Investigating Ordered Phase-Like Domains on the Membrane of Intact B Cells Using Super-Resolution Microscopy

by

Marcos Francisco Núñez

A dissertation submitted in partial fulfillment
of the requirements for the degree of
Doctor of Philosophy
(Biophysics)
in the University of Michigan
2019

Doctoral Committee:

Associate Professor Sarah L. Veatch, Chair
Associate Professor Julie S. Biteen
Professor Charles L. Brooks III
Associate Professor Ann L. Miller
Professor Jennifer P. Ogilvie

Marcos Francisco Núñez Paz

mfnunez@umich.edu

ORCID iD: 0000-0003-1156-6029

Dedication

"Then darkness took me, and I strayed out of thought and time, and I wandered far on roads that I will not tell…And when I was finally ready to return to that place where I was unmade, [they] stood by my side, [they] held my hand, and never let go."
- Junot Díaz & JRR Tolkien

Dedico la labor y cumplimiento de esta tesis a mi
hermano Juan Manuel Núñez Paz y hermana Rocío Alhely Núñez Paz.
Gracias por amarme, apoyarme, respaldarme, cuidarme, y protegerme.
Thank you for walking around lost in the dark with me until we found some light.
Los amo,
- Maco

Juan Manuel Núñez Guillén & Jacobo Eduardo Núñez Guillén
You are capable of achieving the things you never even imagined.
This is proof.
I love you.

Acknowledgements

Quiero agradecerle a toda mi familia por haberme apoyado durante esta carrera. En particular, les agradezco a mi papá y a mí mamá el haber cambiado la trayectoria de sus propias vidas, sacrificando las relaciones con sus amistades y familiares, para que mis hermanos y yo tuviéramos a nuestro alcance las oportunidades que hemos tenido. Les agradezco que no nos empujaron, ni cobraron, ese sacrificio; y porque en todo momento me permitieron sentirme en libertad de perseguir mi pasión, que siempre ha sido por la investigación científica. Gracias por siempre apoyarme en mis estudios al punto de que haya alcanzado mi meta de recibir un doctorado en Biofísica. Gracias por todas las oportunidades que nos han provisto a mis hermanos y a mí. Los quiero mucho.

I would like to thank my advisor, Professor Sarah Veatch, who is the brilliant scientist that has both sacrificed, and invested the time and effort, to guide me through this Thesis and, more importantly, to develop me as a scientist over the past six years. I also thank my committee members Professors Ann Miller, Julie Biteen, Jennifer Ogilvie, and Charlie Brooks, who have provided helpful feedback, mentorship, and support from the start of my graduate career.

I thank my labmates, past and present: Elin Edwald, Matt Stone, Brian DeVree, Sarah Shelby, and Thomas Shaw, for teaching me, being patient with me, and helping me with my various projects during my time in lab. I would especially like to thank our lab manager, Kathleen

Wisser, because I would not have been able to complete the experiments necessary for my Thesis were it not for Kathleen's help, expertise, and consistent contributions. I feel fortunate to have worked with a lab that was always willing to teach, commiserate, celebrate, troubleshoot, give feedback, and lend a hand. Thank you!

I want to thank Mark Kamimura-Jimenez and Emma Flores for taking particular interest in me and mentoring me during some of the toughest times I experienced in graduate school. Thank you for supporting me, relating to me, and always encouraging me to continue to pick myself up and find a way to keep moving forward. You each made a difference.

I thank the Paramount High School teachers that encouraged me to pursue higher education, believed in me, and made me believe in myself. I had very little concept of what higher education was, and much less what scientific research was, but even so, they managed to convince me that I was capable of it all. Thank you for that Ms. Romo, Ms. Royo, and Mr. Cantrell. It started in your classrooms in Paramount High School. This document would not exist, and PhD would not be at the end of my name, if you had not convinced me that it was possible.

Lastly, I would like to thank my friends, mi gente, and the people that have supported me emotionally throughout the years. You have all played a crucial role in my being able to graduate and complete this work. So many people have been instrumental, even if for short periods of time, but I want to shout out my 'ride or dies': Candy & Charlie Rivas, Julia Bourg, Oleta Johnson, and Kristin Schimert. You each made me feel like myself and taught me how to be a

more understanding person. I love each of you so much for it, and I thank you for your support and for your friendship. Shout out to Francisco Solorio and Andrew Page for always being down to have fun and for helping me make my way to some of the best times of my life while in graduate school. Lastly, shout out to Karen Montoya for showing up when everyone else had graduated and left—you have been one of the greatest support systems I've had throughout my six year stay here. Te quiero mucho, Manta.

Table of Contents

List of Figures

List of Abbreviations

BCR: B cell receptor
IgM: Immunoglobulin type M
IgG: Immunoglobulin type G
IgG: Immunoglobulin type D
ITAM: Immunoreceptor tyrosine-based activation motif
ITIM: Immunoreceptor tyrosine-based inhibition motif
MHC: Major histocompatibility complex
Syk: Spleen tyrosine kinase
GPI: Glycosylphosphatidylinositol
CTxB: Cholera Toxin subunit b
LAT: Linker for activation of T cells
PM: Palmitoylated and myristoylated peptide
TM: Transmembrane domain of LAT
TCR: T cell receptor
FRET: Förster resonance energy transfer
PSF: Point spread function
(d)STORM: (Direct) stochastic optical fluctuation microscopy
(f)PALM: (Fluorescence) photoactivation localization microscopy
STED: Stimulated emission depletion
2D: Two dimensional
3D: Two dimensional
GUV: Giant unilamellar vesicle
GPMV: Giant plasma membrane vesicle
f(Ab)1: Fragment antibody with only one binding domain
f(Ab)2: Fragment of antibody with two binding domains
PMF: Potential of Mean Force
MSD: Mean-squared displacement
TIRF: Total internal reflection fluorescence (microscopy)
DOPE: Dioleoyl phosphoethanolamine

Abstract

B cells lymphocytes are responsible for mounting an immune response in a variety of species. B cells are typically activated through the antigen-binding site of its B cell receptors (BCR) which are surface-expressed on the plasma membrane. The lipid composition and organization of the B cell plasma membrane has been implicated in B cell-related immune disease and highlights that plasma membrane organization plays important roles in appropriate BCR signal propagation. B cells respond to a wide variety of antigens with varying valency and mode of presentation, although the contribution of plasma membrane lipids to signaling in these different scenarios is not clearly understood. Past work has shown that BCR clustering through streptavidin, a model soluble antigen, results in the stabilization of an ordered phase-like domain capable of sorting minimal peptides and full length regulatory proteins with respect to BCR clusters. BCR can be stimulated through surface presented antigen in vivo & in vitro, and it is hypothesized that forces mediated via the surface can also impact the sorting of regulatory proteins with respect to antigen engaged BCR.

The research presented in this Thesis applies quantitative two-color super-resolution fluorescence localization microscopy to measure the co-distribution of membrane-anchored peptides and proteins on the B cell surface. I engage and cluster proteins on the surface of B cells both with model soluble antigen and with antigen presented on a mobile bilayer surface. I find that BCR clusters formed through engagement with bilayer-presented antigen sort minimal peptides in a similar manner to BCR clusters stabilized with soluble antigen, indicating that these

are also ordered phase-like domains. I find Lyn kinase is more strongly enriched and CD45 phosphatase is more strongly depleted from BCR clusters engaged with bilayer presented compared to soluble antigen, and that tyrosine phosphorylation is enhanced in surface engaged BCR clusters. Additionally, I show that clusters of cholera toxin B subunit (CTxB) also stabilize environments that sort minimal peptides, and I explore how physical parameters such as temperature and domain size impact the sorting strength of these phase-like domains.

Based on these results, I conclude that ordered domains contribute to the organization of regulatory proteins with respect to BCR engaged with both soluble and surface presented antigen, and that ordered domain stabilization is a general characteristic of the B cell plasma membrane and not specific to BCR clustering. I link CTxB cluster size and temperature to ordered phase-like domain sorting strength suggesting cells can tune the strength of lipid domains to modulate signaling. Findings from my Thesis could contribute to the advancement of therapies for diseases in which altered plasma membrane lipid composition impacts the functional organization proteins on the cell surface.

Chapter 1: Introduction

1.1 – Overview:

The research presented in this Thesis investigates the liquid-ordered (Lo) phase-like domains that form in B cell lymphocyte plasma membranes upon engagement of the B cell receptor (BCR) or Cholera toxin B subunit (CTxB) with either surface-presented or soluble antigen. This Chapter introduces BCR function and several existing models of BCR activation. I review the evidence of membrane heterogeneity, its role in B cell signaling, and the need for a unified physical model to describe lipid organization in plasma membranes. I then provide a brief review of super-resolution microscopy techniques and their application for studying B cell lymphocytes. This introductory material is used to motivate and outline the experimental studies pursued in my Thesis.

1.2 – B cell lymphocytes of the vertebrate immune system:

Vertebrates fight disease and infections through the concerted effort of various cytokines and cells of the immune system that recognize, target, and eliminate pathogenic antigens causing disease or infection [1]. There are two subtypes of white blood cells from the vertebrate immune system that occur in the lymphatic system known as T (thymus-derive) and B (bursal or bone marrow-derived) lymphocytes [2]. B cell lymphocytes, or simply B cells, typically function in the lymphatic space of the body, where they encounter antigen, initiate the immune response, and produce antibodies against antigen consequently leading to the body's adaptive (acquired) immunity [3-6].

B cells engage antigen through its B cell receptor (BCR), causing the receptor to become activated, and the receptor-antigen complex to be internalized for antigen processing [7, 8]. The fate of the B cell following receptor-antigen complex binding depends on various factors, including the developmental stage of the cell [9]. Immature B cells in the germinal center will become antigen-presenting cells for T cells in a major histocompatibility complex (MHC)-restricted manner and develop into plasma cells during a genetic clonal expansion [10-12]. B cells that have already developed into long-lived memory plasma cells will instead begin secreting large amounts of highly specific antibodies against the antigen that stimulated BCR that serve to aid the body mount an immune response [3-6]. These antibodies circulate the body, bind their target antigen on pathogens with high affinity and serve as a marker or flag for other components of the immune system, like natural killer cells, to fight infection and disease [1].

Membrane-bound BCRs are composed of two parts, a membrane-spanning immunoglobulin of isotypes IgD, IgM, IgA, IgG, or IgE, and a heterodimer signal transduction moiety called Igα/Igβ (CD79) [13]. The BCR immunoglobulin isotype varies with B cell development, with mature naïve B cells expressing the membrane-bound IgM isotype of BCR [14-17] that becomes activated as a result of primary antibody-based stimulation in the lymphatic system [18, 19]. Both of Igα/Igβ span the plasma membrane and contain a cytoplasmic tail bearing an immunoreceptor tyrosine-based activation motif (ITAM) [20, 21]. Upon antigen-receptor engagement, the ITAM motifs become dually phosphorylated by Src family kinase (SFK) proteins like Lyn and Syk [22-25]. This phosphorylation event leads to the formation of the signalosome, an assembly of intracellular signaling molecules including phospholipase-Cγ2

(PLCγ2), phosphoinositide 3-kinase (PI3K), Bruton's tyrosine kinase (Btk), and Vav, alongside adaptor molecules such as B cell linker (Blnk) [26-30]. The molecular composition of the signalosome determines the variations in the signaling cascade that coordinate the cell's biological response, including signaling through second messengers such as calcium, the induction of gene expression, and the internalization of antigen [12, 31]. BCR signaling inside the signalosome is a regulated process in which negative regulators, including phosphatases like CD45 are also recruited to BCR sites where they downregulate Lyn and attenuate the BCR signal [32, 33]. The careful balance between Lyn and CD45 activity at BCR sites contributes to the signal duration strength of BCR [34].

A significant amount of literature indicates that properties of the plasma membrane itself contribute to the activation of the BCR [35, 36]. First, the plasma membrane provides a two-dimensional (2D) platform on which early BCR signaling occurs. Antigen engagement, ITAM phosphorylation, SFK recruitment, and other events that form part of the early BCR signaling cascade occur on the plasma membrane mainly because so many of the molecular components involved in BCR signaling are either membrane-integral or peripheral proteins [1, 37, 38]. In addition to serving as the primary stage for BCR signaling, past studies implicate plasma membrane composition and organization in immune receptor localization and function [39-42].

1.3 – Lipid organization in the plasma membrane of eukaryotic cells:

The plasma membrane surrounds all cells and defines the boundary between cells and their environment. It is comprised of a lipid bilayer of various types of lipid species, proteins, and carbohydrates that collectively perform functions for the cell. These functions include

moderating traffic into and out of the cell and serving as a platform for many cellular signaling pathways. Proteins such as receptors and transport channels associate with the plasma membrane through structural characteristics including fatty-acid acylation or hydrophobic α-helices [1] (Fig 1A). One vital function accomplished at the plasma membrane of B cells is communicating extracellular antigen binding of membrane expressed BCR to interior of the cell.

Since 1972, the "Fluid Mosaic Model" has provided a basic description of the plasma membrane [43]. The fluid mosaic model provides for membrane-associated proteins to interact with lipids and for protein function to depend on specific lipids. However, this model states that no long-range ordering of proteins exists within the lipid matrix, but rather that proteins freely diffuse in the "sea of lipids" [43]. With this understanding, immune receptor function on the plasma membrane would not be due in any part to lipid composition or organization (Fig 1A). However, we now know that the lipid organization contributes to signaling to some degree [44-50] (discussed in section 1.3.6).

1.3.1 The lipid raft hypothesis.

The fluid mosaic model has been modified since its inception, but the most disputed change has been the lipid raft hypothesis for plasma membrane heterogeneity. The raft hypothesis predicts the existence of lipid rafts on the plasma membrane of cells and postulates their ability to modulate protein, lipid, and carbohydrate interactions through their sorting in a manner consistent with the raft-preference of their corresponding membrane associations [51-53] [51, 53]. Lipid rafts are defined as membrane domains dynamic in lateral mobility and association-dissociation kinetics, heterogeneous in composition, enriched in cholesterol and sphingolipids,

on the order of 10-200nm with the ability to form microscopic domains (>300 nm) upon clustering induced by protein–protein and protein–lipid interactions (Fig 1B) [44, 54].

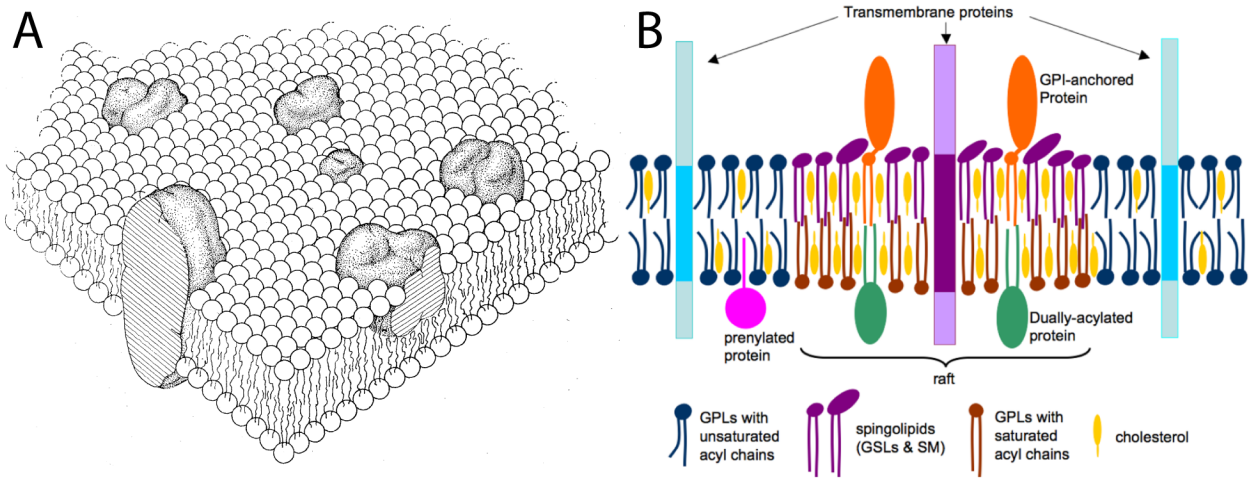

Figure 1: Visual representation of the plasma membrane

(A) Proteins are associated to the lipid bilayer through various modifications including lipid-anchoring and hydrophobic transmembrane-domains. The fluid mosaic model does not depict any long-range interaction or ordering of proteins in a sea of lipids on the plasma membrane. Reprinted from [43] with permission: AAAS License #: 4562410667390. **(B)** Lipid rafts are enriched in sphingolipids, cholesterol, and saturated lipid species. Proteins sort based on the partitioning preference of their membrane association, lipid anchor or transmembrane domain, which enhances or deters specific interactions. Reprinted from [55] with permission: Elsevier License #: 4557480979450.

Model membranes consisting of a mixture of relatively saturated lipids with a high melting temperature, cholesterol, and unsaturated phospholipid species with a low melting temperature separate into two distinct liquid phases [56]. The liquid-ordered (Lo) phase is a highly packed phase enriched in saturated lipid species and cholesterol and the liquid-disordered (Ld) phase which is more fluid and comprised mainly of unsaturated lipids [56-58]. However, due to the tight molecular packing and enrichment of cholesterol and saturated lipids, the Lo-phase is often considered a model for lipid rafts [44]. It should be noted though, that the lipid raft specifically applies to nanoscale domains to in cells, and Lo/Ld phases to model membranes, which are thought to be governed by a different, but overlapping, set of physical mechanisms [54]. While the phase separation of lipids is an acknowledged contributor to the formation of membrane

domains, I acknowledge that both proteins and lipids likely contribute to the generation of these membrane structures [54, 59].

1.3.2 Early evidence supporting the existence and biological function of lipid rafts in cells.

Although the existence and functionality of lipid rafts were proposed in 1997 [51], observations of phase-like behavior in membranes have existed longer than the fluid mosaic model has been proposed [51, 53, 60-66]. Early evidence for lipid rafts came largely from biochemical treatments of the plasma membrane in which detergent-insoluble portions of the plasma membrane, termed "Detergent Resistant Membrane (DRM)", were extracted and discovered to be enriched in sphingolipids and depleted of glycerophospholipids [67] resembling Lo domain. This same type of treatment was applied in various studies to probe which other proteins co-extracted with the DRMs. One such study found that PLAP, a glycophosphatidylinositol (GPI)-anchored protein, consistently extracted with DRMs during Triton X-100 solubilization. PLAP was sorted in the Golgi before being trafficked to the membrane, which suggested that membrane domains are initially sorted in the trans golgi network following protein modification prior to transport to the membrane [68].

However, it wasn't just the association of proteins with DRMs that supported the evidence of lipid rafts, studies revealed some receptors differentially associate with DRMs depending on the signaling state further supporting the functionality hypothesis of lipid rafts. IgE receptor activation was originally thought to depend solely on protein–protein interactions [69], although several observations soon indicated that rafts were also involved in this process [70]. For

example, resting state FcεRI is non-DRM associated in Triton X-100 but becomes DRM-associated upon cross-linking based stimulation [71].

A second set of biochemical treatments that contributed to the evidence for lipid rafts in cell plasma membranes came from the observation that a disruption of lipid rafts byway of a major raft component, cholesterol, significantly impaired signaling processes that appeared to be otherwise raft-associated. For example, immune receptor IgE signaling was found to be abolished when plasma membrane cholesterol was extracted through the use of the chemical compound with methyl-β-cyclodextrin (MβCD) [72]. Additional supporting evidence came from MβCD treatment of rat neurons causing a change in the function of a raft-associated potassium channel [73]. Lastly, cholesterol depletion was found to inhibit receptor tyrosine phosphorylation in basophils [72], and T cell receptor activation and signaling in T cell lymphocytes [65].

These studies along with many others [51, 53, 60-64, 74], contribute to a model in which lipid rafts exist on the plasma membrane and function to sort specific proteins.

1.3.3 Challenges to the raft hypothesis due to alternative interpretations of widespread methods.

It was eventually discovered that despite the large body of work contributing to lipid raft observations, the biochemical treatments of the plasma membrane were perturbative, indirect, or open to alternative interpretations [75].

Two of the most commonly used methods for lipid raft detection included DRM extraction with Triton X-100 [67] and sensitivity to cholesterol depletion through the use of methyl-β -

cyclodextrin (MβCD)[76]. For example, DRMs were hypothesized to be detergent insoluble due to the tight packing of lipids in rafts but through the use of ITC, DSC, and NMR, it was observed that Triton X-100 actually increased the transition temperature and formed Lo domains by strongly interacting with Palmitoyloleoylglycero Phosphocholine (POPC) producing "insoluble" sphingomyelin-cholesterol domains [77-79]. It was concluded that DRMs were mistakenly equated with lipid rafts [75].

While Triton X-100 is the most commonly detergent used to study DRMs, other detergents that are less fluidizing are also used. Studies systematically comparing the extent and lipid and protein content of DRMs using different detergents have revealed a great variation in their results [80]. These results indicate that DRMs differ substantially from rafts since a basic assumption of lipid rafts is they exist as a consequence of a spontaneous de-mixing of two liquid phases in the lipid bilayer [79].

Experiments using cholesterol depletion also required re-evaluation after studies revealing its perturbative effect on the actin cytoskeleton through the distribution of phosphatidylinositol (4,5) bisphosphate (PIP_2)at the plasma membrane [81]. Microdomains like lipid rafts were considered scaffolds for PIP_2 signaling, that enabled PIP_2 to selectively regulate different processes in the cell. Enrichment of PIP_2 in lipid rafts was based on cholesterol depletion and detergent extraction studies [82]. PIP_2 also has a role for the organization the cytoskeleton by stabilizing cortical actin and influencing the turnover of cytoplasmic stress fibers [81]. Additionally, past experiments revealed that cholesterol depletion interfered with basal, ligand-independent recycling of the neurokinin A receptor, thereby providing alternative explanations for the cholesterol dependency

of PIP_2 breakdown.[82]. Therefore, whether cholesterol disrupted specific PIP_2 microdomains or whether the effect on PIP_2 was a secondary effect in response to the disruption of lipid rafts and protein–lipid organization of the plasma membrane became unclear. [83].

Cholesterol depletion also affected lipid raft structure itself. Cholesterol has been shown to promote phase separation [84, 85], thought to occur because of the favorable packing interactions between saturated lipids and sterols [86]. Thus, in phospholipid & sphingolipid mixtures, cholesterol decreases the amount of sphingolipid required to form the Lo phase, thereby directly impacting the phase behavior of raft-resident lipids [85, 87]. Therefore, this likely explains why cholesterol depletion seems to disrupt lipid rafts and affect raft function [88].

It should be noted that these studies do not disprove the lipid raft hypothesis, instead they highlight the need for additional methods of observation, including those that are direct and non-perturbative.

1.3.4 Phase separation observed in isolated biological membranes suggest plasma membrane could support lipid rafts.

Some of the recent supporting evidence for biological membranes exhibiting lipid raft structures comes from giant plasma membrane vesicles (GPMVs) isolated from living cells. GPMVs are blebs induced through chemical treatment [89, 90] from isolated eukaryotic cells. The membranes of these vesicles serve as useful models for studies [91, 92] because they share a similar composition to the cellular plasma membranes from which they were isolated [93-98]. The membrane composition of GPMVs isolated from rat basophil leukemia cells (RBLs) for

example contain 20-40 mol% cholesterol, sphingolipids, phospholipids, and gangliosides typically associated with the plasma membrane, along with many transmembrane and peripheral plasma membrane proteins [91, 97, 99].

In 2007, liquid-liquid phase separation was observed for the first time in GPMVs indicating that plasma membranes, with compositions similar to those of the mammalian cells from which the vesicles were isolated, could support phase separation [97]. What offered more support for the raft hypothesis was that the proteins and lipids co-sorting into each of the distinct phases were considered typical raft residents (GPI-anchored, glycosphingolipid GM1) or non-raft residents (prenylated and unsaturated lipids) [97, 98]. Additionally, the phase behavior in GPMVs was confirmed to be cholesterol dependent [100], consistent with predicted raft behavior.

Lastly, the co-existing phases in GPMVs were identified as the Lo and liquid-disordered (Ld) phases based on diffusivity and order measurements [58, 100] further providing evidence that the membranes of these vesicles could support lipid rafts. Since these vesicles are derived from living cells and contain many the same membrane species as intact cells, it stands to reason that similar physical principles are governing lipid organization in the membranes of both vesicles and living intact cells. Therefore, the plasma membranes of living cells could potentially exhibit lipid rafts.

1.3.5 Plasma membrane vesicles isolated from living cells exhibit critical fluctuations.

Experiments studying GPMVs derived from several cell types observed that they undergo a phase transition in the range of 15°C to 25°C where a single phase at higher temperatures de-

mixes into coexisting Lo and Ld phases at lower temperatures [101]. Microscopic analysis of characteristics including domain edge fluctuations at lower temperature and composition fluctuations at higher temperatures indicated the membrane's proximity to a miscibility critical point and found to be consistent with theory [102, 103].

A key feature of systems exhibiting critical behavior is that they are universal, meaning that many of the system's properties can be understood without considering the details of the system [104, 105]. Past theoretical work modeled the membrane of GPMVs using another critical system, 2D Ising model simulations. From these simulations, it was argued that lipid raft heterogeneity in cells could arise as a consequence of existing near a critical point determined by the membrane's temperature and composition [59]. Specifically, it is proposed that cell plasma membranes exhibit a critical miscibility transition at temperatures 15-30 degrees below growth temperatures, and that lipid rafts are subtle fluctuations that occur in membranes as a result of this near-by phase transition [101].

1.3.6 Evidence for a role for lipid rafts in B cell receptor signaling.

The plasma membrane composition and organization has been implicated in BCR signaling [35, 36]. The plasma membrane is thought to achieve this role through the sorting of regulatory proteins of BCR signaling. Sorting of these proteins has been shown to occur predominantly via their membrane association [1, 37, 38]. Antigen-mediated clustering of the BCR is quickly followed by the association of BCR into biochemically defined lipid rafts where it encounters other raft-resident proteins, like Lyn kinase, and becomes spatially segregated from non-raft resident proteins, like CD45 phosphatase (Fig 2) [36]. The sorting of these regulatory proteins

based on their membrane anchors is thought to contribute to the spatial sequestration, and consequently to an environment that favorably results in the phosphorylation of BCR ITAM domains and signal propagation (Fig 2) [36]. Additionally, Lyn's kinase activity is regulated by phosphorylation at one of two sites: pY397 activates kinase activity while pY508 inhibits it [106]. The phosphorylation sites on Lyn are regulated by different proteins. An interesting trend that has shown up in previous studies is that some of Lyn's positive regulators and negative regulators have different phase preferences, which suggests that phase-like sorting might govern or contribute to BCR activation by way of Lyn kinase activity [107-109].

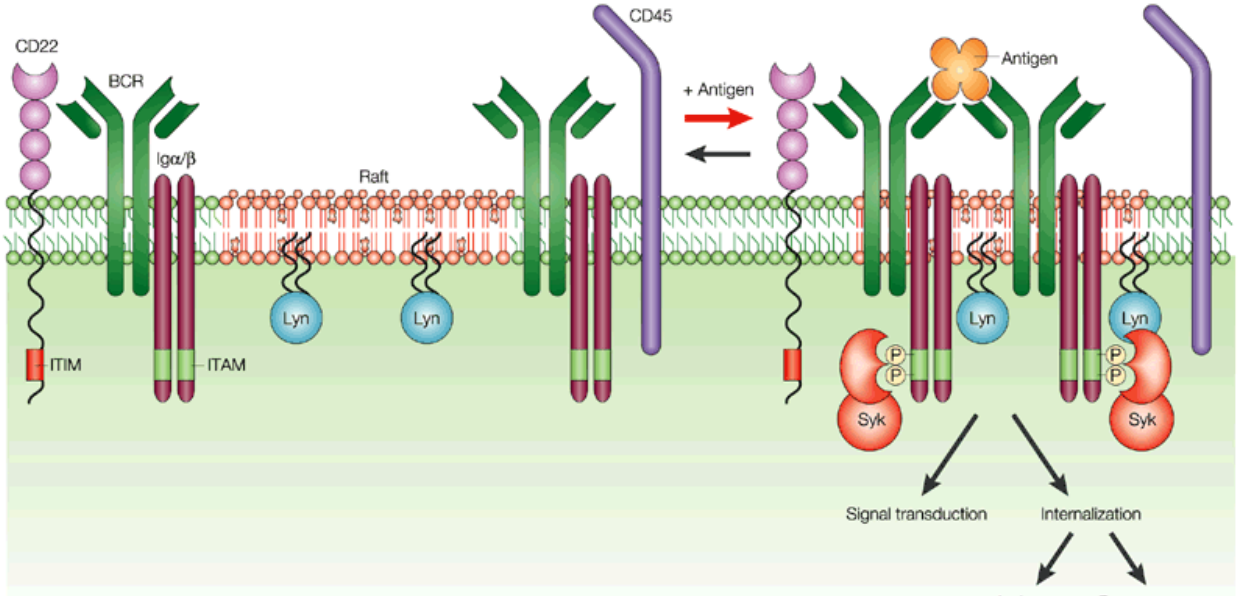

Figure 2: Lipid rafts contribute to BCR signaling
The lipid raft model for BCR signaling postulates that BCR associates with lipid rafts upon antigen-based clustering stimulation. In lipid rafts BCR clusters are activated by raft-resident Src family kinases like Lyn and sequestered from non-raft resident deactivating phosphatases like CD45. Lipid rafts are thought to contribute to BCR signaling by sorting proteins in such a way that promotes an activating, phosphorylating environment that promotes BCR signaling. Reprinted from [36] with permission: Springer Nature License #: 4557790163781.

The phase-based sorting trend is not specific to Lyn, it is more common to BCR signaling as a whole. For example, transmembrane adaptor proteins like LAT2 and LIME are palmitoylated membrane-associated scaffolds for BCR signal transduction [110-112]. Palmitoylation is a post-

translational S acylation modification of a protein in which a palmitate is added through a cysteine-linked modification, and has been shown to preferentially associate otherwise Lo-partitioning transmembrane proteins with the Lo-phase in GPMVs [113]. Another example in which Lo-like domains are implicated in BCR signaling is with the CD81 dependent association of the CD19/CD21 complex with lipid rafts resembling the composition of the Lo phase. The CD19/CD21 complex is an essential B cell coreceptor that works to decrease the threshold for B cell activation by enhancing signaling [114]. The cooperation between the CD19/CD21 complex and BCR depends on the ability of tetraspanin CD81 to incorporate the co-ligated complex into Lo-like domains [115]. Lastly, the receptors for the Fc region of IgG (FcγRIIB) whose main function is to inhibit activating signals typically by co-ligating directly to BCR are thought to do so through their direct incorporation into biochemically defined lipid rafts. Inhibition first requires the phosphorylation of the cytoplasmic domains on the immunoreceptor tyrosine-based inhibitory motif (ITIM) of FcγRIIB [116, 117], which is achieved through its incorporation into lipid rafts where BCRs are actively signaling. Once phosphorylated, subsequent binding of SH2-domain-containing inositol phosphatases (SHIPs) leads to the downregulation of the immune synapse formation and inhibition of the BCR signaling cascade [118-120].

Methods like the biochemical techniques [67, 76] and biological membranes isolation [97, 98, 121] described in sections 1.3.2 and 1.3.4 have contributed significantly to the lipid raft model for BCR signaling. With the incorporation of different imaging techniques, the evidence supporting this model has become even stronger. Imaging with probes like the Laurdan stains which incorporate into the plasma membrane and are often used as a proxy for lipid packing and phase-order domains taken mark lipid rafts [122]. Imaging tools like Förster resonance energy

transfer (FRET) can detect interactions between 1-10nm [123-130] and has been used to measure interactions between various specific membrane proteins and lipids [125, 131-133]. This sensitivity makes FRET a powerful method for measuring the interactions between proteins and lipids at the nanoscale in both model membranes [134] and live cells [135], not only to probe the existence of lipid rafts but also to define their size [134, 136].

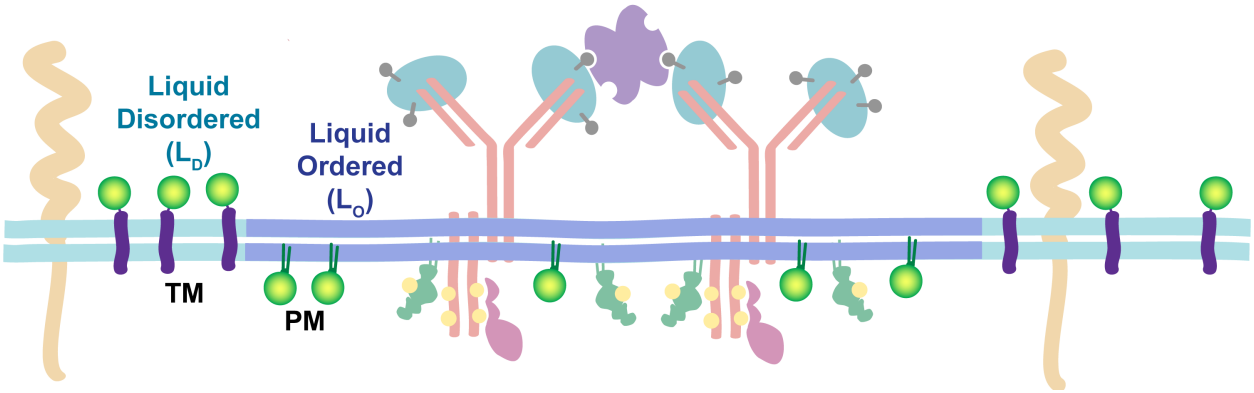

Figure 3: BCR clustering-based stimulation stabilizes Lo-like domains
The minimal phase-marking peptides PM (ordered) and TM (disordered) sort into corresponding phases in GPMVs and relative to BCR clusters in B cells. Figure adapted from cartoons provided by Dr. Sarah Shelby.

Several super-resolution optical microscopy approaches have been developed recently [137, 138] to visualize nanoscale structures and dynamics in cells, including lipid-mediated protein clustering [139]. We recently contributed to lipid raft model for BCR signaling by demonstrating the presence of heterogeneous lipid domains in the plasma membranes of intact B cells that resemble the Lo and Ld phases in GPMVs [50, 97]. We directly visualized the presence of Lo-like and Ld-like phases on the plasma membrane of B cells supporting that the plasma membrane exhibits phase-like behavior [50] (Fig 3). I will refer to the liquid-order phase-like domains on cell membranes as Lo-like, and the liquid-disorder phase-like domains as Ld-like since phase separation has not been observed in cells. Several features of the Lo-like domains in cells are predicted to correspond to properties of lipid rafts: nanoscopic, dynamic environments enriched in cholesterol, sphingolipids, and acylated proteins [140, 141]. However, we have only observed

the nanoscale sorting of phase-markers of known preference from GPMV studies to identify the Lo-like and Ld-like phases in cells [50]. Convergence between the rest of the properties of lipid rafts, and the newly discovered phase-like domains in cells remains to be tested.

We observed clustered B cell receptors (BCR) reside in Lo-like domains and are capable of sorting key regulators of B cell signaling, such as Src-family kinases (SFKs). Upon antigen-mediated BCR clustering, SFKs are recruited to Lo-like domains and contribute to the activation of BCR, facilitating downstream signaling that constitute the B cell response [142-144]. We also demonstrated that Lo-like domains concentrate active Lyn kinase and deplete one of its negative regulators, CD45, providing an environment that favors the activation of BCR.

1.3.7 Stabilization of critical fluctuations in biological membranes for experimental observation.

The theoretical model introduced in section 1.3.5 also predicts that the application of a stabilizing force, such as at sites of coupling the membrane to the cytoskeleton, will stabilize fluctuations and enable their experimental observation [59]. Our lab previously stabilized critical fluctuations in Giant Unilamellar Vesicles (GUVs) made with critical compositions and GPMVs derived from RBLs by adhering the vesicles to a supported lipid bilayer [145]. Adhesion sites were mediated through Lo- or Ld-preferring molecules. The local lipid environment around the adhesion site was sensitive to lipid order when the adhesion site itself had an order preference, which would serve as the weak applied energy field necessary to stabilize the critical fluctuation.

This past study in model membranes motivates similar experiments in intact cells, were plasma membrane fluctuations are stabilized via protein clustering through an external force. The 2D

Ising model-based predictions describe an experiment [145] that could be used for testing consistency between critical fluctuation model and the behavior of the phase-like domains in intact cells [50]. In this hypothetical experiment, the stabilized Lo-like domains on B cell plasma membranes could be perturbed in their composition or temperature in order to test for consistency with the expected sorting behavior based on the 2D Ising model predictions. This type of experiment could provide a quantitative approach for validating the critical fluctuation model for membrane organization in B cell plasma membranes.

1.3.8 A unified physical model of plasma membrane phase-like behavior is needed to further understand biology and diseases.

Experimental observations have made it clear that phase behavior exists in GPMVs which could give rise to lipid rafts, suggesting that they could also exist in living intact cells [101]. Since GPMVs are derived from living intact cells, a physical model describing the membrane phase-like behavior would need to capture the behavior observed not only in vesicles but also in cells. A unified model of membrane organization would contribute to a gap in knowledge the field has been pursuing for the past few decades. This model would allow us to validate if the physical mechanisms governing membrane organization in GPMVs also gives rise and govern the same types of structures in intact cells. This model would also allow us to make testable predictions of how lipid organization would respond to various external stimuli or manipulations thereby revealing what types of mechanisms cells might use to modulate their own lipid organization. This type of knowledge would have impacts not only for biology but also for human health and disease.

There are existing drugs and therapies that alter membrane composition in order to alter signaling and alleviate specific symptoms like polyunsaturated fatty acid supplementation which is used to treat over-active immune-related inflammation [146] and ether-lipid (alkyl-phospholipid) analogues such as edelfosine, miltefosine and perifosine for cancer therapy [147]. Lastly, biochemical perturbations that alter lipid phase separation properties of GPMVs [101, 145, 148] can also alter SFK activity and downstream function in cells [149-152]. This past work indicates lipid domain structure is important for SFK-based signaling, which highlights the importance of understanding lipid organization of plasma membranes for biological signaling. Although advances in molecular biology have resulted in incremental knowledge about how these biological compounds and therapies that can be used effectively, the precise disease-relevant mechanism of action of these compounds remains elusive [153]. A unified physical model of plasma membrane phase-like behavior would go beyond alleviating symptoms and allow the study of human diseases with a physical and predictive approach.

Establishing a set of physical principles by which lipid organization in plasma membranes affects signaling would inform how these disease, drugs, and therapies work and would potentially lead to development of new therapies that could complement available treatments [153].

1.4 – Alternate models for B cell receptor activation:

The lipid raft model for BCR activation postulates that he plasma membrane composition and organization are essential for BCR signaling [35, 36]. The plasma membrane is thought to achieve this role through the sorting key regulators like Lyn kinase and CD45 phosphatase in a

manner consistent with the partitioning preference of their corresponding membrane association [1, 37, 38]. Evidence supporting this model comes from the observation that antigen-mediated clustering of the BCR is quickly followed by the association of BCR into lipid rafts where it encounters Lyn and other raft-resident proteins while becoming spatially segregated from CD45 and other non-raft resident proteins [36], such that the lipid raft establishes an environment that favorably results in the phosphorylation of BCR ITAM domains and signal propagation.

While it is clear that key kinases like Lyn and phosphatases like CD45 play major roles in BCR signaling, the events following early BCR signaling are still an area of ongoing research [9, 26-30, 32, 33]. Various models have emerged in an effort to explain the molecular mechanism governing BCR activation [154]. I will summarize some of these models used to describe B cell activation following BCR-antigen engagement are presented in the following subsections.

1.4.1 Dissociation model

The dissociation model [155] proposes that upon antigen binding of the receptor a BCR dissociates from the inhibitory oligomer into an active monomeric state. In the following section I will discuss the research that support this model.

Naïve B cells express the IgM subtype of BCR on their plasma membranes [15, 16], whereas mature B cells express both IgM and IgD subtypes, each of which contains identical antigen-binding specificities [156, 157]. The two BCR subtypes differ only in the constant regions of their respective mHCs (μm and δm), and that the Igα-Igβ complex is identical for the two subtypes, apart from minor differences in the glycosylation of Igα [158-160]. However, the

structural identity between IgM and IgD BCR made it difficult to understand the measured differences in signal transduction between the two subtypes of receptors [161-163].

One of the initial pieces of evidence that lead to the development of the dissociation model came from the observation that membrane-bound portion of BCR and Igα-Igβ subunits bind 1:1 to form the receptor complex [24, 164]. In this complex, the hydrophilic amino acids of the immunoglobulin's (Immunoglobulin) membrane-bound heavy chain (mHC) transmembrane region would be partially exposed to the hydrophobic lipid environment, but should become stabilized if they were shielded in a BCR oligomeric state [24, 165]. This lead to the discovery that both IgM and IgD subtypes of BCR run as large macro-molecular complexes in a blue native polyacrylamide gel electrophoresis(BN-PAGE) analysis suggesting that they are present in oligomers on the plasma membrane [24]. Additionally, a mutation of all hydrophilic amino acids on the transmembrane region of the δm mHC was found to reduce the size of the observed macro-molecular complexes suggesting the only variation between IgM and IgD as the oligomer building site [24].

The presence of BCR oligomers was supported in living cells using bifluorescence complementation (BiFC) [166]. With this method, a BCR IgD subtype mutant unable to form oligomers was identified with several amino acid mutations at the transmembrane region of the δm mHC B [166], supporting results obtained with BN-PAGE. Lastly, the monomeric BCR mutant was found to be more actively signaling than the BiFC-stabilized BCR dimer which further strengthened the dissociation model [166]. Additional support for this model has come from super-resolution studies direct using stochastic optical reconstruction microscopy

(dSTORM) to measure the BCR organization in primary B cells showing that both IgD and IgM subtypes are mostly organized as pre-formed nanoclusters in resting cells [167]. A separate study combined two-color direct dSTORM and two-marker transmission electron microscopy TEM to provide evidence that the IgM and IgD are not only localized in separate "protein islands" resembling oligomers [168].

The last set of experiments providing support for the dissociation model comes from Fab-based proximity ligation assays (Fab-PLA) which can detect the proximity of two proteins on the surface of cells [169, 170]. The organization of IgM and IgD BCR subtypes was studied using Fab-PLA and revealed that they reside in distinct membrane compartments with a different protein and lipid compositions [171]. Additionally, this results obtained with this method suggested that two closely situated BCR of either subtype separate, or dissociate, upon activation [171]. These findings collectively support the dissociation activation model, in which B cell activation is accompanied by the dissociation of an activated BCR monomer from inhibited pre-formed BCR oligomers [155, 168, 172].

1.4.2 Kinetic segregation model: in which CD45 ectodomain depletes it from BCR clusters.

A separate model of BCR activation is borne out of observations made in T cell experiments. T cell lymphocytes and B cell lymphocytes are closely related, sharing various characteristics, and work closely with one another to mount an immune response [1, 6]. These two lymphocytes express a different canonical antigen receptor on its surface, TCR as opposed to BCR which engage one another during the antigen presentation process to form the immune synapse [173]. An additional feature that is common among these cell types is that receptor organization during

activation is thought to influence receptor function [174, 175] given that the organization of regulatory proteins relative to their receptors also influences signaling [176, 177].

In T cells however, studies have revealed that CD45's large extracellular domain largely contributes to its exclusion from TCR clusters during activation due to steric hindrance [174, 175, 178]. T cells typically recognize antigen on the surface of other cells. In order for TCR to engage surface-bound antigen, the space between the membrane of the two cells is reduced to sizes smaller than CD45's ectodomain [179, 180], and the immune synapse forms. Studies have shown that the membrane is not only responsible for coordinating the organization of TCR accessory proteins, but it also orchestrates the 3D-spatial sterics which largely constrain the organization of CD45 to the periphery of the immune synapse [175, 179]. This is important because CD45's phosphatase activity is thought to counteract Lyn's kinase activity which would upregulate TCR, amplify TCR signaling, and promote the immune synapse to form [181]. Without CD45's dramatic exclusion, TCR would likely not be activated to the degree that it is. These observations lead to the development of the kinetic segregation model for TCR signaling [178]. Due to the many similarities between B cells and T cells, could describe a similar mechanism for BCR activation and signaling in B cells [35, 182].

BCR is known to activate in response to various antigens, but the response types, strength, and cluster organization are all parameters that can differ based on antigen-binding valency, affinity, density, mobility, and form of presentation to the receptor [155, 166, 183-195]. Considering the kinetic segregation model in T cells (section 1.4.4) and its possible application to B cells, it is important to investigate what differences might arise when BCR is stimulated with soluble

antigen as opposed to surface-presented antigen (Fig 4). We identified Lo-like domain stabilization upon BCR clustering using a model artificial and soluble ligand — streptavidin [50]. BCR was labeled at the Fc (μ domain) region with a biotinylated f(Ab)1 IgM fragment. Large BCR clusters were formed to activate BCR by adding soluble streptavidin which then cluster the biotinylated fab-labeled BCR. Although B cells engage both soluble and membrane-anchored- antigen in vivo [190], studies suggest that surface-presented antigen may constitute the dominant form of antigen-dependent BCR stimulation [188, 191-195]. Therefore, it is important to consider differences in receptor stimulating conditions in this case because they each result in very different signaling outcomes, although they both experience an active BCR state.

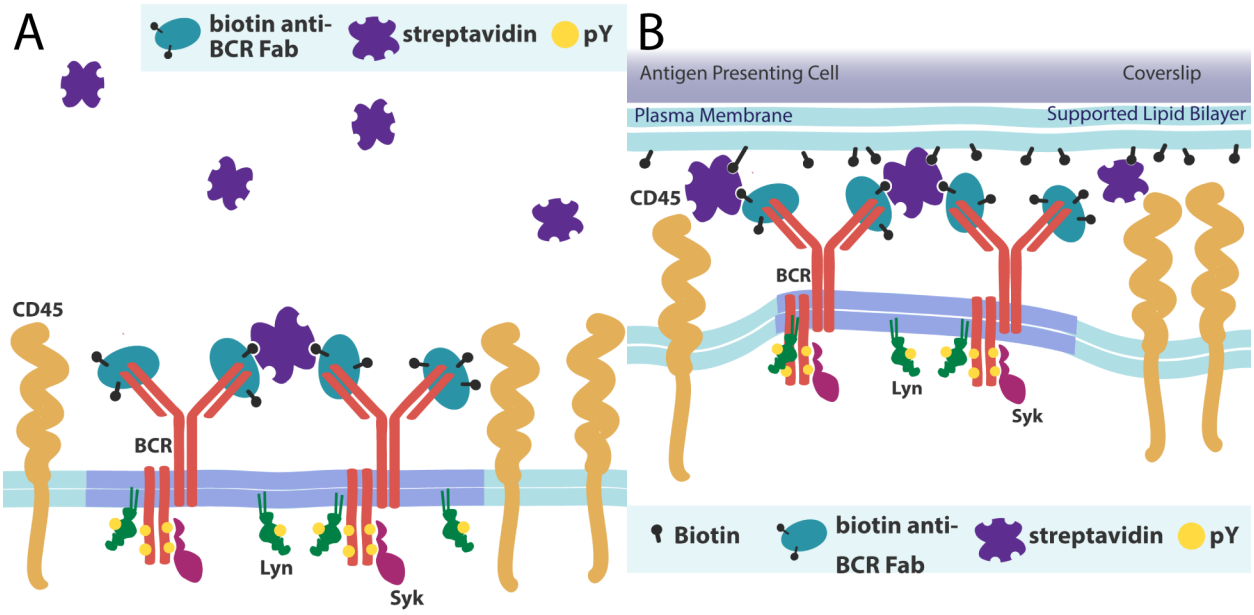

Figure 4: Comparison of soluble and surface-presented stimulation of BCR
(A) Soluble-based stimulation of BCR for the model antigen used in this Thesis. The contribution of lipid rafts in this method of stimulation is highlighted here. **(B)** The same model antigen is bound to a surface, a supported lipid bilayer, on to which B cells are introduced for BCR stimulation. The surface-presented method is thought to have contributions for BCR signaling in addition to lipid rafts due to the steric hindrance imposed by the proximity of the two membranes. Figure adapted from cartoons provided by Dr. Sarah Shelby.

1.4.3 Conformational change model

The conformational model hypothesizes that upon antigen docking to the binding pocket of the BCR, the receptor experiences a conformational change that communicates the binding signal to the cytoplasmic ITAM domains of the Igα-Igβ heterodimer.

Similar to the kinetic segregation model, this hypothesis is informed by similarities observed with TCR [35]. In TCR, the conformational model has been supported by the observation that TCR engagement with ligand exposes a proline-rich region in the CD3ε component of TCR prior to phosphorylation of ITAMs resulting in the recruitment of an adaptor protein implicated in mediating cytoskeletal reorganization [196, 197]. This result suggested that a conformational change experienced by TCR in response to ligand binding was responsible for recruiting an adaptor protein responsible for signaling prior to the essential tyrosine phosphorylation. Additionally, the conformational change in TCR also caused the exposure of basic residues in CD3ε containing the ITAMs to the cytoplasm and accessibility to SFKs following TCR stimulation[198].

Although x-ray crystallography studies of BCR have yet to reveal crystal structures in which a conformational change near the ITAM region is observed [199, 200], it should be noted that a complete crystal structure of an antigen-bound BCR complex has not been solved and therefore does not rule out the possibility that this model is indeed valid [201]. In fact, crystal structures of intact IgG indicate interdomain flexibility within the immunoglobulin [202]. Additionally, crystal structures of the Fc region of IgE [203] and Fc region of IgG [204, 205] bound to Fc receptors or free revealed rearrangement of the Fc region upon Fc receptor binding, which

collectively indicates the conformational flexibility of the IgG and IgE and suggests that the same flexibility might be a characteristic of IgM [201].

There has been structural and functional evidence of BCR supporting the conformational model for B cells. For example, a studies on the Igα-Igβ cytoplasmic ectodomain and its assembly with the membrane bound immunoglobulin revealed that both Igα and Igβ bind to the membrane-proximal Cμ4 domain of the membrane bound immunoglobulin through a contact surface involving multiple charged residues [205]. In separate studies it was reported that Igα-Igβ tails undergo conformational changes during BCR activation as evidenced by FRET signal changes between CFP- and YFP-tail-labeled Igα-Igβ [172](Tolar et al. 2005). Therefore, these data support the hypothesis that antigen could induce an conformational change to the receptor in the Igα-Igβ heterodimer thereby transducing information to the cytoplasmic domains.

The conformational model was further strengthened when evidenced for a mechanism of how a conformational change in the Cμ4 domain resulted in the observed BCR clustering and slowing that characterizes antigen-based stimulation [206]. Immobilization of BCR in the signalosome was found to occur independently of the cytoplasmic domains of BCR, the Igα-Igβ heterodimer. Instead, BCR clustering was identified to occur through the membrane-proximal Cμ4 domain of the membrane bound immunoglobulin [207], which forms a homodimer at the bottom of the canonical Fc structure shared in all immunoglobulin molecules [208-210]. Not only did monovalent membrane antigens stimulated BCRs lacking the Cμ4 domain fail to cluster and signal, but Cμ4 domains were sufficient to clustered spontaneously and activated B cells. Together these results support the idea that a conformational change is communicated through

the receptor upon antigen binding which promotes the clustering of the receptor and promotes signal propagation — the conformation change model.

1.5 – Super-resolution microscopy:

Possibly the largest obstacle preventing significant advances in the field of membrane biology has been the lack of methods with the sensitivity to observe lipid domains in intact cells. Following the discussion in section *1.3*, the most recent advancement in the field came after the development of super-resolution microscopy and its incorporation to this field of research. In this section I will give a brief overview of this microscopy technique, its applications, and how I use it in my research.

1.5.1 Imaging the plasma membrane requires high contrast, specificity, and resolution.

Brightfield imaging is the most basic form of optical microscopy illumination. With this type of microscopy, a dark sample is illuminated with bright white light and observed through a series of lenses that create an image and magnify the samples features. Studies however require much greater specificity than simply illuminating an entire sample with white light. The plasma membrane is a crowded environment comprised of thousands of different types of proteins and lipids that do not absorb light and as a result are not visible. Therefore, studying the role that lipids in the plasma membrane contribute to BCR signaling requires imaging with much greater contrast. Fluorescence imaging provides that type of contrast.

With fluorescence imaging, a protein of interest is typically isolated for imaging by tagging with a fluorophore. The fluorophore is typically introduced through an organic dye or a fluorescent

protein. During imaging, the valence electrons of the fluorophore are excited with light of $\lambda_{excited}$. The electrons experience some energy loss in this excited state through vibrations in a phenomenon known as the stoke's shift [211]. So, as the electron spontaneously emits a photon to return to its ground state, the electron it emits will be of lower energy than the light it was excited with and therefore emit light with a longer wavelength such that $\lambda_{\text{excited}} < \lambda_{\text{emitted}}$. In order to image multiple fluorophores at once, the absorption and emission spectra of the fluorophores simply would need to be separated enough to isolate the colors without bleed-through from other channels. Isolation of individual colors is typically achieved through the use of filters. Through the use of more advanced microscopy techniques like total internal reflection fluorescence (TIRF), we are able isolate the plasma membrane for imaging and increase the contrast of our images [212, 213].

However, the resolution of my images is still restricted by the diffraction limit of visible light. The ability to resolve two molecules, or fluorophores in my experiments, is characterized by the ability of my imaging system to distinguish their point spread functions (PSF) (Fig 5). The Rayleigh criterion for microscope resolution states that the ability to distinguish two objects is limited by the wavelength of light with which it is imaged $r = 0.61\lambda/NA$, where NA is the numerical aperture of the lens and λ is the wavelength [214, 215]. Since fluorescent imaging relies on visible light, the smallest distance we can resolve through typical diffraction limited techniques is on the order of 250nm. This poses a problem when trying to image nanoscale structure on the surface of cell plasma membrane, and in fact has prevented much advancement in the lipid raft field.

There are imaging modalities like Scanning Electron Microscopy (SEM) or X-Ray Crystallography that depend on λ much smaller than those from the visible spectrum and therefore provide much higher resolutions. Fluorescent imaging benefits from the ease of sample preparation and the ability to label and tag proteins of interest. The Nobel prize winning technique of 2014, super-resolution microscopy, overcame the diffraction limit of light while still imaging conventional immunohistochemistry labels and fluorescent protein tags with wavelengths of light in the visible spectrum.

1.5.2 Principles of super-resolution microscopy.

In its most fundamental definition, super-resolution imaging is used to image fluorescent structure with sub-diffraction resolution. This is achieved in a variety of ways, but conceptually they all seek to detect single molecules such that their individual point spread functions are distinguishable from others (Fig 5D).

Here I briefly describe some common super-resolution microscopy techniques.

1.5.2.1 SIM: Structured Illumination Microscopy.

Structured-illumination microscopy (SIM) works by using patterned illumination to excite a fluorescent sample [216]. This patterned excitation typically has a sinusoidal shape which generates a similarly shaped fluorescence emission pattern that is diffraction-limited [217]. The sample is imaged iteratively under a series of periodic excitation patterns comprising a small number of spatial frequencies, each of which causes a specific region of frequency space to be translated into the detection passband [217].

The patterns are phase-shifted such that the contributions from different regions can be separated and computationally restored to their proper position in frequency space. A final image is thus reconstructed from multiple images collected by scanning and rotating the pattern that has a lateral resolution approximately twice that of diffraction-limited instruments, approximately 100nm [214, 218]. The additional spatial modulation from the excitation pattern brings the enhanced spatial resolution into the reconstructed image [219, 220].

1.5.2.2 STED: StimulaTed Emission Depletion.

With stimulated emission depletion (STED) microscopy [221-223] sub-diffraction resolutions are achieved by selective deactivation of fluorophores at specific positions of the diffraction-limited excitation regions [224]. With this technique, the fluorescent confinement of molecules is achieved by co-aligning an excitation beam with a second beam, called the STED beam. The STED beam interrupts the normal fluorescence process by forcing excited electrons to relax into higher vibrational states than the fluorescence transition would normally enter, causing the emitted photon to be red-shifted and then spectrally-filtered [221, 225].

The STED beam is engineered with a doughnut-shaped focal intensity distribution such that there is zero-point intensity of stimulated emission in the center, allowing for maximum fluorescent emission by the co-aligned excitation beam [224]. While the focal intensity distribution of the STED beam is diffraction limited, high laser intensities saturate the stimulated emission transition and keep virtually all the fluorophores in the dark state, that is except for those in the region surrounding zero-point intensity, whose size reaches sub-diffraction values

and decreases with increasing STED beam intensity [221-224]. STED microscopy provides cellular imaging with resolution down to 20nm [226].

1.5.2.3 Localization microscopy: (STORM: Stochastic Optical Reconstruction Microscopy; PALM: PhotoActivated Localization Microscopy; PAINT: Points Accumulation for Imaging in Nanoscale Topography).

Single-molecule localization microscopy provides fluorescence images of probes with sub-diffraction resolution. In this section I will describe three different localization-based super-resolution microscopy techniques, all of which fundamentally rely on the "blinking" of fluorophores to image and localize single-molecules for super-resolution image reconstruction. These techniques vary in how their fluorophores "blink", either by photoswitching from bright to dark, one excitation/emission wavelength to another, or simply from a bound state to unbound. However, they all exploit the ability to image fluorophores or fluorescent proteins and localize their individual position for subsequent image reconstruction.

Whichever localization-based super-resolution microscopy technique is used, once single molecules can be imaged (Fig 5B), their positions are determined with high precision by finding their center peaks [227, 228]. This is achieved by fitting the observed intensity pattern of single molecules, termed point spread functions (PSF), to a 2D-Gaussian function for which the center becomes an estimate of a molecule's position, referred to as a localization [229] (Fig 5C). The uncertainty in determining the molecule's position, or localization precision, scales with the inverse square root of the number of photons ($1/\sqrt{N}$) emitted by the molecule [214, 227, 230]. The localization precision can be as small as 1nm for bright molecules emitting as much as 1

million photons [228, 231], although due to experimental constraints we are limited to specific organic dyes and achieve resolutions closer to 20-30nm.

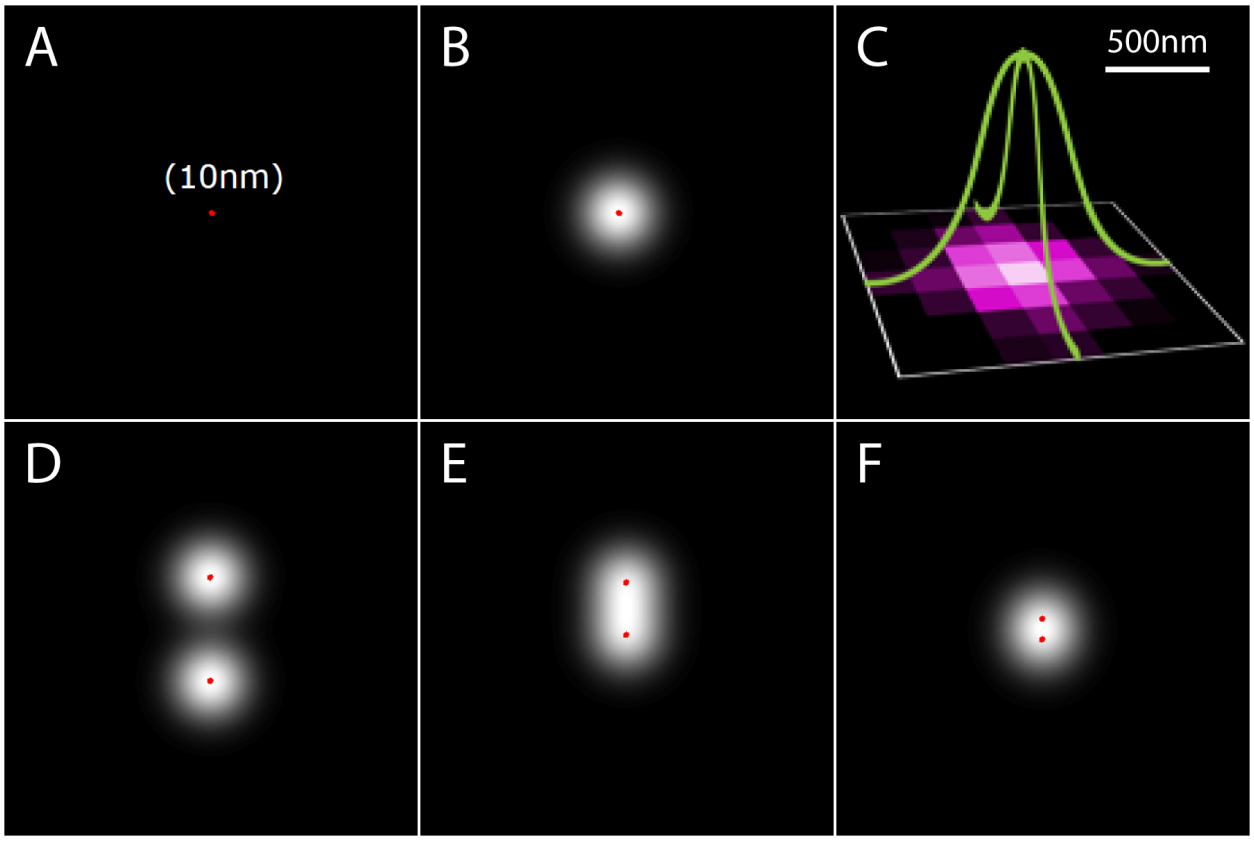

Figure 5: Single Molecule point spread function (PSF)
(A) A 10nm wide single-molecule emits light would be observed as a **(B)** diffraction-limited 250nm blurred spot. **(C)** The point spread function (PSF) corresponds to the intensity profile generated by the diffraction-limited spot using visible light. **(D)** Two single-molecules are resolvable while their PSFs remain separate and identifiable. **(E)** As the single-molecules approach each other, their PSFs overlap and become more difficult to distinguish, **(F)** until it is impossible to distinguish the two probes. Figure adapted from animation provided by Professor Sarah Veatch.

Point accumulation for imaging in nanoscale topography (PAINT) is a localization-based method of imaging that relies on monitoring the interaction of individual diffusing fluorophores in solution with the surface of a substrate [232]. The probes transiently interact with the surface and are immobilized long enough for their PSF to be localized. Thus, a fluorescent signal is only observed when bound to the substrate surface. A key aspect of this approach is the requirement to keep the density of probes at the substrate below 1 molecule/μm^2 for each observation [233]. However, since the flux of probes at the sample is essentially constant over long lengths of time,

acquiring single molecule localizations approaches an incredibly large number and yields highly resolved images [234]. This method has been used to image lipid bilayers, contours of these bilayers, large unilamellar vesicles, and DNA origami [235].

(Direct) stochastic optical reconstruction microscopy (STORM/dSTORM) [236, 237] and (fluorescent) photoactivation localization microscopy (PALM/fPALM) [238] are two additional point-localization based methods and super-resolution microscopy techniques I use for the experiments in this Thesis. STORM and PALM depend on the stochastic blinking and subsequent single-molecule localizations of fluorophores in a sample to produce an image with sub-diffraction resolution. For both STORM and PALM, the fluorophore is stochastically excited such that only a subset of the fluorophores on the samples is emitting a fluorescent signal. The density of probes emitting light is controlled such that spatially distinct single-molecule localizations can be observed and fit by approximation to the PSF. Stochastic excitation of subset of fluorophores is achieved differently for STORM and PALM.

With STORM, the fluorophore is typically an organic dye that is excited into a triplet state which is dark and does not emit energy [239, 240]. This is achieved through the use of high-energy laser power and reducing imaging buffers with oxygen scavenging systems [240]. The removal of oxygen from the system helps prevent the photobleaching of the fluorophores and the conversion of the electrons from their excited state to the dark triplet state [237]. In the dark triplet state, the fluorophore's electrons can photoswitch back and forth between the normal excited state to briefly emits bursts, or blinks of light [239]. This "blinking" is what allows fluorophores that are still imaged with diffraction limited light, to be localized with much greater

certainty than 250nm. Since any observance of a fluorescent emission on an image is now corresponding to a single fluorophore, that 250nm PSF, is be fit to a gaussian function with much greater precision which will result in a resolution higher than 250nm (Fig 6).

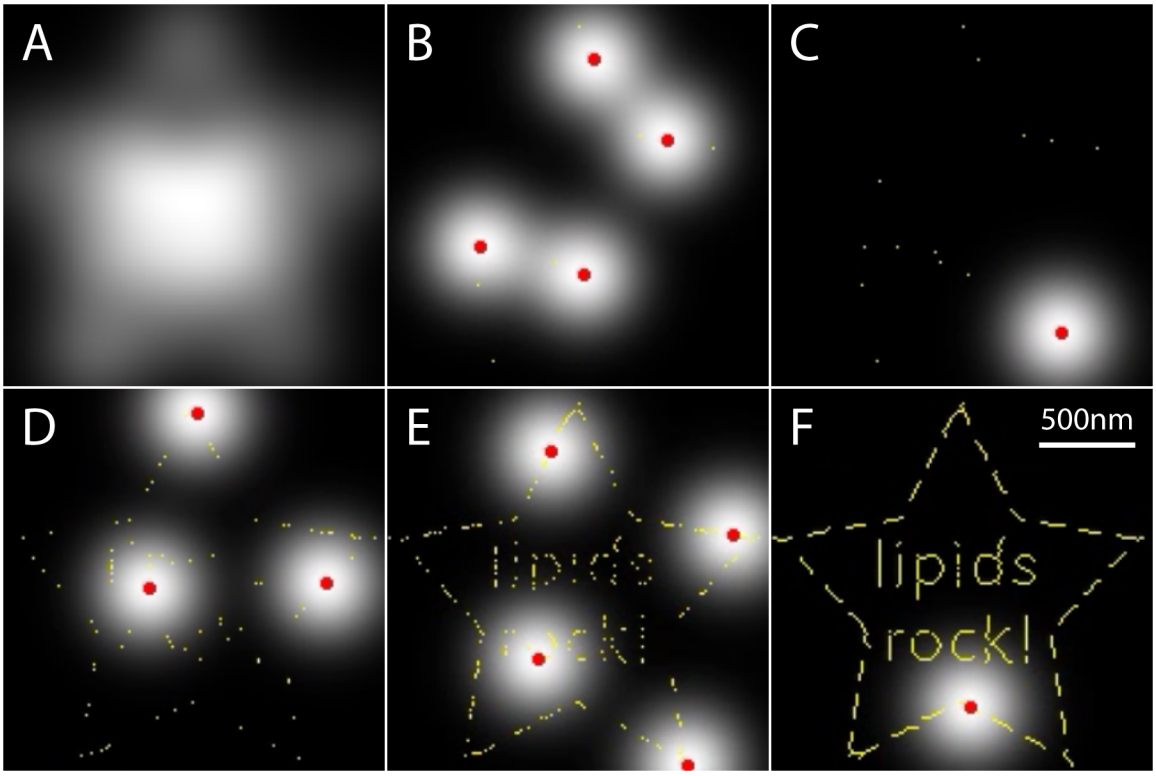

Figure 6: Schematic of 3 localization-based techniques: STORM, PALM, & PAINT
(A) Multiple diffraction-limited single-molecules do not indicate any structure or writing. **(B)** A subset of single-molecules are excited and localized, allowing for their individual PSFs to be distinguished. **(C)-(E)** This process is repeated iteratively across multiple frames, **(F)** until the all of the localizations are super-imposed on a single super-resolved reconstructed image which contains structure and writing not observable through diffraction-limited imaging. Figure adapted from animation provided by Professor Sarah Veatch.

With PALM, the fluorophore is typically a fluorescent protein that is photoactivated from a non-fluorescent conformation, to a fluorescent conformation by means of a second wavelength in addition to the excitation wavelength [241]. The second wavelength is an activating laser beam at low-power that stochastically photoconverts a subset of the fluorophores in the sample such that only those fluorophores will emit light once excited with the excitation beam that is simultaneously illuminating the sample. As the fluorophores emit their photons they photobleach

and return to ground state or revert to the non-fluorescent conformation, waiting to be photoconverted and excited once again [238]. Imaging a subset of the photoconverted fluorophores with PALM is equivalent to the stochastic blinking that is observed with STORM. The photoconversion is the stochastic selection of probes that allows the single-molecule fitting of localizations and improvement of resolution from 250nm to down to 10-30nm [238]. With our imaging set-up, I am able to localize fluorophores within 20-30nm.

1.5.3 BCR structure & function has been studied using super-resolution microscopy techniques.

Super-resolution techniques like STORM have been used to study the organization of the IgM, IgD, and IgG, three of BCR's isotypes, which indicate that BCR organize into clusters preceding antigen engagement and that the type of clustering observed following antigen engagement is specific to the three isotypes [167, 168, 242].

Super-resolution microscopy has also been used to investigate molecular interactions in addition to BCR's organization. For example, studies using STORM have implicated the cytoskeleton in modulating BCR diffusion rates [167, 243]. In fact, a recent study measured the size, density, and distribution of tetraspanin-enriched microdomains on the plasma membrane of B cells using two-color STED microscopy [244]. Two-color simultaneous PALM and STORM have been implemented to measure the direct binding of BCR and Lyn in live cells following antigen stimulation [245]. STORM and PALM were also used to observe the presence of Lo-like domains on the plasma membrane of B cells [50]. 3D-SIM was implemented for the first study of changes in nuclear DNA structure of any disease using super-resolution microscopy

comparing wild type B cell and T cell lymphocytes, Hodgkin cells, and Reed–Sternberg cells [246].

However, an area that requires further investigation in particular is the role of the plasma membrane for BCR signaling. Especially in consideration of the differences that arise depending on the form of antigen presentation, whether soluble or surface presented. While we have presented evidence that Lo-like domains are present and could contribute to the sorting of BCR and regulatory proteins for soluble-based stimulation, the same remains to be answered for surface-presented stimulation.

1.5.4 Challenges in imaging BCR signaling on the plasma membrane.

There are various obstacles to consider when imaging B cell lymphocytes. These include protein labeling, BCR triggering, temporal resolution, and statistics [247]. The BCR signalosome is a crowded environment and B cell signaling is comprised of many membrane-associated proteins [248, 249]. Therefore, studying the role the membrane contributes to BCR signaling requires a large availability of proteins available for study. Immunohistochemistry provides the largest variety of labels, although there are considerations that must be taken into account like the loss of antigenicity due to chemical fixation, or the inability to avoid triggering signaling in live cells simply by labeling with antibody. Fluorescent-tagged proteins offer a good work-around for this issue, however expression efficiency can often be too low for imaging, or so overexpressed that it introduces signaling artifacts. In general, this indicates that labeling of endogenous proteins through immunohistochemistry rather than expressing exogenous ones through transient transfection is preferable. The constraint to consider however is that intracellular proteins are not

readily accessed in intact cells, which restricts labelling to the extracellular regions of cell-surface proteins assuming they don't trigger a cellular response.

The previous paragraph brings up a second obstacle in imaging the role of the plasma membrane in B cells — BCR triggering. A variety of parameters can cause the B cell to begin signaling, most of them involve directly binding the protein labels introduced to the cells [26]. This is an important parameter to consider particularly when designing an experiment given that dynamics and distribution of BCR and Lyn were shown to change following antigen stimulation [245]. The onset of signaling should tightly controlled either through the addition of soluble ligand or through the deposition of cells onto antigen presenting surfaces in order to capture the earliest events in signaling [26]. In order to be able to capture the earliest events following the onset of BCR stimulation, both high temporal and spatial resolutions are required. This third obstacle is often a difficult one to overcome because most imaging modalities often trade one type of resolution for the other [247].

One of the last obstacles in studying the role of the plasma membrane in B cell signaling is sampling statistics. In general, high enough sampling statistics of fluorophore localizations are desired to obtain a super-resolved image that captures as many of the original protein localizations [50]. However, immunohistochemistry only labels a subset of these proteins, and depending on the imaging modality that is implemented, only a subset of the labeled molecules might actually be localized for image reconstruction. That is to say, in an effort to achieve single molecule signals, a lot of molecules are turned off, which affects the sampling statistics of the reconstructed image and quantitative analysis that can be performed. Sampling can be improved

by higher labelling efficiency or higher transfection efficiency, although overexpression still poses a problem.

1.5.5 PALM & STORM provide versatility & high resolution for imaging B cell plasma membranes.

STORM and PALM are point localization based super-resolution microscopy methods that generate highly resolved images by precisely localizing individual photoswitching or photoactivatable fluorophores [238-241, 250]. These methods benefit from a high compatibility with labels for immunohistochemistry or transgenic protein tags. Continually improving optics, fluorophores, lasers, and cameras are continuously pushing the achievable boundary of resolution. Recently there has been significant advancements in camera sensitivity and speed which allow live-cell imaging of BCR and membrane dynamics at reasonable resolutions [245, 251]. An obstacle we often encounter with this method of imaging is over-counting of fluorophores such that the reversible photoactivation of fluorophores will skew point-based localizations in appearing clustered [252]. While a method has been presented for filtering the over-counting effect from images, it is not always reliable [139]. Achieving a high precision of localization of probe requires that a large number of photons are emitted and acquired per frame [214]. Recent advancements in stable fluorescent probe development have produced very bright, spectrally separated fluorophores that work well in STORM/PALM live cell experiments.

I study the B cell plasma membrane with PALM and STORM because it offers a wide set of protein targets for labeling, live cell imaging capabilities, and high resolutions for the interactions I am studying. The largest obstacle remains being the sampling statistics of labeling,

particularly for fixed-cell experiments. In order to account for the low-sampling statistics of my single-measurements, I typically acquire large sample sizes. It should be noted that in this set of experiments I primarily perform STORM and PALM of fixed cell samples, the reagents and methods used allow the possibility of expanding these measurements to live-cell experiments in the future.

1.6 – Current studies and Thesis outline:

The experiments described in this Thesis use super-resolution microscopy to explore differences in Lo-like domain structure and adaptor protein sorting in response to changes in clustering size, antigen presentation, and ambient temperature. This work is motivated by the recent observations of order-like domains stabilization on the B cell membranes [50] and the increasing implications of membrane composition in biological signaling [39-42] and diseased states [101, 145-152, 253].

In Chapter 2, two-color super-resolution localization microscopy is used to measure the concentration of phase markers and adaptor proteins in BCR clusters in the context of surface-presented antigen. The goal of this Chapter is to identify a role for membrane Lo-like domains in BCR activation when antigen is presented on a supported lipid bilayer. I find that BCR clustering through surface-presented antigen stabilizes robust Lo-like domains. I measure enhance sorting of two key regulators that correlates with higher levels of phospho-Tyrosine activity in surface-presented samples. From my results I conclude that the more robust Lo-like domain stabilization elicits a higher response from B cells in surface-presented samples compared to soluble ones. I also measure the relative energetic contribution the membrane imparts to sorting of CD45 at

BCR in response to surface presented stimulation. I find CD45's sorting in surface-presented samples is due to the membrane in addition to other contributions not measured in soluble stimulated samples. I present my ideas on where those contributions could come from.

In Chapter 3, two-color super-resolution microscopy is used to measure the concentration of phase markers in CTxB clusters on B cell membranes. The goal of this Chapter is to identify if CTxB, a clustering structure separate from the BCR signaling apparatus, is also capable of stabilizing Lo-like domains on the membrane of B cells. I find that clusters of CTxB formed with both soluble and bilayer-loaded streptavidin on the membranes of B cells stabilize Lo-like domains using similar methods to Chapter 2. These Lo-like domains are more robust, greater in size and exhibit enhanced sorting strength of phase markers when the clustering structure, CTxB in this case, is formed using a supported-lipid bilayer. My results indicate that the size and strength of sorting of Lo-like membrane domains are parameters that both scale with the size of the CTxB clusters. Lastly, I find that sorting of the disordered phase marker was enhanced at 4°C. I present my ideas on how these results could couple to possible mechanisms cells use to modulate the Lo-like domain structure and function on their own plasma membranes.

In Chapter 4, I summarize my results and place them in the context of the larger field. I also discuss the new measurements that this work motivates, and its implications for human health.

Chapter 2: B Cell Receptor Clusters Activated by Surface Presented Antigen Are Robust Ordered Phase-Like Domains

*This Chapter is reproduced from a submitted manuscript: Núñez, M.F., and Veatch, S.L. 2019. "B cell receptor clusters activated by surface presented antigen are robust ordered phase-like domains." Frontiers in immunobiology.[50]

MFN contributed to the data acquisition and analysis, writing of the original draft and editing. SLV contributed to the conceptualization of the project, data analysis and analytical method development, supervision, writing of the original draft, and editing.

2.1 – Overview:

B cells are responsible for reacting to broad stimuli from other cells and within the environment [2, 254, 255]. These signals are often initiated through the clustering of cell surface receptors and co-receptors by extracellular ligands and result in cellular level responses such as the release of cytokines, processing and presentation of antigen peptides to T cells, differentiation, clonal expansion, apoptosis, or combinations of these outcomes [9, 256-258]. Signaling through the highly expressed B cell receptor (BCR) occurs when the BCR encounters natural antigens, multivalent artificial antigens, or monovalent artificial antigens bound to surfaces [259]. Often times, BCR binding to ligands acts to cluster BCRs on the cell surface, initiating a signaling cascade that results in phosphorylation of BCR immunoreceptor tyrosine activation motifs (ITAM) by the Src family kinase Lyn [26, 35]. Once phosphorylated, the ITAM regions become sites of docking for other signaling mediators, such as Syk, that propagate the cellular-level immune response.

While many structural and functional consequences of receptor clustering in B cells are well characterized, mechanisms describing how BCR clustering leads to the robust phosphorylation of

BCR ITAMs remains an open topic of active debate. One proposed mechanism is that receptor clustering leads to receptor partitioning with ordered membrane domains sometimes referred to as lipid rafts. Once sequestered in these domains regulators of BCR signaling, such as Lyn and CD45, are sorted to facilitate ITAM phosphorylation. These studies are supported by a large quantity of past observations using detergent extraction [260, 261], FRET imaging [131, 132], and our recent study that utilized super-resolution fluorescence localization microscopy [50]. Other authors have proposed that engagement with surface presented antigens leads to receptor clustering and activation through the formation of a tight contact between the B cell plasma membrane and a surface, in a way that excludes membrane proteins with bulky ectodomains, such as phosphatases[175, 262]. In this model, lowering the concentration of phosphatases proximal to BCRs also favors ITAM phosphorylation. Yet other mechanisms have been proposed for BCR engaged with natural ligand, where conformational changes increase the accessibility of BCR ITAMs to kinases, facilitating their activation[206]. These proposed mechanisms are not mutually exclusive and may work in concert to initiate B cell responses. It is also possible that specific mechanisms dominate under specific stimulation conditions, enabling the flexibility of B cells to respond to a diverse repertoire of antigens. Although B cells engage both soluble and membrane-anchored- antigen *in vivo* [190], studies suggest that surface-presented antigen may constitute the dominant form of antigen-dependent BCR stimulation [188, 191-195].

Plasma membranes isolated from B cells and other cell types separate into coexisting liquid-ordered and liquid-disordered phases at low temperature [97, 121, 263]. Liquid phase domains present in isolated plasma membrane vesicles are macroscopic and have different lipid and

protein compositions. In particular, saturated lipids and palmitoylated proteins are enriched in the liquid-ordered phase, while single-pass transmembrane proteins that lack palmitoylation sites are enriched in the liquid-disordered phase [264, 265]. Intact B cell plasma membranes do not phase separate, but are predicted to contain domains resembling phases that are small and dynamic. Our past work demonstrated that domains resembling ordered or disordered phases could be stabilized in B cell membranes by cross-linking membrane proteins or peptides with soluble multivalent antigen, and that cross-linked BCR clusters have local environments that resemble ordered phase domains [50]. In that case, we found that the sorting of Lyn and CD45 based simply on their interactions with membrane domains was sufficient to initiate receptor activation upon clustering with multivalent soluble antigen. The goal of the current study is to identify a role for membrane domains in BCR activation when antigen is presented on a supported membrane.

In this study, I compare the membrane contribution to B cell signaling in samples stimulated with soluble or with surface-presented antigen using the same cell line, reagents, and probes characterized in our previous study. I use streptavidin to cluster biotinylated $f(Ab)_1$ fragments reactive against the Fcμ domain of mouse IgM as an artificial BCR antigen. In order to mimic the surface-bound antigen presentation that occurs *in vivo* streptavidin is presented to BCR on a supported-lipid bilayer. I acquire super-resolution images of fluorescently labeled proteins and peptides alongside BCR on the B cell surface and perform a cross-correlation analysis to quantify the sorting of phase-like markers and signaling regulators with respect to clusters of BCR. I find that BCR clusters engaged with surface presented robustly sort peptide markers of membrane phases. These domains, along with additional interactions, determine the local

concentration of CD45 and Lyn and likely other signaling molecules involved in initiating a cellular level immune response. Overall, I conclude that multiple interaction modalities likely combine to BCR activation when engaged with surface presented antigens.

2.2 – Materials and methods

2.2.1 Antibodies modification

For B cell receptor detection, CH27 B cells were labeled with a biotinylated and fluorescently conjugated $f(Ab)_1$ fragment against IgM. The biotinylation and fluorophore conjugation of the Goat $f(Ab)_1$ anti-Mouse IgM (Jackson ImmunoResearch Labs Cat# 115-007-020, RRID:AB_2338477) antibody are done simultaneously. 2.25µL of 15 mM amine reactive biotin-X, SE (Invitrogen: B1582) and 0.45µL of 10mM NHS-Ester Atto655 (Millipore-Sigma: 76245) were mixed with 150µL of 1.3mg/mL of the $f(Ab)_1$ fragment at pH 8.5 and rotated for 1 hour at room temperature in an aqueous solution buffered by 0.01M NaH_2PO_4 with 0.01M NaH_2CO_3. After incubation, the modified $f(Ab)_1$ fragment was purified and separated from unbound dye through a gel filtration column (GE Healthcare illustra NAP Columns from Fisher: 45-000-151) in 1X-PBS+1mM-EDTA. The modified antibody was further purified by centrifugation in a Vivaspin-500 Polyethersulfone concentration spin column with a 30kDa cutoff (Vivaspin: VS0121). The modified antibody was then conjugated to additional NHS-Ester Atto655 a second time by mixing 0.4µL of 10mM of the NHS-Ester Atto655 with the modified antibody at room temperature in pH 8.5 for 1 hour. The antibody was purified through the gel column and spin column again before its optical spectrum was obtained to estimate degree of label (~ 3 dye/antibody).

For PhosphoTyrosine detection, chemically fixed cells were permeabilized in 0.1% Triton X 100 then labeled with anti-phosphotyrosine 4G10 Platinum mouse monoclonal antibody of the IgG2b subclass (Millipore Cat# 05-1050, RRID:AB_916371). The primary antibody was detected using a secondary goat anti mouse IgG Fcγ subclass 2b antibody (Jackson ImmunoResearch Labs Cat# 115-005-207, RRID:AB_2338463) . The secondary antibody was conjugated to Alexa Fluor 532 using methods described for the $f(Ab)_1$-Atto655 and biotin modification described above.

For CD45 detection, chemically fixed CH27 B cells were incubated with anti-mouse CD45R (B220) primary antibody clone RA3-6B2 conjugated directly to Alexa 532 (Thermo Fisher Scientific Cat# 14-0452-81, RRID:AB_467253) .

2.2.2 DNA constructs

The plasmids used for this study were used and described previously [50]. Briefly, Lyn-eGFP and PM-eGFP plasmids [129] were gifts from Barbra Baird and David Holowka (Cornell University, Ithaca, NY) and were cloned using standard techniques to replace eGFP with mEos3.2. Plasmid DNA encoding mEos39.2 protein and YFP-TM were gifts from Akira Ono (University of Michigan, Ann Arbor, MI). The YPF-TM plasmid encodes the transmembrane domain of LAT (Linker for Activation of T-cells) fused to the YFP such that the fluorescent protein is on the extracellular side of the cell. This plasmid was cloned using standard techniques to replace YFP with mEos3.2. The mEos3.2 tagged constructs used here are in Clontech N1 plasmid vector background (Clontech, Mountain View, CA).

2.2.3 Cell culture and plasmid transfection

CH27 mouse B-cells (Millipore Cat# SCC115, RRID:CVCL_7178), a lymphoma-derived cell line [266], used in the soluble and surface-presented experiments, were acquired from Neetu Gupta (Cleveland Clinic). Cells were maintained in culture as previously described [245]. CH27 cells were transiently transfected by Lonza Nucleofector electroporation (Lonza, Basel, Switzerland) with electroporation program CA-137. Typically, 10^6 CH27 cells were transfected with 1.0 mg of plasmid DNA. For soluble measurements, transfected cells were grown on glass-bottom Mattek petri dishes overnight for next-day sample preparation. For surface-presented measurements, transfected cells were grown overnight in T-25 cell culture flask with filter caps in 5mL of growth media. The following day, the transfected cells were harvested and pelleted at 500g for 5 minutes before being labeled for sample preparation.

2.2.4 Flow chamber and supported lipid bilayer assembly

Large Unilamellar Vesicles (LUVs) were formed through extrusion. First, a 3mg lipid mixture of 99.5 mol% DOPC (Avanti, 850375C) and 0.5% mol% Biotinyl-DOPE (Avanti, 870273C) in Chloroform was dried with N_2 while being vortexed in a clean glass tube. The dry lipid film deposited along the glass tube was further dried in vacuum for 30 minutes before water hydration. The resulting MultiLamellar Vesicles (MLVs) were subjected to 10 freeze-thaw cycles. Finally LUVs were obtained by extruding the MLVs 30 times with a mini-extruder (Avanti, 610000) using 10mm diameter filters (Whatman Drain Disc, 230300) and a membrane of 0.1μm pore-size (Whatman Nucleopore Track-Etched Membrane, 800309). The LUVs were stored at 4°C and used within 2 weeks.

Each individual flow chamber was assembled in lab the day of the experiment. First, a 25x75x1mm plain microscope slide (Fisherbrand, 12-550D) and no. 1.5 22x22mm glass coverslip (Fisherbrand, 12-541B) were rinsed with water, dried with N_2, rinsed with ethanol, dried with N_2 again, and finally rinsed with chloroform before being dried with N_2 one last time. The microscope slide and coverslip were plasma cleaned for 5 minutes using a basic plasma cleaner (Harrick Plasma, PDC-32G). Once finished, 2 strips of PARAFILM were cut into 1 x 2.5 cm and placed on top of the microscope slide. The PARAFILM strips were placed in the middle of the microscope slide with 1 cm of space between them. The coverslip was placed on top of the PARAFILM, and the entire flow chamber was placed on a hot plate at 100C until the PARAFILM had melted and sealed the slide and coverslip together. PBS was introduced into the chamber to prime the volume of the chamber and ensure no air bubbles.

Supported lipid bilayers were fused from LUVs. 60µL of the LUV mixture was introduced to the flow chamber and incubated at room temperature for 30 minutes, then washed with PBS and incubated for 1 hour at room temperature to allow the bilayer to equilibrate. Next, 200µL of a 1µg/mL streptavidin solution was introduced to the flow chamber and incubated for 10 minutes at room temperature. The flow chamber was then washed with 1mL of Tyrode's buffer (NaCl 15.0 mM, KCl 5.0 mM, $CaCl_2$ 1.8 mM, $MgCl_2$ 1.0 mM, Glucose 6.0 mM, 20mM HEPES, pH 7.4) to remove unbound streptavidin as well as to exchange the buffer in the chamber for live-cell attachment and stimulation. The final assembled flow chamber and supported lipid bilayer were used the same day they were assembled.

2.2.5 Labeling and sample preparation

For BCR labeling and stimulation of surface-presented antigen measurements, live CH27 cells in suspension were pelleted at 500g for 5 minutes at 4°C then incubated on ice for 10 minutes with 5µg/mL of anti IgM $f(Ab)_1$ modified with biotin and Atto655 in the Tyrode's buffer defined above. Cells were washed twice through centrifugation at 500g for 5 minutes at 4°C and ultimately suspended in room temperature Tyrode's buffer. The receptor was clustered by introducing labeled B cells into the flow chamber containing a streptavidin-loaded bilayer. Cells incubated on the bilayer for 5 minutes in Tyrode's buffer at room temperature prior to fixation. For BCR labeling and stimulation of soluble antigen measurements, B cells were plated on Mattek round glass-bottom petri dishes and labeled with 5µg/mL anti IgM $f(Ab)_1$ fragment modified with biotin and Atto655. Cells were incubated for 10 minutes at room temperature, washed with Tyrode's buffer, and incubated with 1µg/mL streptavidin in Tyrode's buffer for 5 minutes at room temperature.

Cells were chemically fixed in 2% paraformaldehyde (PFA), 0.15% Glutaraldehyde, solubilized in 0.5X PBS. For bilayer stimulated samples, fixative was introduced to the flow chamber containing CH27 B cells and incubated for 20 minutes at room temperature. For cells stimulated with soluble antigen, the same fixative was added directly to the petri dish containing the cells. In both cases, fixation was quenched by incubating with PBS containing 3% BSA for 20 minutes at room temperature.

For CD45 detection, cells were incubated with 1µg/mL CD45-AF532 in block buffer (3% BSA, 3% Fish Gelatin in 1X-PBS) for 2 hours at room temperature. Cells were washed extensively

with PBS to remove unbound antibody. Phosphotyrosine labeling was accomplished after blocking and cell permeabilization with 0.1% Triton-100X in block buffer (5% Fish Gelatin, 5% BSA, PBS) for 20 minutes at room temperature. Samples were washed with block buffer then incubated with a 1:1000 dilution of 4G10 Platinum, anti-phosphotyrosine antibody (Millipore-Sigma: 05-1050) in block buffer for 1 hour at room temperature. Samples were washed with PBS to remove unbound primary antibody before incubating with the fluorescently labeled secondary antibody. Cells were incubated with 0.2μg/mL of goat anti mouse IgG Fcγ subclass 2b antibody conjugated to Alexa Fluor 532 (~5 dye/protein) in block buffer for 1 hour at room temperature. Samples were washed extensively with PBS to remove unbound secondary antibody.

2.2.6 Imaging

Samples labeled with BCR-Atto 655 and mEos3.2 were imaged in a buffer found to be optimal for Fluorescence Localization Microscopy with these probes: 30 mM Tris, 9 mg/ml glucose, 100 mM NaCl, 5 mM KCl, 1 mM KCl, 1 mM $MgCl_2$, 1.8 mM $CaCl_2$, 10 mM glutathione, 8 mg/ml catalase, 100 mg/ml glucose oxidase, pH 8.5 [50]. CD45 and phosphotyrosine samples were labeled with BCR-Atto 655 and CD45-Alexa 532 or 4G10::IgG2b-AF432 and imaged in a buffer more suitable for the dye pair [50, 240]: 50 mM Tris, 100 mg/mL glucose, 10 mM NaCl, 100 mM 2-mercaptoethanol, 50 mg/ml glucose oxidase, 200 mg/ml catalase, pH 8.

Imaging was performed using an Olympus IX81-XDC inverted microscope. TIRF laser angles where achieved using a cellTIRF module, a 100X UAPO TIRF objective (NA = 1.49), and active Z-drift correction (ZDC) (Olympus America) as described previously [50, 245, 267]. Images were acquired on an iXon-897 EMCCD camera (Andor) with an exposure time of 20

milliseconds. Atto 655 was excited using a 647 nm solid state laser (OBIS, 100 mW, Coherent). Photoactivation of mEos3.2 was accomplished with a 405 nm diode laser (CUBE 405-50FP, Coherent) and simultaneously excited with a 561 nm solid state laser (Sapphire 561 LP, Coherent). Alexa 532 was excited using a 532 nm diode-pumped solid-state laser (Samba 532–150 CW, Cobolt). Laser intensities were adjusted such that single fluorophores could be distinguished in individual frames, and were generally between 5 kW/cm2 and 20 kW/cm2. Atto655 and mEos3.2 excitation and emission was filtered using a LF405/488/561/647 quadband cube (TRF89902, Chroma, Bellows Falls, VT). Atto655 and Alexa532 excitation and emission was filtered using a 405/488/532/647 quadband cube (Chroma, Bellows Falls, VT). Emission was split into two channels using a DV2 emission splitting system (Photometrics) with a T640lpxr dichroic mirror to separate emission: ET605/52m to filter near-red emission, and ET700/75m to filter far-red emission (Chroma).

Diffraction-limited fluorescent images of BCR- and pTyr-labeled cells were obtained using a 100X oil-immersion objective under the same excitation and camera gain imaging conditions using the microscope system described above. Images of cells in each color were acquired in TIR simultaneously to report on the probe intensity specifically at the bottom membrane of the cells.

2.2.7 STORM image reconstruction

Candidate finding for single-molecule fitting was accomplished by fitting the intensity profile of local maxima in background subtracted and wavelet filtered images using 2-D Gaussian functions as described previously [50]. Once candidates were fit and localized, they were culled to remove outliers based on size ratio, intensity, and localization error for each color using

software described previously [252]. The near-red channel was overlaid onto the far-red channel using an image transform matrix calculated from fiducial bead marker images obtained during each experiment. The images were aligned to account for stage drift which resulted in the final reconstructed STORM image from the culled, transformed, and aligned localizations. Final image resolution was calculated for each color using previously described methods [252].

2.2.8 Correlation analysis and comparison

Auto-correlation and Cross-correlation functions were tabulated from masked, reconstructed super-resolution images using previously described methods [50, 139, 245, 252]. Errors in single cell measurements as a function of radius are estimated by quantifying the variance in the cross-correlation function as a function of angle at fixed radius and correcting for the finite localization precision of the measurement [50]. Average cross-correlation functions are obtained through a simple average over single cell measurements, and errors presented on average curves represent the standard error of the mean. The PMF is calculated to be PMF = -kBTln(C(r)), and errors on these curves are propagated from the errors in C(r) (dC(r)) as dPMF = dC(r)/C(r).

In some figures, properties of correlation functions are extracted through fitting to an exponential function, 1+Aexp(-r/ro), using the lsqcurvefit function in Matlab. Here A+1 corresponds to the extrapolated amplitude of the correlation function at r=0 and r_o represents the characteristic length-scale of the correlations.

2.2.9 Diffraction-limited BCR and phosphotyrosine fluorescence histograms

Images corresponding to the two emission channels were overlaid with the aid of images of fiducial beads. Cell footprints were identified and masked by hand, and image intensities were corrected to account for the camera offset. Intensities were recorded for pixels within masks and the average intensity per cell footprint was tabulated. Histograms were constructed from the average values as well as the individual pixel values, where each pixel was considered an independent measurement.

2.2.10 Simulations of component partitioning into domains

A binary map of domains was constructed by randomly placing circles of fixed radius (12 pixels) on a 256 by 256 pixel grid using periodic boundary conditions. This binary map was then used to define the probability distribution that a component would be present at a given location in space, where different probabilities were assigned to positions within and outside of binary domains. This scheme was implemented by randomly selecting a pixel, and accepting placement of a component at that pixel based by comparing the probability associated with that pixel to a uniform random number distributed between 0 and 1. Roughly 200,000 components were placed in each of the images shown, which corresponds to an average occupancy of 3 components per pixel over the entire image. Cross-correlation functions were then tabulated between the binary mask and the image of placed components. All analyses were carried out in MATLAB.

2.3 – Results:

2.3.1 BCR engagement with bilayer presented antigen results in the sorting of minimal peptides that mark ordered and disordered membrane domains.

I monitored the recruitment and exclusion of phase-marking minimal peptides with respect to BCR clusters engaged with bilayer-presented streptavidin using methods similar to those I used previously for soluble streptavidin [50]. Briefly, CH27 B cells transiently expressing one of two minimal phase marking peptides were labeled with anti-IgM $f(Ab)_1$ conjugated to both biotin and the organic fluorophore Atto655. The minimal peptides used in this study were chosen because they partition strongly into liquid-ordered (PM) or liquid-disordered (TM) phases in isolated plasma membrane vesicles, and because they differentially partition into ordered and disordered phase-like domains in intact B cells. PM is the minimal anchor motif of Lyn kinase which is post-translationally modified with myristoyl and palmitoyl acylations, whereas TM is the transmembrane anchor helix of LAT with palmitoylation modifications removed via mutation. Cells were activated by allowing them to settle on a bilayer containing biotinylated lipids coupled to streptavidin, which acts as a model high affinity multivalent antigen (Fig 7A). Streptavidin mobility was verified in parallel measurements using fluorescently labeled streptavidin (Fig 8). Samples were prepared in a simple flow-chamber to facilitate fast settling of cells onto the bilayer surface. Under these conditions, BCR labeled B cells attached and began clustering within 1 minute of being loaded into flow chambers, and calcium mobilization occurred within seconds of cells settling onto membranes, as indicated by monitoring the intensity of Fluo-4 pre-loaded into cells (Fig 9). Cells were chemically fixed 5 minutes after

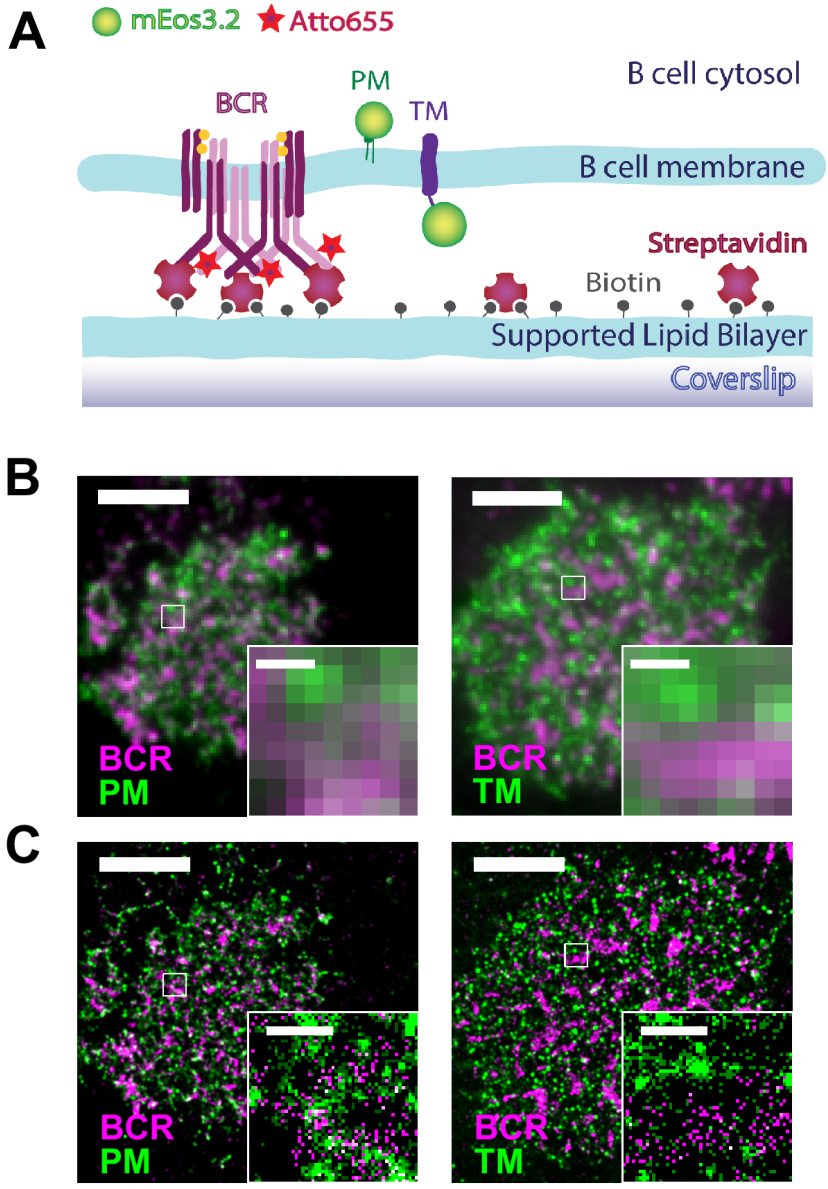

Figure 7: Surface stimulation of IgM BCR in CH27 cells

(A) Schematic of experimental setup of supported bilayer containing biotinylated lipids bound to mobile streptavidin acts as our model antigen. CH27 B cells expressing the IgM isoform of the BCR are pre-bound to anti μ f(Ab)1 antibodies conjugated to both biotin and the organic fluorophore Atto 655. When cells come into contact with the supported bilayer, f(Ab)s bound to the BCR engage with streptavidin leading to BCR clustering and B cell activation. **(B)** Diffraction limited images showing BCR (magenta) and one of two membrane anchored peptides (PM or TM, green). Images are generated by averaging over single molecule measurements as described in Methods. **(C)** Reconstructed super-resolved images generated from the same data shown in B. Scale-bars in B,C are 5μm in the main images and 500nm in the insets.

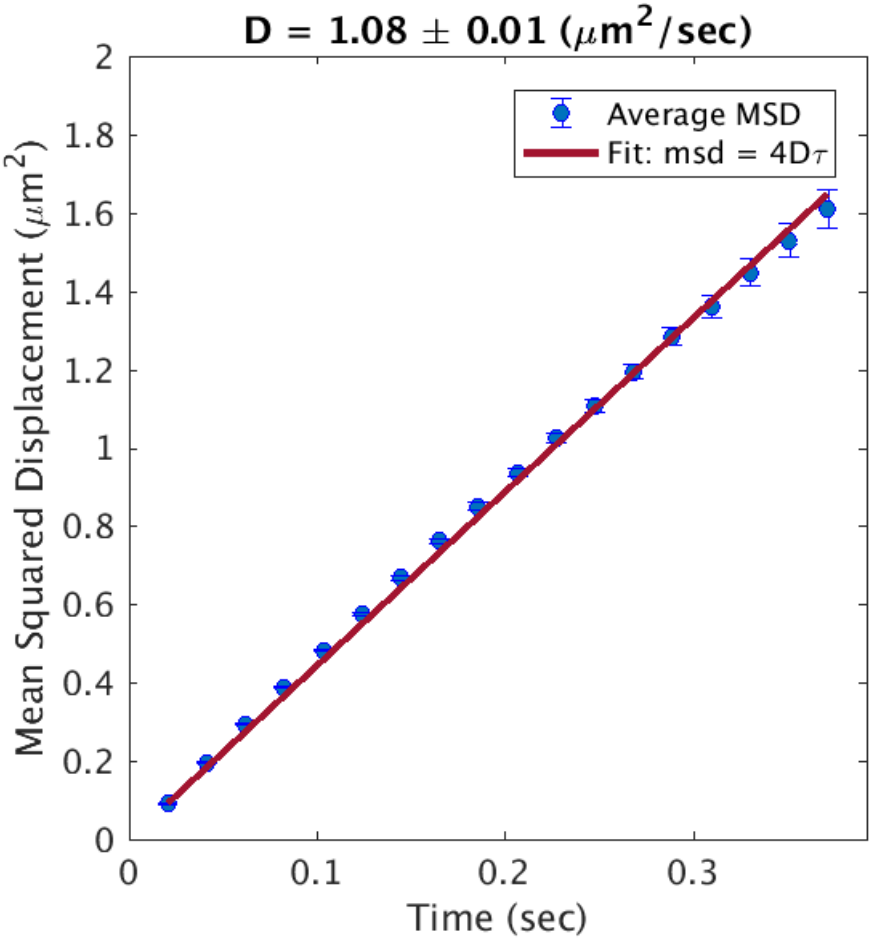

Figure 8: Streptavidin is mobile on supported lipid

Streptravidin-Alexa Fluor 647 fluorescence was tracked when loaded onto a supported lipid bilayer fused from large Unilamellar vesicles comprised of 99.5mol% DOPC and 0.5mol% biotinyl-cap-DOPE. The mean squared displacement of each single-molecule track was averaged by hundreds of localized probe tracks across 10 movies. Averaged streptavidin-AF647 MSD curve is presented with the standard error of the mean (blue). The diffusion coefficient of streptavidin was estimated by fitting the averaged MSD to a line (red) with slope = 4Dτ and a y-intercept fixed at 0. Streptavidin has a diffusion coefficient of 1.08 μm^2/sec, which is on the order of the diffusion coefficient of a mobile lipid in a bilayer and indicate that the antigen is mobile on the bilayers fused in our flow chambers.

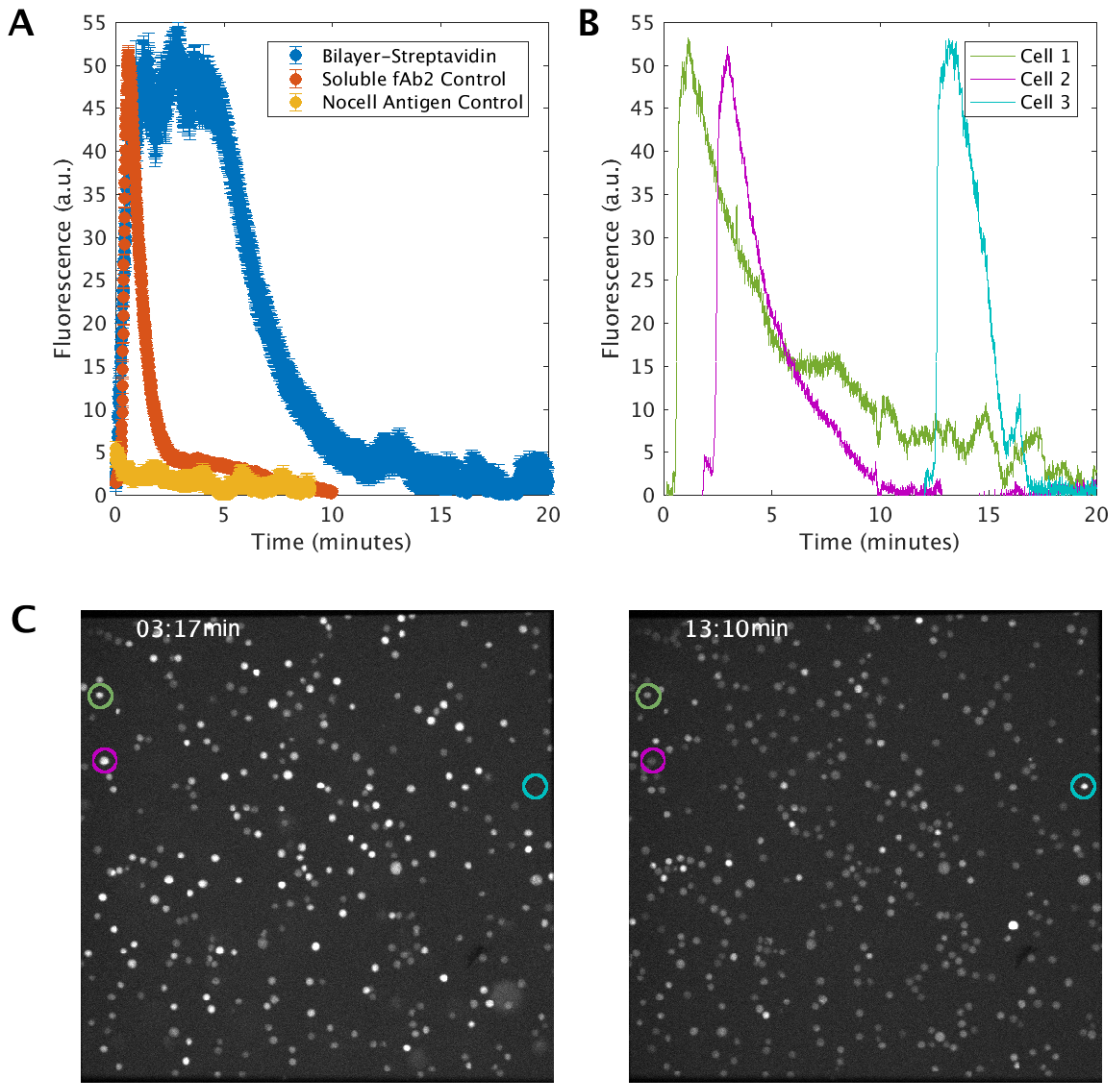

Figure 9: Ca2+ response of CH27 B cells occurs shortly after encountering mobile streptavidin loaded on a supported lipid bilayer

(A) Fluo-4 labeled CH27 cells were introduced to a supported bilayer. The Ca^{2+} response is proportional to Fluo-4 fluorescence intensity and measured for B cells stimulated with streptavidin-loaded bilayer, with soluble $f(Ab)_2$, or not stimulated at all. The last measurement consisted of observing the Fluo-4 loaded B cells landing on clean (no antigen) glass. The fluorescent time traces for hundreds of Fluo-4 loaded cells were measured and used to report the average Ca^{2+} response. The average Ca^{2+} response of B cells introduced to a streptavidin-loaded bilayer (blue) was typical in its onset (rapid), amplitude (large), but its duration was abnormal (broad). **(B)** Single-cells exhibit a typical Ca^{2+} response although the onset of which is not synchronized **(C)** B cell Fluo-4 intensity at two time points after cell deposition on streptavidin-loaded bilayer. The three curves in B correspond highlighted cells. These bilayers were fused in a petri dish which introduced a much larger volume and asynchrony for t=0 at the onset of landing and stimulation for cells compared to the bilayers fused in flow chambers. In flow chambers, I observe BCR begins clustering under a minute, however I cannot acquire images prior, during, or immediately after cell introduction to the flow chamber due to mechanistic limitations.

loading into the flow chamber, then mEos3.2 and Atto655 labels were imaged simultaneously under conditions that allowed for stochastic blinking to obtain single molecule localizations. At least 10,000 images were acquired and averaged to generate the representative diffraction limited images of PM and TM expressing cells shown in Fig 7B. Single molecules were also localized from each image frame as described in Materials and Methods and used to reconstruct the representative super-resolution images shown in Fig 7C.

Diffraction limited and super-resolved images indicate that BCR organizes into non-circular domains at the cell surface, in good agreement with previous studies that use similar activation conditions and image with diffraction limited microscopy [188, 268, 269]. In contrast, both PM and TM peptides appear more uniformly distributed in both diffraction limited and reconstructed super-resolved images. Often, PM and TM peptides appear as small puncta in reconstructed super-resolution images. These tight puncta in the mEos3.2 channel are most likely a consequence of observing the same mEos3.2 fluorophore multiple times over the course of imaging. This over-counting effect is a common feature many super-resolution localization measurements and does not indicate that peptides are themselves organized into clusters [252].

Co-distributions of BCR with minimal peptides were quantified using pair cross-correlation functions, C(r), which are tabulated as described in Materials and Methods. The cross-correlation function reports the relative density of localizations of one color probe a distance r from the average probe of the other color within a specified region of interest. C(r) is normalized so that values greater than 1 indicate co-clustering, values less than 1 indicate depletion, and values equal to 1 indicates a random co-distribution within the specified error bounds. Cross-

correlation functions are tabulated for individual cells, and curves obtained from the images shown in Fig 7C are shown in Fig 10A. For single cells, error bounds are estimated from the angular average of C(r) and the measured localization precision of localizations [50]. The cross-correlations shown in Fig 10B are obtained by averaging curves tabulated for 31 individual cells expressing PM and 19 expressing TM. The reported error bounds represent the standard deviation of this mean.

Both the single cell measurements in Fig 10A and the average cross-correlation functions in Fig 10B indicate that PM is robustly enriched and TM is robustly depleted from BCR clusters. The average cross-correlation curve between BCR and PM has a maximum of $C(r)=1.31\pm0.04$ for $r<25$nm, indicating that the average concentration of PM is roughly 30% higher within BCR clusters than in the membrane overall. In contrast, the average cross-correlation curve between BCR and TM has a minimum of $C(r)=0.80\pm0.04$ for $r<25$nm, indicating that the concentration of TM is 20% lower in BCR clusters than in the membrane as a whole. Since the minimal peptides PM and TM are not known to exhibit direct interactions with proteins, I conclude that their sorting behavior arises from their interactions with membranes and that BCR clusters are ordered membrane domains.

Interestingly, the range of correlations between BCR and PM extends to larger separation distances ($r_o=210\pm20$nm) than the range of anti-correlation between BCR and TM ($r_o=150\pm30$nm), where r_o is obtained by fitting cross-correlation functions to an exponential of the form $C(r) = 1+Aexp(-r/r_o)$. Both of these values are larger than the size of BCR clusters themselves ($r_o=130\pm10$nm) obtained by fitting the BCR auto-correlation function, G(r), to the same exponential function, $G(r) = 1+Aexp(-r/r_o)$. Unlike cross-correlation functions, auto-

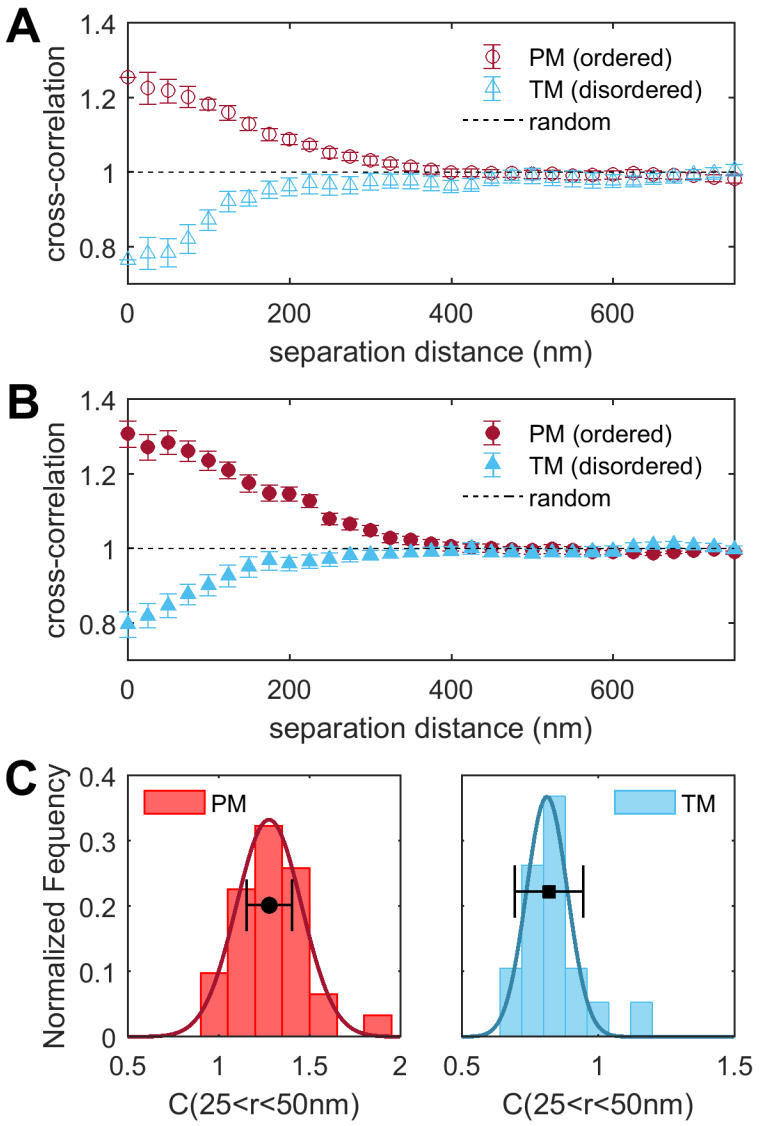

Figure 10: Colocalization of BCR clusters and minimal peptide markers of ordered and disordered domains

(A) Cross-correlation functions tabulated from the reconstructed images shown in Fig 7C. Curves are normalized so that values of 1 indicate a random co-distribution, values greater than 1 indicate colocalization, and values less than one indicate exclusion. Error bars are estimated from the counting statistics of the images themselves as described in methods. **(B)** Cross-correlation functions determined by averaging over >30 cells for each peptide. Error bars represent the standard error of the mean. **(C)** Histograms showing the value of C(r) in individual cells for the point corresponding to 25<r<50nm. Also shown is the mean ± the average error extracted from single cell measurements for the same point. For PM, the distribution is wider than the average single cell errors, indicating that some variation can be attributed to cellular factors. For TM, the distribution falls within single cell errors, indicating that the variance arises primarily from counting statistics.

correlation functions are impacted by the over-counting of individual labeled molecules, which results in these functions having elevated amplitude at short radii. This will tend to decrease estimates of cluster sizes evaluated by the simple fitting procedure described above, therefore I take this value to represent a lower limit of the average BCR domain size. Overall, this analysis indicates that TM depletion extends to or slightly beyond the boundary of clustered BCR domains whereas PM enrichment extends well beyond the boundary of BCR domains.

Fig 10C displays the statistical variation of cross-correlation amplitudes between cells expressing either PM or TM peptides, along with the variance expected based on errors extracted from single cell measurements (black horizontal error bars). The magnitude of errors in single cells strongly dependent on the surface expression level of peptides in this measurement (typically 1-10 peptides per μm^2) [270]). For PM, the observed cell-to-cell variation exceeds that expected from single cell measurements, indicating that cellular factors are likely contributing in some way to the observed variance. In contrast, the observed cell-to-cell variation for TM is well described by the variance associated with single cell measurements alone.

2.3.2 Surface presentation of antigen results in more robust BCR clustering and peptide sorting as compared to soluble antigen.

Fig 11 compares peptide recruitment and depletion with respect to BCR clusters formed through engagement with surface presented and soluble antigens. Fig 11A shows reconstructed images of CH27 B cells expressing either PM or TM engaged with streptavidin antigen either presented on the surface of a supported bilayer or in solution. One striking difference between these two sample preparation methods is the size of the resulting BCR clusters. When streptavidin is

presented on a lipid bilayer, BCR clusters are extended and non-circular, whereas BCR clusters in cells stimulated with soluble streptavidin form tight puncta. This qualitative observation is quantified by determining the average BCR cluster size (r_o) and correlation amplitude (A) by fitting BCR auto-correlation functions from single cells to an exponential form, $G(r) = 1+Aexp(-r/r_o)$, and results are shown in Fig 11B. The average cluster size for surface presented antigen (r_o=126±3nm) is much larger than that observed with soluble antigen (r_o=45±2nm), whereas the average amplitude of correlations is much lower for surface presented antigen (A=8±1) than for soluble antigen (A=70±9).

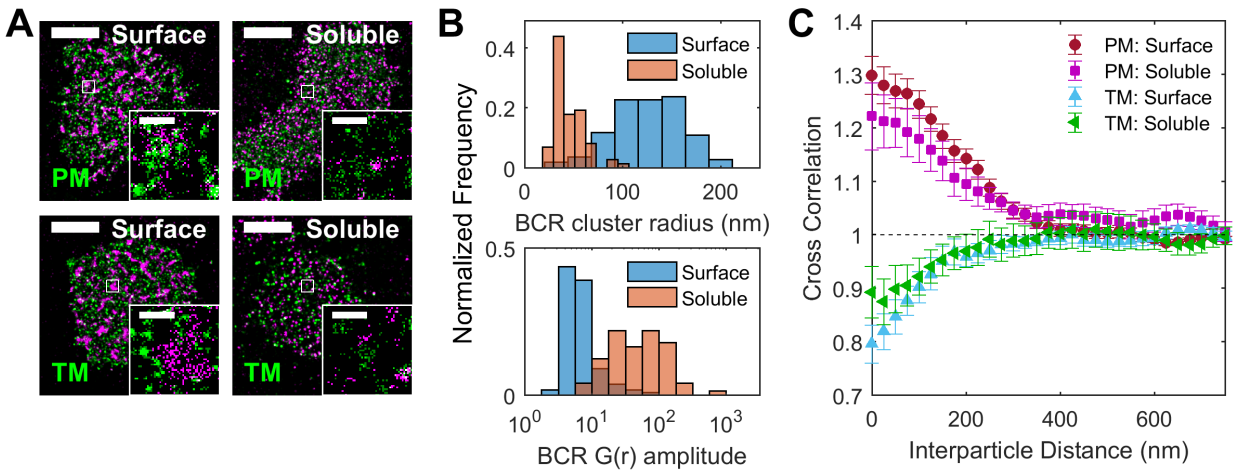

Figure 11: Comparison of TM/PM sorting with surface presented and soluble multivalent antigens

(A) Representative reconstructed super-resolved images of BCR with PM (top) or TM (bottom) in cells stimulated with surface presented (left) or soluble (right) streptavidin antigens. Scale-bars are 5μm in the main images and 500nm in the insets. **(B)** Quantification of BCR clusters in the different stimulation conditions. BCR clusters are larger when engaged with surface presented antigen compared to soluble antigens (top; $<r_o>$ = 126±3nm and $<r_o>$= 45±2nm respectively). The amplitude of BCR auto-correlation curves (G(r)) are lower when BCR is engaged with surface presented antigen compared to soluble antigens (top; <A>= 8±1 and <A>= 70±9 respectively). **(C)** Cross-correlation functions for both peptides under both stimulation conditions. Error bars represent the standard error of the mean between cells. **Soluble data was previously published in an article I coauthored: Stone, M.B., Shelby, S.A., Núñez, M.F., Wisser, K., and Veatch, S.L. 2017. "Protein sorting by lipid phase-like domains supports emergent signaling function in B lymphocyte plasma membranes." Elife [50]*

There are also striking visual differences in peptide partitioning with respect to BCR clusters in the represented super-resolution images shown. Namely, PM is clearly enriched and TM is clearly excluded from BCR clusters in images of cells engaged with surface-presented ligands, while localization (and exclusion) is less visually apparent in images of cells engaged with soluble ligands. Interestingly, I observe very similar enrichment and depletion of PM and TM probes with respect to BCR clusters under the two stimulation conditions when co-clustering is quantified through correlation functions (Fig 11C). Under both stimulation conditions, the PM peptide is enriched ($C(r)>1$) and the TM peptide is excluded ($C(r)<1$) from BCR clusters. Cross-correlation amplitudes are slightly enhanced with respect to BCR clustered via surface presented antigen.

2.3.3 Surface presentation of antigen results in more efficient sorting of regulatory proteins as compared to soluble antigen.

Although minimal peptides sort with similar magnitudes with respect to BCR clusters formed via surface presented and soluble antigens, the regulatory proteins CD45 and Lyn are more effectively sorted in the case of bilayer presented antigen (Fig 12). Fig 12A shows representative reconstructed images of BCR alongside transiently expressed Lyn or endogenously expressed CD45 stimulated with surface presented or soluble streptavidin antigen. Cross-correlation functions tabulated from multiple cells (Fig 12B) indicate that both Lyn and CD45 are more effectively sorted with respect to BCR clusters when BCR is engaged with surface presented antigen than when BCR is engaged with soluble antigen. The correlation function is related to a quantity called the potential of mean force (PMF), which is the effective interaction required to

give rise to the measured co-distribution for a system at equilibrium. PMF curves for both minimal peptides and full length proteins are shown in Fig 12C.

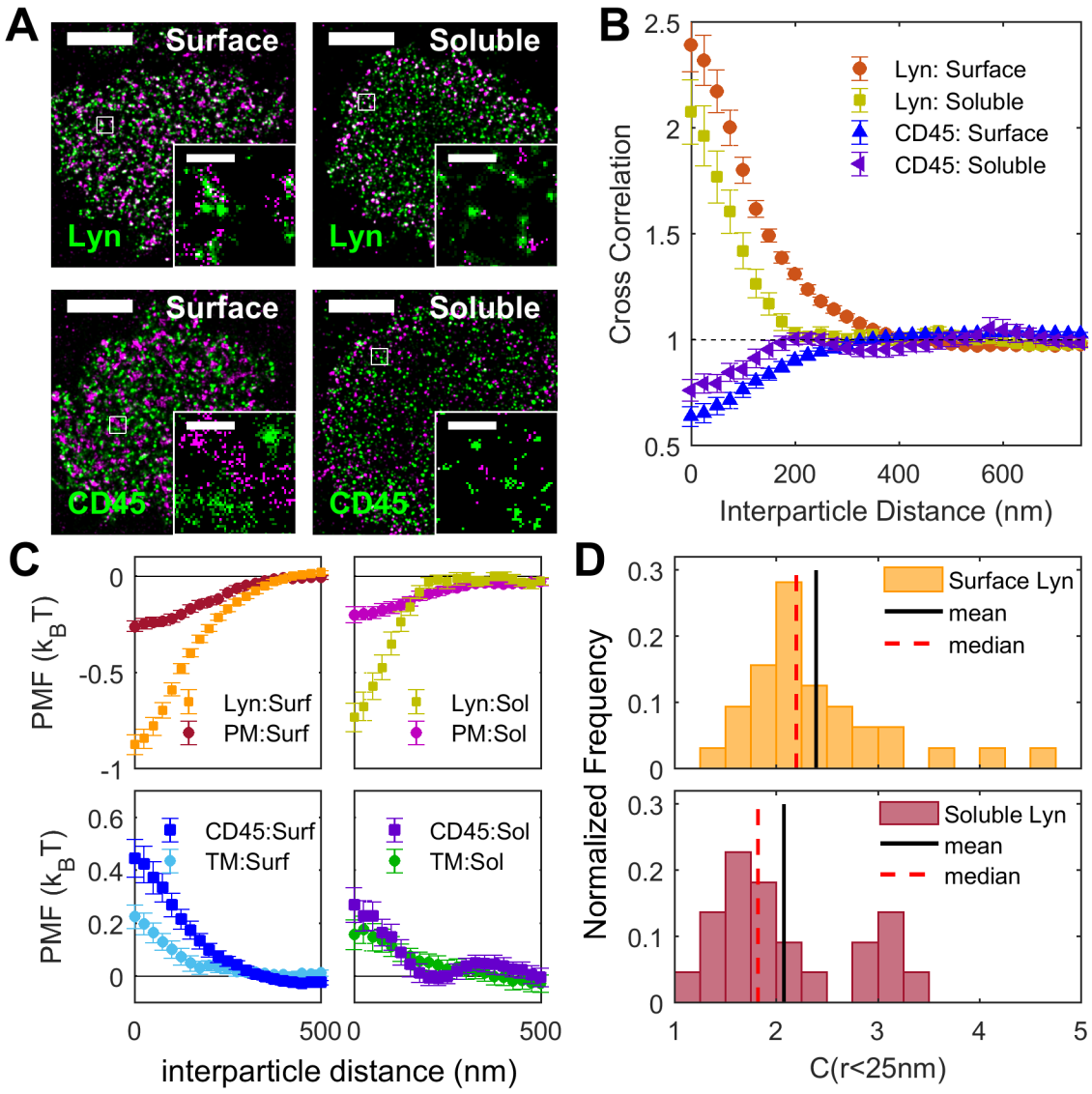

Figure 12: Sorting of Lyn and CD45 with respect to BCR clusters with both surface presented and soluble antigens

(A) Reconstructed super-resolution images of BCR (magenta) and either transiently expressed Lyn (green; top) or endogenous CD45 (green; bottom) in cells stimulated with surface presented (left) or soluble (right) streptavidin. Scale-bars are 5µm in the main images and 500nm in the insets. **(B)** Cross-correlation functions tabulated from multiple cells like those shown in A. Error bars are the standard deviation of the mean between cells. **(C)** Potential of mean force (PMF) curves tabulated from cross-correlation curves from Fig 12B and Fig 11C according to the relation PMF=-k_BT ln(C). **(D)** Histograms showing the value of C(r) in individual cells for the point corresponding to r<25nm. Distributions contain outliers at high values of C(r<25nm) that contribute disproportionately to the mean. Outliers are observed under both stimulation conditions and distributions are general shifted to higher values in the surface presented condition.

Full length Lyn interacts directly with phosphorylated BCR and the large cross-correlation amplitude between these two proteins represents a combination of both protein-protein and membrane-mediated interactions between these two proteins. This conclusion is supported by the PMF curves shown in Fig 12C that indicate that Lyn's anchor motif (PM) contributes roughly ¼ of the interaction energy between Lyn and BCR for surface stimulation and 1/3 of the interaction energy with antigen is presented in a soluble form. CD45 is more excluded from surface engaged BCR clusters than the minimal peptide anchor TM, suggesting that the effective repulsion between these two proteins arises from a combination domain mediated and alternate interactions. By comparing the PMFs of BCR/CD45 and BCR/TM, roughly ½ of the energy required for the observed exclusion arises from membrane-mediated interactions. In contrast, both CD45 and TM are excluded from BCR clusters engaged with soluble antigen to the same extent, indicating that membrane-mediated interactions are sufficient to give rise to the observed distribution of CD45 under this stimulation condition.

I observe larger cell-to-cell variation in cross-correlation magnitudes in measurements involving Lyn than for the other proteins and peptides investigated. In particular, the majority of cells populate a normal distribution centered at a median value, while several cells exhibit high cross-correlations that fall well outside this normal distribution, and these outliers contribute disproportionately to the mean (Fig 12D). It is possible that these cells are undergoing an asynchronous signaling event that gives rise to stronger interactions between Lyn and BCR clusters. Despite this complicated cell-to-cell variation, I can conclude that Lyn is more strongly recruited to surface antigen engaged BCR clusters because both the median and mean of cross-

correlation amplitudes are shifted to higher values than detected for the case of soluble antigen engaged BCR.

2.3.4 BCR clusters engaged with surface presented antigens are highly tyrosine phosphorylated.

Lyn is a kinase involved in phosphorylating the BCR and other components of the signaling complex at tyrosine residues, whereas CD45 is a phosphatase that removes tyrosine phosphorylation from Lyn, thereby downregulating BCR signaling. Our observations of enhanced sorting of the regulatory proteins Lyn and CD45 in cells stimulated with surface presented antigen led us to speculate that BCR clusters in these cells are more highly activated than those found in clusters engaged with soluble antigen. To test this hypothesis, I visualized BCR alongside an antibody against total phosphotyrosine (pTyr). Representative reconstructed super-resolution images of CH27 cells engaged with surface presented and soluble streptavidin antigens are shown in Fig 13A. In both cases, pTyr staining appears highly colocalized with BCR clusters. This observation is quantified by the cross-correlation functions in Fig 13B that produce curves with very high cross-correlation amplitudes.

The cross-correlation functions of Fig 13B and the quantification in Fig 13C are both normalized by the average surface density of pTyr and BCR over the whole cell. The high cross-correlation amplitudes indicate that the vast majority of observed pTyr localizations occur within BCR clusters, but this quantification does not compare absolute pTyr levels within BCR clusters. In general, our super-resolution imaging technique is not well suited for quantifying the density of labeled molecules, especially in cases where they are highly clustered. There are numerous factors that lead to both over- and under-counting of single molecules within clusters that

confound this type of measurement such as reversible blinking, multiple labeling of single proteins, probe quenching, and probe photobleaching [270]. To circumvent these experimental difficulties, I instead collected diffraction limited images of both BCR and pTyr to quantify relative pTyr levels in cells with different stimulation conditions.

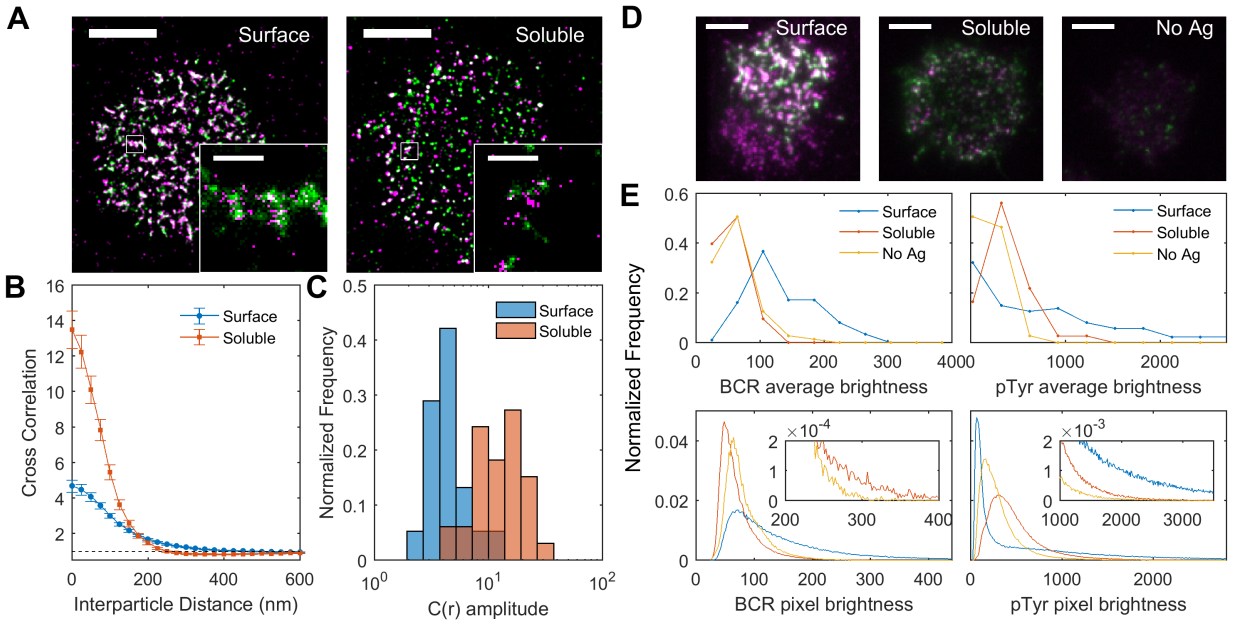

Figure 13: Activity of BCR clusters as reported by general phosphotyrosine (pTyr) staining **(A)** Representitive super-resolution images of BCR (magenta) and pTyr stained with the antibody clone 4G10 (green) for cells for cells activated with surface presented (left) and soluble (right) streptavidin antigen. Scale-bars are 5μm in the main images and 500nm in the insets. **(B)** Cross-correlation functions tabulated from multiple cells like those shown in A. Error bars represent the standard error of the mean between cells. **(C)** Histogram showing the amplitude of C(r) from single cells. **(D)** Diffraction limited images of BCR (magenta) and pTyr staining (green) for cells stimulated with surface presented (left) or soluble (middle) antigens, or for cells that are unstimulated (right). Scale-bars are 5μm. **(E)** Quantification of multiple (>50) cells for each condition shown in D. Curves shown histograms of BCR (left) and pTyr (right) average intensity over entire cells (top). Also shown are histograms of pixel individual pixel intensities for both BCR and pTyr.

Fig 13D shows representative images of BCR and pTyr imaged in cells stimulated with surface presented or soluble antigens, or in cells lacking exposure to antigen. From the images it is clear that BCR intensity is enhanced in cells engaged by surface presented antigens. This is likely because BCRs present on the dorsal surface of the cell either diffuse or are trafficked to the

ventral side where they engage with antigen and ultimately concentrate BCR. Absolute pTyr levels also appear higher in cells engaged with surface presented antigen compared to soluble antigen. In addition, I often observe that pTyr distributions appear to be polarized within cells stimulated with surface-presented antigen, with areas of the cell footprint staining highly for pTyr while others exhibit low pTyr staining.

These qualitative observations are quantified in the histograms shown in Fig 13E which quantify the average intensity over the cell footprint and pixel intensities of both BCR and pTyr detected in >50 individual cells per condition. In this case, the average intensities represent the total cellular levels of the labeled component while the pixel intensities reflect the local concentrations of these components. This quantification verifies that the average intensity of BCR is enhanced in cells engaged with an antigen presenting supported bilayer, and that there is a higher BCR local density of BCR within clusters in cells engaged with surface presented antigen than in cells engaged with soluble antigens. Overall pTyr levels are the highest in cells engaged with surface presented antigen, and these cells contain a large number of pixels with elevated pTyr intensity. The histograms also indicate the large cell-to-cell heterogeneity in the surface presented condition. The distribution of average intensity values is very broad across cells, with some cells exhibiting very high and others low pTyr average intensities. The histograms of pixel intensity indicate that a large fraction of pixels exhibit pTyr levels that are lower than those found in control cells that are not exposed to antigen. This histogram also has a tail that extends to very high intensity representing areas with high pTyr levels. Overall, these results support the conclusion that pTyr levels are higher and more heterogeneous in cells exposed to surface presented streptavidin than in cells exposed to soluble streptavidin.

2.4 – Discussion:

This study quantifies the membrane composition proximal to BCR clusters established through interactions with surface presented antigens using multicolor super-resolution fluorescence localization microscopy, and compares to similar BCR clusters formed after interactions with the same multivalent soluble antigen. I used the model multivalent antigen streptavidin, which binds with high affinity to biotin moieties conjugated to $f(Ab)_1$ antibodies which decorate the BCR IgM isotype on the cell surface. I used the same antigen to stimulate cells in both soluble and surface presented forms, enabling the direct comparison of membrane organization and signaling outcomes arising from these two engagement modes. Disadvantages of this model antigen are that it binds with much higher affinity than natural ligands and that it does not engage the antigen recognition site of BCR, therefore the signaling outcomes may bypass aspects of BCR function that depend on natural ligand directly binding the antigen site of the receptor. Instead, this stimulation scheme isolates the cellular responses that occur in response to receptor clustering.

Our studies add to a large body of work comparing BCR stimulation with surface presented and soluble antigens. Notably, past work has demonstrated that diverse monovalent antigens can stimulate B cells when presented on surfaces but many fail to stimulate cells when presented in solution [185, 207, 271-273], It is known that BCR, when engaged with surface bound antigens, undergoes a conformational change that facilitates enhanced BCR oligomerization [206, 207]. In addition, coupling B cells to surfaces by engaging integrins acts to lower the threshold of B cell activation for antigen affinity and density [269] and facilitates B cell spreading [268] and survival [274, 275]. Engaging BCR via a mobile surface presented antigen enhances B cell signaling further, likely because active processes within cells, driven by actin, can more easily

gather BCR/antigen complexes into larger domains [183]. Overall, this past work demonstrates that BCR clustering and downstream signaling responses are more robust when BCR is engaged by mobile, surface presented antigen than when BCR is engaged with soluble multivalent antigen. The goals of the current study are to explore if these more robust BCR clusters stabilize ordered phase-like domains, as I previously reported for BCR engaged with soluble antigen, and identify if membrane domains contribute to sorting of Lyn and CD45, two key regulators of early BCR activation.

2.4.1 BCR clusters engaged with surface presented antigen stabilize robust ordered phase-like domains.

I find that BCR clusters established via interactions with either surface presented or soluble antigen are enriched in a peptide marker of the liquid-ordered phase (PM) and depleted of a peptide marker of the liquid-disordered phase (TM), in good agreement with past studies that characterized the BCR microenvironment as an ordered membrane domain [36, 50, 131, 132, 261]. It is striking that the magnitude of correlation functions for PM and TM are similar given that the properties of BCR domains differ so dramatically when clustered with surface presented versus soluble antigen. This result can be partially explained simply based on the weak partitioning of peptides with respect to BCR clusters under all conditions, as shown in Fig 14. In this simulated example, cross-correlation amplitudes between domains and a strongly partitioning component

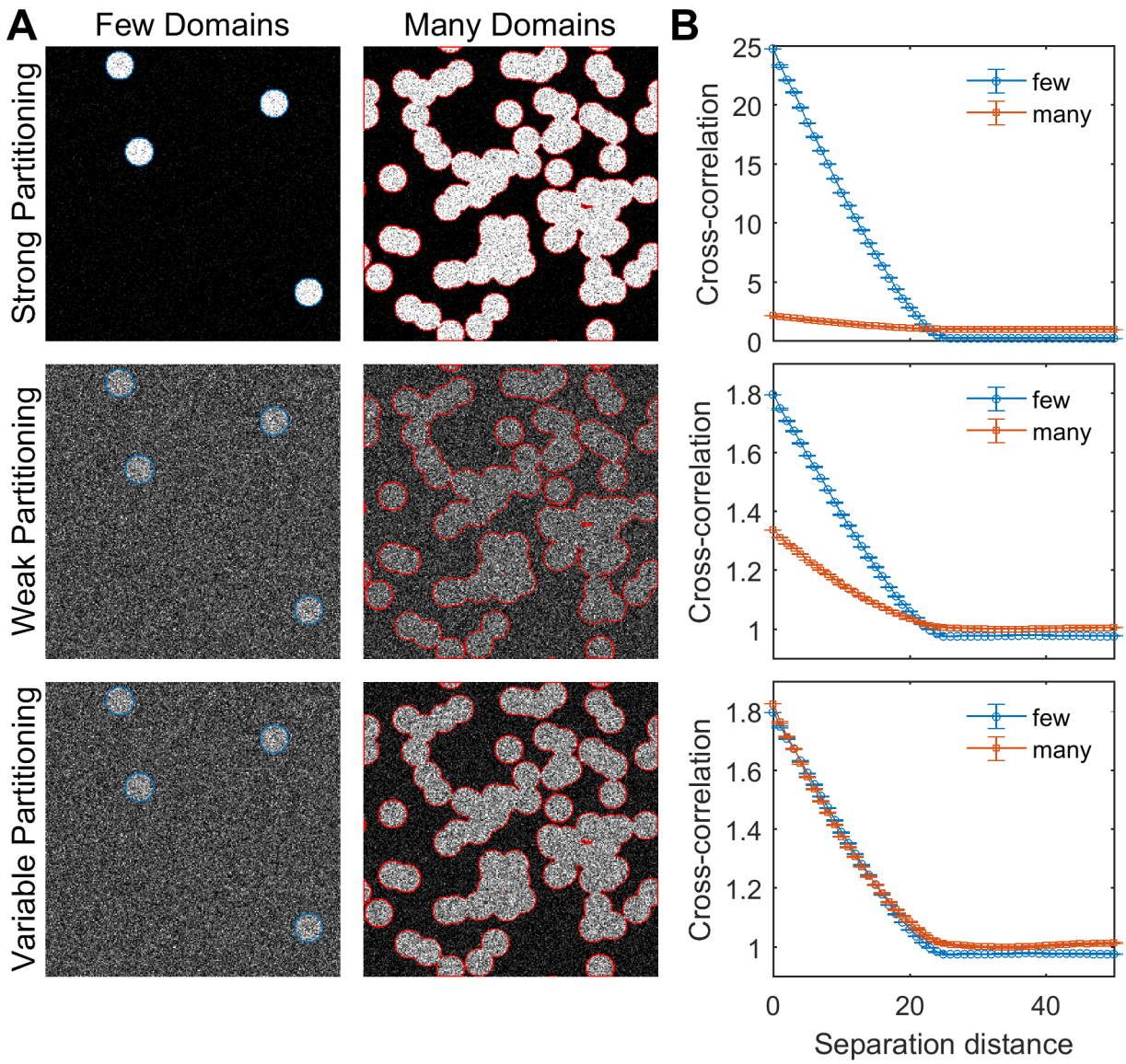

Figure 14: Interpretation of Cross-correlation amplitudes in systems with different area fractions occupied by domains

(A) Simulated images of strong (top), weak (middle), and variable (bottom) partitioning of a component within a membrane with either a small number (left) or a large number (right) of equally sized domains. The outlines drawn indicate the boundary of domains from the binary mask. This simulation intended to roughly mimic the differences in BCR clustering under conditions of soluble antigen (few domains) or surface presented antigen (many domains). **(B)** Cross-correlation between the components shown in A and binary mask indicating the location of domains. For the case of strong partitioning (top), the amplitude of the cross-correlation function varies dramatically between conditions, but the discrepancy is less pronounced for the case of weak partitioning (middle). In order to produce equal correlation functions in this simulation, the coefficient for partitioning into the domains was increased for the case of many domains. This also acts to increase the contrast visible in the simulated image.

differ by more than an order magnitude when the number of domains is changed and the relative concentration of the component with respect to domains remains constant. In contrast, the change in amplitude between these two conditions changes by less than a factor of 2 when a weakly partitioning component is investigated. In simulations, it is possible to maintain the same cross-correlation function only by increasing the partition coefficient of the component for the simulation with larger domains. One possibility is that this enhanced partitioning in surface stimulated cells arises from a higher local concentration of BCR and possibly other signaling components, as indicated in the diffraction limited BCR and pTyr labeling intensities shown in Fig 13D & Fig 13E.

Unlike our past study that exclusively used soluble antigen, peptide enrichment and depletion with respect to BCR clusters is visually apparent in both diffraction-limited and reconstructed super-resolution images of cells engaged with surface presented antigen. This observation is highlighted in the reconstructed images shown in Fig 11A. With surface presented antigen, PM is clearly incorporated into extended BCR clusters whereas TM is visibly excluded from these domains. In contrast, sorting of peptides is less visually apparent with respect to the small, sparsely distributed BCR domains that form after exposure to soluble antigen. Despite this clear visual difference, the magnitude of cross-correlation functions are roughly equivalent in these two systems. This is consistent with the simulation at the bottom of Fig 14, where enhanced partitioning was required to maintain the same correlation function in the presence of more domains. Intuitively, this is because the correlation function is normalized by the average concentration of both BCR and peptides over the cell footprint, and not by the concentration of peptides away from domains. When cells contain a large surface fraction of domains, the

average density over the whole footprint can be very different than the concentration away from domains. In this case, the amplitude of the correlation function will be reduced compared to the contrast visible in an image.

2.4.2 Membrane anchor sequences of Lyn and CD45 contribute to their localization with respect to BCR clusters.

The results shown in Fig 12 demonstrate that both Lyn and CD45 sort with respect to BCR clusters and that interactions between their membrane anchors and membrane domains contribute to this localization. Under both soluble and surface presented stimulation conditions, Lyn is more strongly recruited to BCR clusters than its minimal anchor peptide PM. This result is expected because it is known that Lyn interacts directly with BCR through phosphorylated ITAMs [144]. Examining the potential of mean force indicates that interactions between the membrane domain and the anchor peptide contribute a significant fraction of the energy required to give rise to Lyn's organization. Lyn is more strongly recruited to BCR clusters in the case of surface presented antigen likely because clusters contain more activated BCR than present in BCR clusters engaged with soluble antigen. This is seen in the diffraction limited measurements of Fig 13D and Fig 13E that detect roughly twice as much BCR on the ventral cell surface when stimulated with surface presented antigen accompanied by elevated phosphotyrosine levels. A larger concentration of activated BCR in clusters presents a larger density of potential binding sites for Lyn which is expected to increase Lyn's recruitment to BCR clusters.

CD45 is more excluded from BCR clusters than the transmembrane peptide TM when cells are exposed to surface presented antigen compared to cells exposed to soluble antigen. This

suggests that interactions between CD45 and membrane domains is sufficient to account for its organization with respect to BCR clusters under soluble stimulation conditions but not when BCR is engaged with surface presented antigen. CD45 and other phosphatases implicated in regulating BCR signaling have large extracellular domains, and past studies have attributed phosphatase exclusion from immune receptor clusters engaged with surfaces to steric effects whereby these proteins are prevented from entering membrane regions that are in tight juxtaposition to an opposing membrane [262, 276]. Our results are consistent with this model, which is referred to as the kinetic segregation model [175], where in this case steric exclusion contributes roughly half of the potential of mean force required to give rise to the observed CD45 distribution. This may represent an example whereby membrane domains and steric exclusion work in concert to exclude phosphatases from sites of BCR engagement.

2.4.3 Tyrosine phosphorylation levels are increased under conditions of enhanced protein sorting.

Lyn and CD45 are involved in regulating early stages of BCR tyrosine phosphorylation, as well as the pTyr state of scaffolding elements and other signaling regulators within the BCR activation pathway. As a consequence, enhanced spatial sorting of Lyn and CD45 in the case of surface presented antigen is expected to give rise to elevated pTyr levels in the vicinity of BCR clusters, consistent with the observations summarized in Fig 13. While the cross-correlation functions of Fig 13B indicate that pTyr staining is highly enriched at BCR clusters, the amplitudes of cross-correlation functions are not easily compared. First, the BCR clusters differ dramatically in the two stimulation conditions, making direct comparison of a strongly partitioning component via this quantitation method, as described in Fig 14. Secondly, the cross-

correlation function is normalized to the average density, therefore converting cross-correlation amplitudes into a density, which is a better measure of local pTyr activity, requires a separate measurement of this quantity which varies dramatically across stimulation conditions. I accomplished this through the diffraction limited measurements of Fig 13D & Fig 13E, which show enhanced pTyr levels both within BCR clusters and in the cell overall.

Interestingly, I observe that many surface stimulated cells appear polarized in their pTyr staining, with regions of surface stimulated cells showing pTyr staining below that observed levels in unstimulated cells on a glass surface. Numerous past studies have detailed the polarization or capping that occurs in response to soluble antigens, or the formation of larger synapses in response to surface presented antigens. Typically these processes are observed when cells are stimulated at 37°C or when cells are examined after longer stimulation times than investigated in this study [120, 132, 183, 188, 189, 242, 268, 272]. Even so, it is possible that the polarization observed in the current study represents a related effect in these samples, possibly expedited due to an enhanced initial activation of these cells compared to cells stimulated with soluble antigen. Activated Lyn also plays important roles in down-regulating BCR signaling, by phosphorylating PAG/CBP that recruits CSK to the membrane [277], and Lyn deficient B cells are chronically activated [278, 279]. It is possible these pathways are initiated in the cells and regions of cells with extremely low pTyr levels observed in these studies.

2.5 – Concluding remarks:

In this study, I have quantified several properties of BCR clusters stimulated through engagement of the model multivalent antigen streptavidin. Notably, I find that BCR clusters

robustly and differentially sort two peptides that mark the liquid-ordered and liquid-disordered phases in isolated vesicles. Moreover, peptide sorting is more robust in cells stimulated with surface presented antigen than in cells stimulated with soluble antigen, and sorting is apparent through visual inspection of reconstructed super-resolution images of surface stimulated cells. Enhanced sorting of the regulatory proteins Lyn and CD45 is also observed in surface stimulated cells, and I estimate the fractional contribution that membrane domains play in these sorting of these proteins. CD45 is more excluded from BCR clusters engaged with surface presented antigen, likely because its bulky extracellular domains are excluded from regions where the B cell membrane comes into close juxtaposition to the supported membrane, consistent with previously published results by other groups. As expected, BCR clusters in cells stimulated with surface presented antigen are more highly tyrosine phosphorylated, possibly due to the enhanced sorting of signaling regulators. Overall, this work supports the idea that BCR clustering can initiate signaling through a variety of different protein-protein and protein-lipid interactions that can vary in relative magnitudes under different stimulation conditions. Independent of how receptors become activated, the resulting domain shares properties with the liquid-ordered domains in isolated plasma membrane vesicles.

Chapter 3: Cholera Toxin B Clusters Stabilize Lo-Like Domains on the Plasma Membrane of CH27 B Cells

3.1 – Overview:

Chapter 3 focuses on studying physical characteristics of liquid-order (Lo)-like domains on the plasma membranes of B cells. In Chapter 2 I observed that surface-presented streptavidin formed larger clusters of BCR that also corresponded to robust Lo-like domain stabilization and enhanced sequestration of regulatory proteins. In this Chapter I characterize the Lo-like domains on the plasma membrane of B cells in an attempt to elucidate some of the physical principles governing membrane heterogeneity in intact cells.

Past experiments have observed GPMVs undergo a phase transitions in the range of 15 to 25°C where one phase at high temperatures phase separates into the liquid order and liquid-disordered phases at low temperatures [101]. Microscopic analysis of domain edge fluctuations, composition fluctuations, and phase transitions indicated the GPMVs proximity to a critical point [102, 103]. Systems exhibiting critical behavior are universal and past theoretical work has modeled GPMVs using 2D Ising model simulations, which are also critical [104, 105]. These simulations indicated that the observed heterogeneity in GPMVs could be a result of the GPMV's membrane proximity to a critical point defined by membrane temperature and composition [59]. This model also predicts that the application of a clustering force would stabilize composition fluctuations long enough to be observed experimentally, which was

achieved in GUVs and GPMVs [145]. The observations of Chapter 2 in which clustering BCR stabilizes Lo-like domains is reminiscent of this prediction.

In this Chapter, I build off the robust clustering and stabilization of Lo-like domains achieved with bilayers in Chapter 2, to study the parameters that modulate Lo-like domains with a clustering structure that is not linked to the BCR signaling cascade. In this Chapter I use a common liquid-order marker, Cholera Toxin B subunit (CTxB), to determine if Lo-like domain stabilization is a phenomenon specific to BCR clustering or if it is a general characteristic of the B cell plasma membrane. I find CTxB clustering stabilizes Lo-like domains, and observe in increase in Lo-like domain sorting strength for surface-engaged CTxB clusters compared to soluble-engaged, as well as for a phase marker in B cells that have experienced a temperature perturbation.

3.2 – Materials and Methods:

**I am only including methods that are unique to this Chapter, methods common to Chapters 2 and 3 are located in the Materials and Methods section of Chapter 2 (section 2.2).*

3.2.1 Cholera toxin subunit B modification

For cholera toxin subunit B (CTxB) detection, CH27 B cells were labeled with a biotinylated and fluorescently conjugated CTxB. The biotinylation and fluorophore conjugation of CTxB (Invitrogen) antibody are done simultaneously. To remove Tris, CTxB was dialyzed overnight at pH 8.5 in 1X Borate Buffered Saline (BBS) (Sodium Borate 10mM and NaCL 150mM).1.67µL

of 15 mM amine reactive biotin-X, SE (Invitrogen: B1582) and 0.80µL of 10mM NHS-Ester Atto655 (Millipore-Sigma: 76245) were mixed with 500µL of dialyzed 9.30µM CTxB pH 8.5 and rotated for 1 hour at room temperature in an aqueous solution buffered by BBS. After incubation, the modified CTxB was purified and separated from unbound dye through a gel filtration column (GE Healthcare illustra NAP Columns from Fisher: 45-000-151) in 1X-PBS+1mM-EDTA. The modified CTxB was further purified by centrifugation in a Vivaspin-500 Polyethersulfone concentration spin column with a 30kDa cutoff (Vivaspin: VS0121) and concentrated down to 100µL. The modified CTxB was then conjugated to additional NHS-Ester Atto655 a second time by mixing 2.3µL of 10mM of the NHS-Ester Atto655 with the modified antibody at room temperature in pH 8.5 for 1 hour. The antibody was purified through the gel column and spin column again before its optical spectrum was obtained to estimate degree of label (~ 1 dye/antibody).

3.2.2 CTxB labeling and sample preparation

For samples clustered with soluble streptavidin, transfected CH27 B cells incubated overnight on glass bottom wells (MatTek Coorporation) were labeled with 1.0 µg/mL CTxB-biotin in Tyrode's buffer and incubated at room temperature for 10 minutes. Cells were washed twice with Tyrode's buffer. CTxB was clustered by incubating cells with 2.0 µg/mL streptavidin (diluted in Tyrode's buffer) for 10 minutes at room temperature prior to fixation. Cells were washed with Tyrode's. Cells were chemically fixed in 2% paraformaldehyde (PFA), 0.15% Glutaraldehyde, solubilized in 0.5X PBS for 20 minutes at room temperature. Fixation was quenched by incubating with PBS containing 3% BSA for 20 minutes at room temperature.

For samples clustered with streptavidin loaded bilayers, transfected CH27 B cells were harvested from culture flasks and pelleted at 500g for 5 minutes at 4°C. Plasma membrane GM1 was bound when the cells were resuspended in 1.0 µg/mL CTxB-biotin-Atto655 in Tyrode's buffer and incubated on ice for 10 minutes. Cells were washed twice by means of centrifugation at 500g for 5 minutes at 4°C and ultimately suspended in room temperature Tyrode's buffer. CTxB was clustered by introducing labeled B cells into the flow chamber containing a previously (2.0 µg/mL) streptavidin-loaded lipid bilayer. Cells incubated on the bilayer for 10 minutes in Tyrode's buffer at room temperature prior to fixation. Cells were chemically fixed in 2% paraformaldehyde (PFA), 0.15% Glutaraldehyde, solubilized in 0.5X PBS. Fixative was introduced to the flow chamber containing B cells and incubated for 20 minutes at room temperature. Fixation was quenched by incubating with PBS containing 3% BSA for 20 minutes at room temperature.

B cells chemically fixed at 4°C were washed with 4°C Tyrode's buffer 10 minutes after streptavidin addition, then fixed at 4°C for 20 minutes. Then, samples were warmed to room temperature to quench the fixation and complete sample preparation for imaging. Typically, a 4°C sample was prepared alongside a 22°C sample.

3.3 – Results:

3.3.1 CTxB clusters correspond to ordered-like membrane domains capable of sorting phase marking minimal peptides.

I measured the sorting of phase marking peptides with respect to Cholera Toxin B subunit (CTxB) clustered by soluble streptavidin as described in Methods. Briefly, CH27 B cells

transiently expressing one of two minimal mEos3.2 tagged phase marking peptides were labeled with biotinylated CTxB. The phase marking peptides were used because they partition strongly into liquid-ordered (Lo) or liquid-disordered (Ld) phases in isolated plasma membrane vesicles, and because they differentially partition into ordered and disordered phase-like domains in intact B cells as shown in Fig 15A [50]. PM is the minimal peptide which is post-translationally modified with myristoyl and palmitoyl acylations which partitions with ordered domains, whereas TM is the transmembrane anchor helix of a protein with palmitoylation modifications removed via mutation that partitions with disordered domains. CTxB clusters were formed through incubation with soluble streptavidin conjugated to the organic fluorophore Atto655. Streptavidin-Atto655 contains 4 binding sites for any of the biotin groups conjugated to CTxB, thereby serving to cluster and image sites of CTxB (Fig 15A). Cells were chemically fixed 10 minutes after streptavidin loading, then mEos3.2 and Atto655 labels were imaged simultaneously under conditions that allowed for stochastic blinking to obtain single molecule localizations. Representative reconstructed super-resolution images of PM (Fig 15B) and TM (Fig 15C) expressing cells are shown in Fig 15.

Super-resolved images indicate that CTxB organizes into small, uniformly distributed clusters on the membrane of B cells. Similarly, the phase markers PM and TM appear uniformly distributed. Insets provide zoomed-in visualization of the single-molecule behavior between CTxB and each of the phase markers on the order of nanometers, where 1 pixel corresponds to 25nm (inset scalebar 500nm).

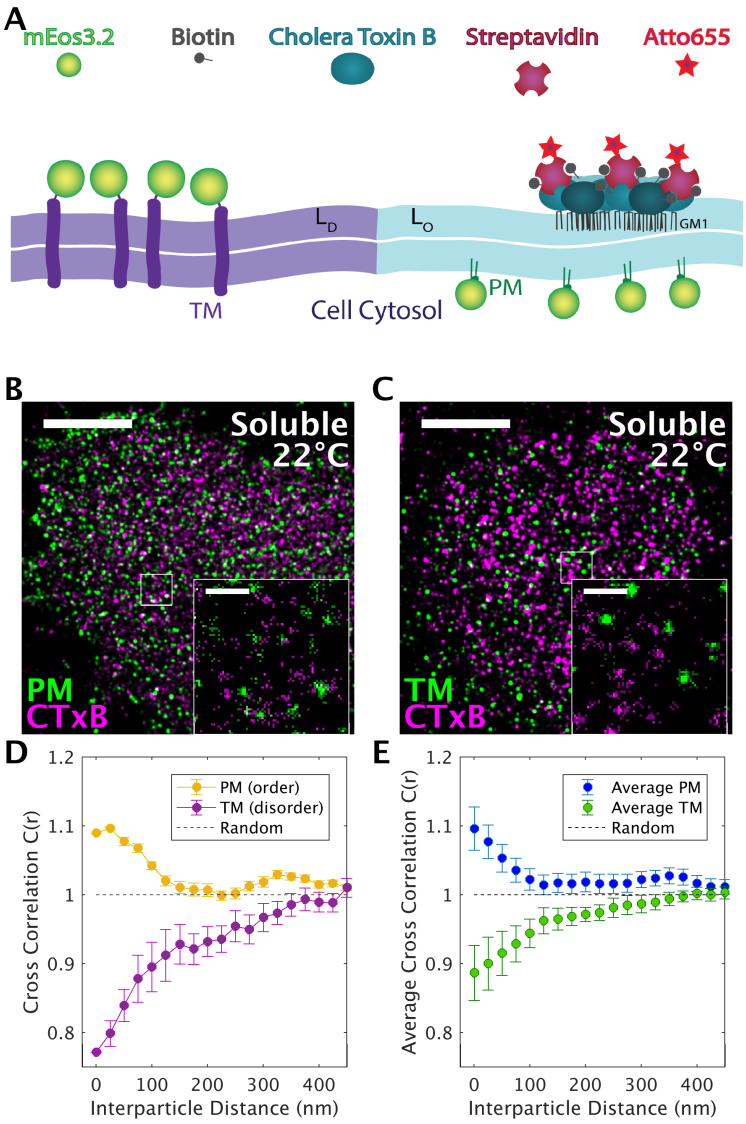

Figure 15: CTxB clusters sort phase markers

(A) Soluble streptavidin conjugated to Atto655 clusters biotinylated CTxB on the plasma membrane of CH27 B cells. **(B)** Reconstructed super-resolved images showing CTxB clusters (magenta) and either one of the membrane anchored phase markers (green). The ordered domain marker (PM-mEos3.2) is anchored at the inner leaflet via lipidation, **(C)** while the disordered marker (TM-mEos3.2) is transmembrane helix that spans both leaflets. Images are reconstructed from single-molecule localizations as described in Methods. Scale-bars in are 5μm in the main images and 500nm in the insets. **(D)** Cross-correlation functions tabulated from the reconstructed images shown in Fig 15B & Fig 15C. Curves are normalized so that values of 1 indicate a random co-distribution, values greater than 1 indicate colocalization, and values less than one indicate exclusion. Error bars are estimated from the counting statistics of the images themselves as described in methods. **(E)** Cross-correlation functions averaged over >25 cells for each phase marker. Error bars represent the standard error of the mean. **This result was previously published in an article I coauthored: Stone, M.B., Shelby, S.A., Núñez, M.F., Wisser, K., and Veatch, S.L. 2017. "Protein sorting by lipid phase-like domains supports emergent signaling function in B lymphocyte plasma membranes." Elife.[50]*

Co-distributions of CTxB with phase markers were quantified from single-molecule localizations of each color using pair cross-correlation functions, C(r), tabulated as described in the methods. C(r) reports the relative density of localizations of one-color probe a distance r from the average probe of the other color within a specified region of interest. C(r) is normalized so that values greater than 1 indicate co-clustering, values less than 1 indicate depletion, and values equal to 1 indicate a random co-distribution within the specified error bounds. Cross-correlation functions are calculated from single-molecule localizations of single cells, that is, one cell will yield one cross-correlation function. The probe co-distributions of CTxB and phase markers in the super-resolved reconstructed images (Fig1B & Fig 15C) were quantified to yield the two cross-correlation functions, each curve corresponding to a single cell (Fig 15D). For single cells, error bounds are estimated from the angular average of C(r) and the localization precision of localizations [50]. The averaged cross-correlations (Fig 15E) are obtained from 58 individual cells expressing PM and 27 expressing TM. The reported error bounds represent the standard deviation of this mean.

Both the single cell measurements (Fig 15D) and the average cross-correlation functions (Fig 15E indicate that PM is enriched, and TM is depleted from CTxB clusters. The average cross-correlation curve between CTxB and PM has a maximum of $C(r)=1.10\pm0.03$ for $r<25$nm, indicating that the average concentration of PM is about 10% higher in CTxB clusters compared to the rest of the membrane. Conversely, the average cross-correlation curve between CTxB and TM has a minimum of $C(r)=0.89\pm0.04$ for $r<25$nm, indicating that the concentration of TM is 11% lower in CTxB clusters compared to the rest of the membrane. The phase markers PM and TM are used in this study not only because of their phase-preference, but because they do not

exhibit known direct interactions with any other membrane species. I conclude that the sorting behavior of PM and TM is a consequence of their interactions with the plasma membrane and that CTxB clusters stabilize Lo-like membrane domains.

I also measured the characteristic correlation length, r_o, between CTxB and each of the phase marking minimal peptides. This parameter reflects the length-scale to which the two probes are energetically interacting attractively or repulsively, thereby reflecting enrichment or depletion before their co-distribution returns to random. The cross-correlation is fit to an exponential of the form $C(r) = 1+Aexp(-r/r_o)$ in order to extract the characteristic correlation length. I find that the range of correlation between phase marking minimal peptides and CTxB are roughly the same: PM and CTxB have a range of correlation of r_o=136±24nm and TM and CTxB have a range of anti-correlation of r_o=142±21nm.

3.3.2 Streptavidin-loaded bilayers create more robust clusters of CTxB on the plasma membrane of B cells compared to soluble streptavidin.

The clustering of CTxB on the membrane of B cells using a lipid-bilayer as the clustering agent was optimized for super-resolution similar to studies involving BCR shown in Chapter 2. CH27 B cells labeled with CTxB-biotin-Atto655 were introduced to a streptavidin-loaded lipid bilayer to cluster for 10 minutes in a simple flow-chamber to facilitate fast settling of cells onto the bilayer surface. After the 10-minute clustering, the cells were chemically fixed and prepared for imaging. The same reagents and dye pairs were used for the surface-presented bilayer experiments as the previous section with the modifications that streptavidin was now loaded onto a supported lipid bilayer rather than in soluble form, and Atto655 was conjugated to CTxB rather

than to soluble streptavidin. While the fluorophore was conjugated to a different protein, the same clustered structure was being imaged (Fig 16A). In soluble streptavidin experiments I observed small clusters of CTxB (Fig 16B), while larger CTxB clusters were observed when they were formed with a streptavidin loaded bilayer (Fig 16C), similar to past observations with BCR shown in Chapter 2. I have previously seen differences in BCR clustering due to the mode of antigen presentation in Chapter 2, and hypothesized that I might similarly see larger clusters of CTxB if I used a supported lipid bilayer loaded with streptavidin to cluster them.

CTxB clusters are quantified using auto-correlation function, G(r) as described in methods (Fig 16D). Similar to cross-correlation functions, a super-resolved image in one color of one cell will yield one auto-correlation. In these sets of experiments G(r) of Atto655 is fit to an exponential function, $G(r) = 1+Aexp(-r/r_o)$ where r_o represents the characteristic length-scale of auto-correlation. Here, r_o can be interpreted as the radius of the average cluster within that cell. The averaged auto-correlation functions have been normalized in order to visualize the differences in their range (Fig 16D). Auto-correlation functions are impacted by the over-counting of individual labeled molecules, which results in these functions having elevated amplitude at short radii. This will tend to decrease estimates of cluster sizes evaluated by the simple fitting procedure described above, therefore this value is taken to represent a lower limit of the average CTxB domain size. I averaged CTxB cluster r_o values by compiling best fit values for cells treated with soluble (85 cells) or bilayer-presented (121 cells) streptavidin. I measured r_o = 45±1nm for CTxB clustered with soluble streptavidin, and r_o = 100±5nm for CTxB clustered using a streptavidin loaded bilayer. This indicates that the clusters formed with a bilayer have a

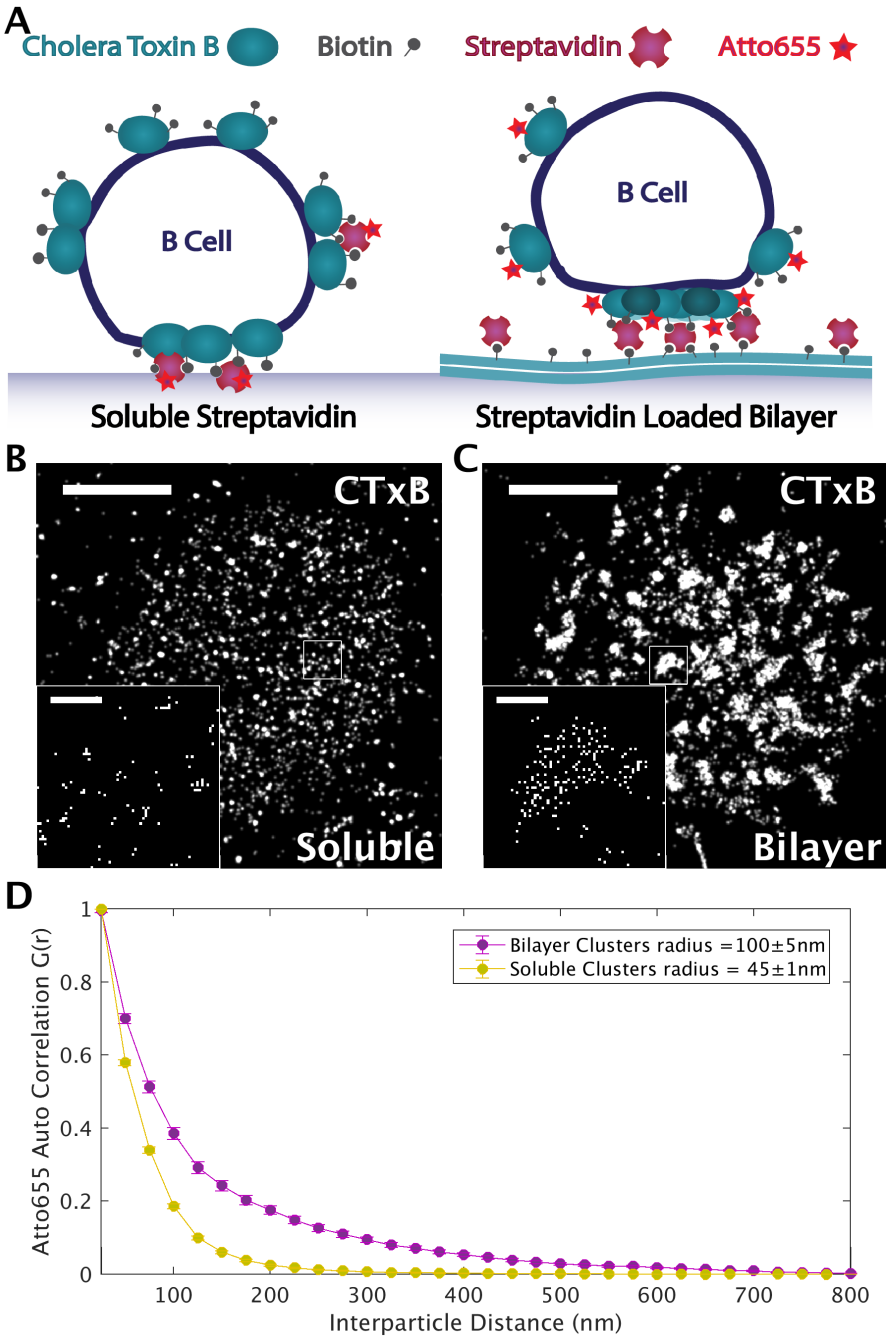

Figure 16: CTxB cluster size varies when streptavidin is presented in solution or on a supported bilayer

(A) Soluble streptavidin conjugated to Atto655 clusters biotinylated CTxB bound to the plasma membrane of CH27 B cells. **(B)** Single-color reconstructed super-resolved images showing CTxB clustered with soluble streptavidin or with **(C)** a supported-lipid bilayer that had previously been loaded with streptavidin. Scale-bars in are 5µm in the main images and 500nm in the insets. **(D)** Averaged auto-correlation functions tabulated from the single-color reconstructed images shown in Fig 16B & Fig 16C. Auto-correlations are normalized to display difference in curve width which is quantified by the decay fit parameter described in methods, displayed in legend. Error bars represent the standard error of the mean.

radius that is at least 2 times longer and an area that is around 4 times as large as the ones formed with soluble streptavidin, since area scales ~ r^2.

3.3.3 Larger CTxB clusters stabilize more robust Lo-like domains.

Super-resolved reconstructed images of CH27 B cells expressing either PM (Fig 17A) or TM (Fig 17B) with CTxB clustered via bilayer presented streptavidin are shown. The visual appearance of the CTxB clustering is similar between TM and PM transfected cells for both cases and resembles the clustering observed in Fig 16C, in that they are large, non-uniform, contiguous, and dense. Cells were imaged with a resolution ranging between 20-30nm for both colors. Bright white spots that indicate co-localization between CTxB clusters (magenta) and PM (green) are noticeable in the reconstructed image (Fig 17A), while these white co-localizations are less prevalent for TM expressing cells (Fig 17B).

Both the single cell measurements (Fig 17C) and the average cross-correlation functions (Fig 17D) indicate that PM is robustly enriched, and TM is robustly depleted from CTxB clustered with a streptavidin-loaded bilayer. The averaged cross-correlations (Fig 17D) are obtained by averaging curves tabulated for 59 individual cells expressing PM and 62 expressing TM. The reported error bounds represent the standard deviation of this mean. PM is 28% more concentrated in CTxB clusters for r<25nm compared to the rest of the membrane as evidenced by the maximum value for the cross-correlation curve between CTxB and PM: C(r)=1.28±0.05. In contrast, TM is 30% less concentrated in CTxB clusters for r<25nm compared to the rest of the membrane as evidenced by the minimum value for the cross-correlation curve between CTxB and TM: C(r)=0.70 ±0.03 for r<25nm. However, the strength of sorting observed in these CTxB

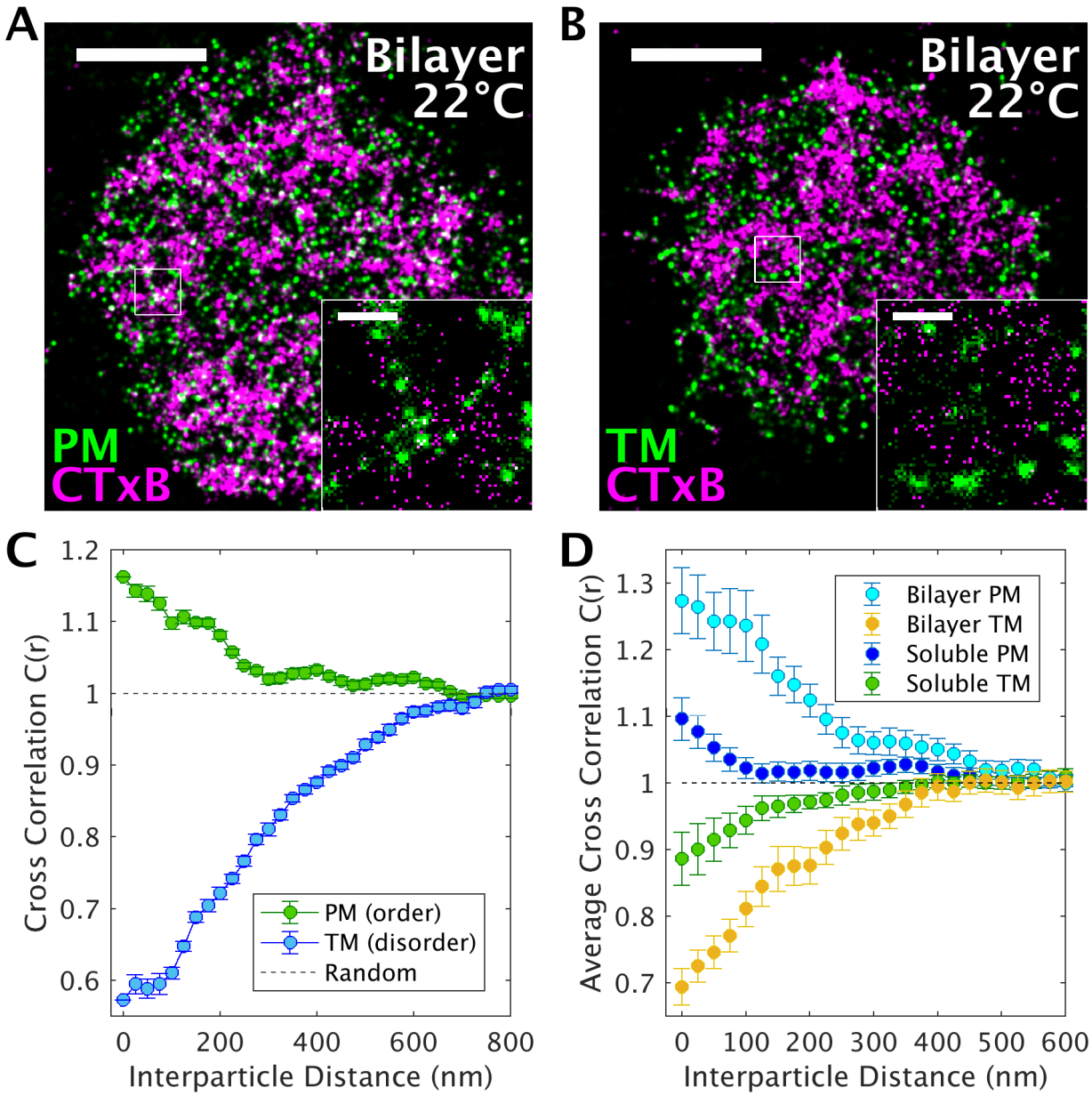

Figure 17: Sorting of phase markers is stronger with larger CTxB clusters

(A) Reconstructed super-resolved images showing CTxB clusters (magenta) and either one of the membrane anchored phase markers (green). The order marker is PM **(B)** and the disorder marker is TM. Scale-bars in are 5μm in the main images and 500nm in the insets. **(C)** Cross-correlation functions tabulated from the reconstructed images shown in Fig 17A & Fig 17B. **(D)** Cross-correlation functions averaged over >50 cells for each phase marker and CTxB clustered on the bilayer. Error bars represent the standard error of the mean. The averaged cross-correlation functions between phase markers and CTxB clustered with soluble streptavidin are re-plotted here from (Fig 15E) for comparison.

clusters are much larger than the ones measured with soluble streptavidin clustered CTxB (Fig 17D). I measure a 3-fold increase in the concentration of PM in CTxB clusters for r<25nm from 10% to 30% when the CTxB clusters are larger. Interestingly, I measured a symmetric 3-fold decrease in the concentration of TM from CTxB clusters for r<25nm from 11% to 30% when CTxB clusters are larger. Since PM and TM exhibit the same phase-partitioning behavior as soluble streptavidin experiments, I conclude that the larger CTxB clusters formed with the bilayer also stabilize liquid Lo-like domains albeit more robust and capable of sorting phase marking minimal peptides with higher concentrations than their smaller counter parts.

I measured the characteristic correlation length between each of the phase markers and CTxB for this set of experiments in order to compare them to those measured in soluble experiments. Not surprisingly, I find that in larger CTxB clusters, the range of correlations between phase markers and CTxB is much longer than in soluble streptavidin experiments: PM and CTxB have a range of correlation of r_o=229±28nm and TM and CTxB have a range of anti-correlation of r_o=205±19nm, while in soluble experiments: PM and CTxB have a r_o=136±24nm and TM a r_o=142±21nm. I conclude that the more robust Lo-like domains stabilized by the larger CTxB clusters not only sort phase markers with higher concentrations but also to longer length-scales.

3.3.4 Robust Lo-like domains stabilized with large CTxB clusters persist at 4°C.

I measured the sorting of phase markers after the B cell membrane's temperature was lowered to 4°C in order to determine if the Lo-like domains stabilized by the streptavidin-loaded bilayer remain and to what degree they might be altered. The temperature perturbation happened following CTxB clustering at room temperature. The cells were chemically fixed at the lowered

temperature so as to capture the co-distribution of CTxB and the phase marking minimal peptides at 4°C. The temperature change was quick enough to mitigate large-scale cell responses, but slow enough for lipids in the membrane to diffuse and re-arrange.

Reconstructed super-resolved images of CH27 B cells labeled with CTxB clustered with a streptavidin loaded bilayer and transiently expressing the order marker PM (Fig 18A) or disorder marker TM (Fig 18B) at 4°C are shown in Fig 18. These CTxB clusters appears similar to the clusters observed at 22°C (Fig 17A & Fig 17B). They are large, non-uniform, and contiguous which seems characteristic of CTxB clusters formed with a bilayer regardless of the temperature. The auto-correlation function was averaged for 61 cells and fit to the exponential function $G(r) = 1+Aexp(-r/r_o)$ to extract the cluster radius as described before (Fig 18C). The clusters had an average r_o=107±6nm which is the same size as the room temperature clusters formed with the bilayer (r_o=100±5nm). I conclude that the CTxB clusters formed on the supported lipid bilayer remain stable in spite of temperature being lowered.

The average cross-correlation functions (Fig 18D) indicates that PM is robustly enriched, and TM is robustly depleted from CTxB clustered with a bilayer at 4°C. The averaged cross-correlations were obtained by averaging the curves tabulated for 18 individual cells expressing PM and 43 expressing TM. The averaged cross-correlation function between PM and CTxB had a maximum value C(r)=1.21±0.06 for r<25nm indicating that PM is 21% more concentrated in CTxB clusters at 4°C relative to its concentration everywhere else on the membrane. The cross-correlation function between TM and CTxB had a maximum value C(r)=0.60±0.04 for r<25nm indicating that TM is 40% less concentrated in CTxB clusters at 4°C relative its concentration

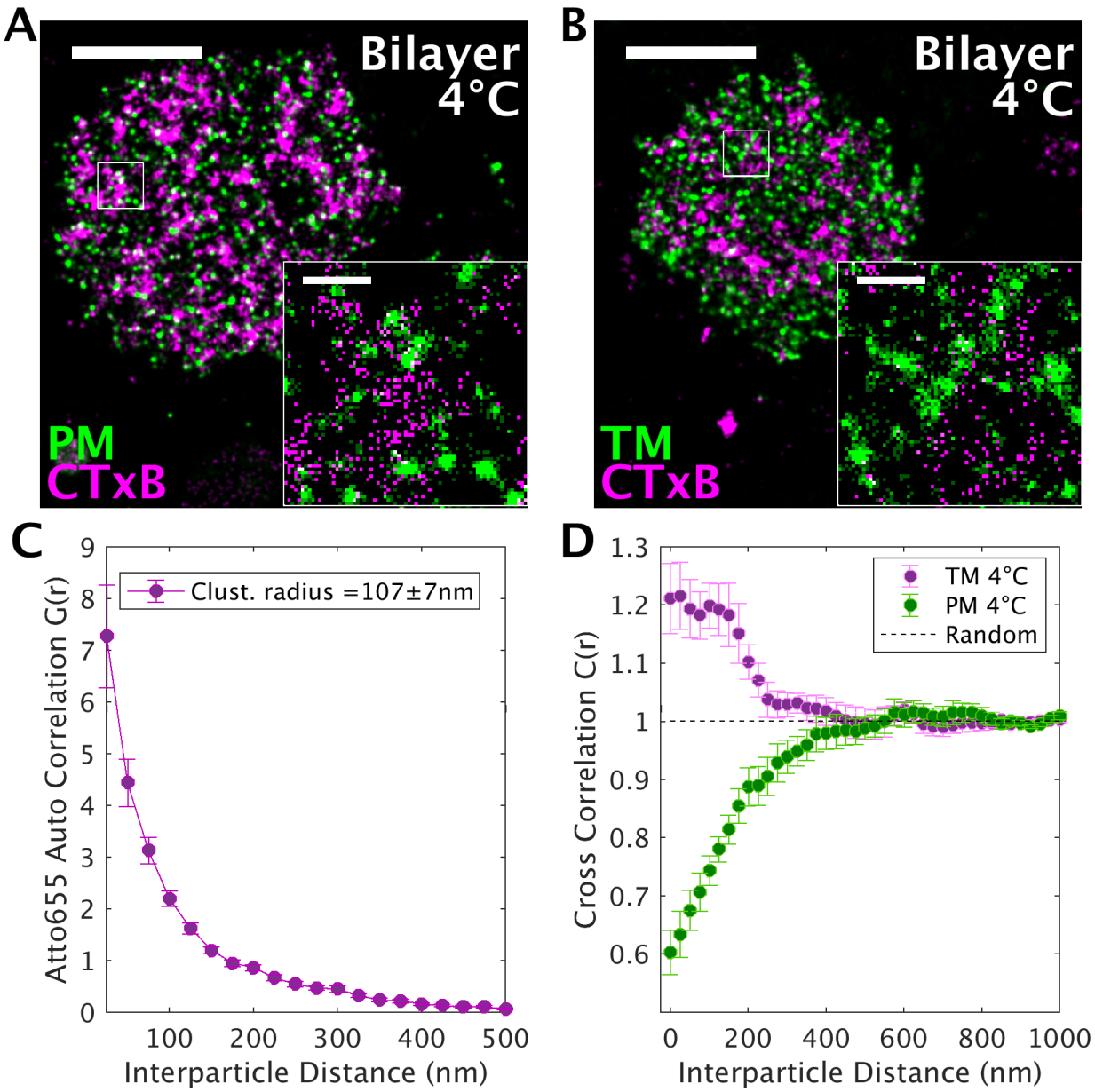

Figure 18: Robust Lo-like domains persist at 4°C

(A) Reconstructed super-resolved images showing CTxB clusters (magenta) formed using a streptavidin loaded bilayer before cell ambient temperature was lowered from 22°C to 4°C. CH27 B cells were expressing either one of the phase markers (green). PM marks the ordered phase **(B)** while TM marks the disordered phase. Scale-bars in are 5μm in the main images and 500nm in the insets. **(C)** Auto-correlation function averaged >60 cells and fit to an exponential function as described in methods. **(D)** Cross-correlation functions averaged over >15 cells for each phase marker and CTxB clustered on the bilayer. Error bars represent the standard error of the mean.

everywhere else in the membrane. As was observed at 22°C, the range of PM and TM correlation or anticorrelation with CTxB is long-range (PM r_o=179±34nm and TM r_o=218±33nm). It should be noted that the PM at this temperature had the smallest sample size (n=18) compared to the other data sets which could explain the large variability in r_o and C(r) for the cross-correlation between CTxB and PM. I note however, that both of the correlation length scales between CTxB and each of the phase marking minimal peptides is larger than the actual CTxB cluster radius (r_o=107±7nm). This indicates that PM and TM are also sorted beyond the boundaries of CTxB clusters at 4°C. Based on these results I conclude that the robust Lo-like domains stabilized by CTxB clustered with the bilayer at room temperature persist on the membrane even at 4°C as evidenced by their capability to sort the phase markers in a phase-dependent manner beyond the boundaries of the clustering structure.

3.3.5 TM sorting is enhanced at 4ºC.

I compared the cross-correlations functions of CTxB and each of the phase markers at the different temperatures to determine if there were any resolvable differences that would indicate a change in their sorting due to temperature (Fig 19). Since the larger CTxB clusters stabilized more robust clusters formed by the bilayer appeared to be stable and continued to exhibit the same phase-like sorting behavior at 4ºC, I compiled the cross-correlation functions between CTxB and each of the phase marking minimal peptides for T=22ºC (Fig 17D) and T=4ºC (Fig 18D) into one plot for comparison (Fig 19). Because these cross-correlations are normalized by their respective average co-distributions such that they decay to C(r) = 1 for r = 1μm, I am able to directly compare these curves from separate experiments. I find that TM is 10% less concentrated in CTxB clusters at 4ºC than at 22ºC for r<25nm relative to the rest of the membrane. This is indicated by the significant difference in the minimum values of their cross-correlation values at 22ºC: C(r)=0.70±0.03 compared to 4ºC: C(r)=0.60±0.04. In comparing the length scale of correlation between CTxB and TM at these two temperatures I find that there is a difference of 13nm that is within the standard error of the mean and therefore not significant.

Additionally, I have established that the CTxB clusters at these two temperatures are the same size. Once again, TM exhibits no known interactions with any membrane species. Thus, I conclude that the sorting of TM by the robust, yet stable Lo-like domains, is enhanced as a result of the temperature being lowered.

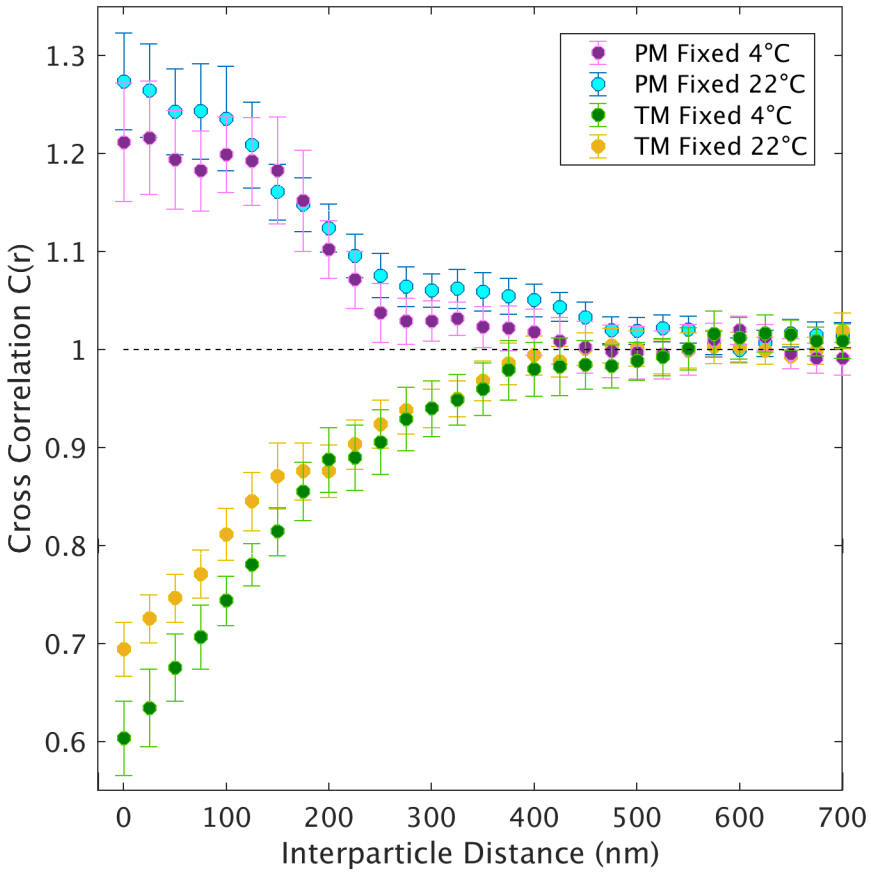

Figure 19: Lo-like domains equally sort phase markers at 4°C and 22°C in CH27 B cell membranes

Cross-correlation functions averaged between CTxB and phase markers for B cells on a supported bilayer at two different temperatures. These curves are replotted from previous plots for comparison (22°C: Fig 17D; 4°C: Fig 18D).

PM on the other hand appears to be equally sorted at both temperatures as evidenced by the roughly equal maximum values of cross-correlation functions between CTxB and PM C(r) for r<25nm at both temperatures. It might appear that PM is 7% more concentrated in CTxB clusters at 22ºC, but the difference in each maximum cross-correlation value is within error and therefor not significant

(22ºC: C(r)=1.28±0.05 compared to 4ºC: C(r)=1.21±0.06). I also noticed that the sample size for the PM measurement at 4ºC was much smaller (n=18) than for other measurements ($TM_{4ºC}$: n=43; $PM_{22ºC}$: n=59; $TM_{22ºC}$:n=62). Therefore, while I am not able to conclude that the PM curves are different, a larger sample size of PM at 4ºC would need to be obtained to conclude that PM is equally sorted at both temperatures by the same Lo-like domains that enhance sorting of TM at 4ºC.

3.4 – Discussion:

In this study I quantified the membrane composition near CTxB clusters on the plasma membrane of mouse CH27 B cells. The CTxB clusters were developed through one of two methods: cells labeled with biotinylated CTxB on a coverslip were labeled with soluble streptavidin, or cells labeled with CTxB-biotin-Atto655 were settled on a streptavidin-loaded bilayer. The membrane composition proximal to CTxB clusters was quantified using multicolor super-resolution fluorescence localization microscopy to measure the co-distributions of CTxB relative to two membrane phase marking minimal peptides used to mark either the Lo or Ld phase. I probe the distribution of the membrane composition near CTxB clusters at two temperatures by directly comparing the sorting of phase markers relative to CTxB.

3.4.1 B cell plasma membranes compositions exhibit Lo-like domains capable of stabilization through CTxB clustering.

I consistently observed PM enrichment and TM depletion at CTxB clusters on the plasma membrane regardless of the method with which the clusters had been formed (Fig 17D). PM and TM sorted relative to CTxB in a manner which is consistent to their phase behavior in cells and

vesicles [50, 58, 113] given that CTxB partitions with the Lo phase in GPMVs [58]. Therefore, the membrane domains CTxB is associating with are also Lo-like, as confirmed by PM's enrichment and TM's depletion. These results are in good agreement with Chapter 2, as evidenced by both BCR and CTxB's ability to sort phase marking minimal peptides.

Taken together, these two studies indicate that the B cell plasma membrane's composition is set such that it allows for Lo-like domain stabilization by two different types of proteins that serve to cluster and organize the membrane species surrounding them. Both of these proteins typically induce signaling as evidenced by their calcium response upon binding [50]. The lipid raft hypothesis suggests that cells use membrane domains to contribute signaling. With BCR clustering it has been shown that the Lo-like domains they stabilize contribute to sorting of key regulators of B cell signaling [50]. It would be interesting to study which other clustering structures stabilize Lo-like domains in B cell membranes and play a role in signaling, like at sites of CD20 clustering on malignant B cells which have been shown to induce apoptosis [280]. This type of information would serve to continue revealing how big or small a role membrane organization contributes in signaling.

3.4.2 Lo-like domains stabilized with larger protein clusters act to enhance peptide sorting.

The larger CTxB clusters formed through bilayer engagement stabilized more robust Lo-like domains compared to the smaller Lo-like domains stabilized by the smaller CTxB clusters engaged with soluble antigen. These results make sense in that the larger protein clustering structure would stabilize larger membrane structure around itself considering that CTxB is an Lo-preferring marker itself. Additionally, the finding that the Lo-like domains stabilized by the

larger CTxB clusters exhibit a 3-fold increase in sorting strength compared to Lo-like domains stabilized by smaller clusters also makes sense with my observation that the larger CTxB clusters increased in area 4-fold since area ~ r^2. While the increase in sorting strength and area are not a 100% match, they are very close, and the 25% mismatch could be attributed to the fact that these phase marking minimal peptides do not partition perfectly into their corresponding phases in model membranes [58].

It would be interesting to study if cells could use the size of Lo-like stabilizing structures to modulate signaling. I have observed a clear size-dependent change in the strength of phase marker sorting for Lo-like domains on the membrane of B cells. Although I'm not expecting to see μm-sized structures, one possible experiment should look into how subtle differences in the size of cluster affect the strength of sorting and whether those differences can lead to a difference in signaling. For example, even within the B cell field, there is some disagreement in the method of B cell activation, whether BCR monomers are the active subunit that break off from inactive oligomers, or if BCR monomers are inactive subunits that must cluster together to activate. It would be interesting to study the difference in an activating cluster, and an inactivating oligomer, to see if their size difference could stabilize Lo-like domains of different sizes and strength, and consequently, different sorting behavior.

3.4.3 Structure of Lo-like domains on the membrane of B cells is temperature dependent.

I found that the sorting strength of the phase marking minimal peptide TM in Lo-like domains was enhanced at 4°C compared to its sorting at 22°C. I did not however observe a significant difference in the sorting of PM between the two temperatures but note that I must acquire a

larger sample size of PM at 4°C before making conclusions about that phase marker. There was no difference in either r_o for C(r) or G(r) at either temperature which indicates that the difference in sorting must be due to a change in the composition in the Lo-like domains. The timescale the temperature was completed on, the slowing of cellular transport and processes at 4°C, should have decreased the likelihood of any large-scale compositional changes to the plasma membrane. Therefore, I conclude that the enhanced sorting of TM must is driven by a change in temperature affecting the organization of the lipids and proteins of the membrane.

3.5 – Concluding Remarks:

I have demonstrated that B cells plasma membranes are generically capable of stabilizing ordered domains. I have accomplished this both by clustering CTxB and BCR. These domains sort phase marker minimal peptides and full-length proteins that contribute to signaling.

My methods can be extended to probe how domain properties depend on membrane composition, temperature, or cellular state. This is significant because it these methods can be used to distinguish competing models of membrane organization [281]. This has the potential to link decades of observations of biochemically defined membrane rafts to the structure and function of intact biological membranes.

Chapter 4: Discussion and Concluding Remarks

4.1 – Overview:

Past studies have provided evidence supporting the lipid raft model of BCR activation in which BCR and its adaptor proteins use membrane interactions to sort and achieve biological signaling [1, 35-38]. We recently visualized the presence of Lo-like domains on the plasma membrane of B cells stabilized by BCR clustered with soluble streptavidin as a model antigen [50]. The new results presented in this Thesis extend to surface presented antigen for BCR stimulation and reveal that Lo-like domains are also stabilized when another plasma membrane-binding protein, CTxB, is clustered.

The experiments presented in this Thesis investigate the differences in sorting of phase partitioning peptides and full-length proteins with respect to BCR or CTxB clusters through the use of two-color super-resolution microscopy. I found that BCR stimulated via engagement with a streptavidin-loaded bilayer formed larger BCR clusters than BCR stimulated via engagement with soluble streptavidin. The larger BCR clusters formed with bilayer presented streptavidin sort phase marking minimal peptides similarly to BCR clusters formed with soluble antigen, consistent with the hypothesis that both clustering modalities result in the stabilization of Lo phase-like domains. Surface engaged BCR clusters sort the regulatory proteins CD45 and Lyn more effectively than expected from their phase partitioning alone, suggesting that factors in addition to the membrane domains contribute to regulatory protein organization.

In a separate set of experiments, I used the same experimental methods to measure the sorting of phase marking peptides relative to biotinylated CTxB clusters formed through engagement with soluble or surface-presented streptavidin. In both cases, I find that peptides sort with respect to CTxB clusters consistent with the hypothesis that they stabilize Lo phase-like domains, and that peptide sorting is enhanced in surface engaged compared to soluble engaged CTxB clusters. Additionally, I find that decreasing the temperature of the B cell plasma membrane to 4°C enhances the sorting of a phase-marker peptide. The following sections of this Chapter place these results in the context of existing literature, summarize my conclusions and provide suggestions for future work.

4.2 –Lo-like domains stabilized with BCR clusters formed using surface presented antigen are sites of high tyrosine phosphorylation.

The goals of Chapter 2 were to find evidence of Lo-like domain stabilization upon BCR stimulation with surface presented antigen and to determine the relative contribution of phase-like domains to localizing regulatory proteins during BCR stimulation with surface presented antigen or soluble antigen. My observation that the local environment of BCR clusters resembles ordered domains is in good agreement with past studies that identify antigen-based stimulation of BCR acts to stabilize ordered membrane domains in biochemical and FRET based assays [36, 131, 132, 261]. Lyn and CD45 are key regulators of early BCR signaling and sort in a manner that is consistent with the phase preference of their corresponding membrane-association. Lastly, I found that B cells stimulated with bilayer-presented antigen also contained higher levels of phosphotyrosine which indicates higher levels of signaling activity. These findings are in good

agreement with past work indicating the B cell response is more robust to surface-presented antigen than soluble antigen [183, 185, 188, 191-195, 206, 207, 271-273].

I observed that surface engaged clusters of BCR were larger and contained more receptors which together could impact the apparent magnitude of phosphotyrosine levels for the comparison between the two modes of antigen presentation. The higher levels of phosphotyrosine could have arisen as a consequence of an increase in the number of available tyrosine sites and not specifically due to an increase in BCR signaling activity. In order to validate my finding, markers with higher specificity of BCR activity should be used. The phosphotyrosine antibody used in this study, 4G10, is a generic phosphotyrosine antibody, but other more specific antibodies are available for phosphorylated BCR and phosphorylated Lyn which could be applied to measure BCR using the two-color super-resolution experiment I have described in this Thesis.

The experiments conducted in this Thesis suggest a reason for enhanced activation of BCR signaling when stimulated with surface-presented antigen. I found that membrane domain association dominates the exclusion of CD45 from BCR clusters engaged with soluble antigen. While in the surface-stimulated samples CD45's sorting was due to a combination of its membrane association and additional unidentified interactions. It seems like the unidentified interactions are likely due to steric exclusion of CD45's large extracellular domains. This hypothesis aligns with past studies attributing phosphatase exclusion from the immune synapse in T cells due to steric effects imposed on the phosphatase's extracellular domain as a consequence of the proximity of the T cell membrane and the antigen presenting cell's

membrane [179-181, 282]. These and other observations are summarized in the kinetic segregation model [175] of T cell signaling, and I conclude also apply to B cell lymphocytes.

The degree of enhanced exclusion of CD45 and BCR cluster size are consistent with past observations in surface-stimulated B cells [283]. My findings add to this past study by imaging the organization of CD45 at higher resolution and mapping the local membrane composition stabilized by surface engaged and soluble-engaged BCR clusters. Both the past study [283] and current study in this Thesis do not observe the dramatic CD45 exclusion that is observed in surface-stimulated T cells [181] and lead to the development of the kinetic segregation model for T. cell signaling [175]. As a reminder, the kinetic segregation model states that sterics imposed by immune synapse architecture physically exclude CD45 phosphatase from sites of TCR signaling due to CD45's bulky extracellular domain. One likely explanation for the discrepancy between T cells and B cells is that CD45 phosphatase is essential for T cell signaling [284] but not for B cells, as CD45 knockouts do not exhibit significantly impaired B cell responses [285, 286]. CD148 is a different phosphatase involved in BCR signaling and studies indicate that CD45/CD148 double knockouts do have impaired BCR signaling [35, 262], suggesting that CD148 is important for BCR signaling. Additionally, CD148 has a larger extracellular domain than CD45, and is highly expressed in B cells [262]. Therefore, I expect CD148 to be excluded more strongly than CD45 was from surface engaged BCR clusters.

4.3 – Lo-like domain stabilization is a common trait of B cell plasma membranes.

The goal of Chapter 3 was to identify if Lo-like domains stabilization was a phenomenon specific to BCR clustering, or if it was a more generic property of the plasma membrane of B

cells. CTxB was chosen for this study because it is both a strong marker of the Lo-phase and of lipid rafts in model membranes [44, 287, 288]. My observation that CTxB clustering stabilizes Lo-like domains on the plasma membranes of B cells supports the hypothesis that intact cells organize ordered membrane domains through similar mechanisms that could give rise to biochemically defined membrane rafts [54]. My finding adds to a recent study in which Lo-like domains on the membrane of internal organelles of living yeast cells were enriched in typical raft residents [289].

Biochemically defined membrane rafts are expected to be generated on intact cells through contributions from both proteins and lipids. In my experiments with CTxB and BCR, the clustering of membrane-bound proteins was used for Lo-like membrane domain stabilization, which is in agreement with previous studies [54] and theory [145]. Additionally, labeling CTxB labeling of B cells is known to induce signaling (Schnitzler et al., 2007). My findings contribute to a set of studies in which Lo-like domains are stabilized at sites of signaling-related protein clusters on the plasma membrane: CTxB or BCR clusters in this Thesis, and IgE-FcεRI in mast cells [290]. I conclude that the clustering of immune-related signaling proteins stabilizes Lo-like domains cell plasma membranes.

4.4 – Surface-based clustering of CTxB but not BCR enhances phase marker sorting.

One interesting observation that was consistent between both CTxB and BCR experiments was that surface-presented methods produced larger clusters than the soluble method of clustering. However, what was inconsistent was the change in sorting of phase markers. The larger CTxB clusters formed with surface-presented antigen enhanced sorting of phase markers 3-fold

compared to the soluble CTxB clusters. On the other hand, the sorting of phase markers in the larger BCR clusters formed with surface-presented antigen appeared equal to the sorting of phase markers in smaller BCR clusters formed with soluble antigen. This result was unexpected, in particular because the surface presentation was consistent in producing larger clustering structures for both CTxB and BCR, as well as enhanced regulatory protein sequestration in BCR clusters.

A possible explanation could come from the observation that CH27 B cells are sensitive to phosphatidylcholine (PC) lipids [291] and the bilayer used in these experiments were composed of 99.5 mol % DOPC. While the BCR of CH27 B cells will be activated by the PC lipid head group of a DOPC bilayer in the presence or absence of streptavidin, I made the assumption that the B cell response induced by biotin-streptavidin would much stronger than the one induced by the natural PC ligand and thus render any simultaneously occurring PC-BCR stimulation negligible. This assumption could be wrong thereby contribute an additive clustering and stimulation effect to the CTxB experiments, which may explain why the CTxB and BCR measurements detect similar sorting of phase markers. While the same amount of streptavidin is added to the bilayers for CTxB and BCR experiments, there is now the added contribution of CTxB clusters stabilizing Lo-like domains that might produce the enhanced sorting in CTxB-Streptavidin + PC-BCR stimulation compared to BCR-streptavidin stimulation alone.

In addition, we have previously observed that CTxB clustering of B cell plasma membrane induces a calcium response in B cells and proposed that larger Lo-like domains should elicit larger cellular calcium responses [50]. Past experiments have shown that CTxB binding induces

a set of signaling events tied to B cell activation, including surface molecule expression and cytokine production [292]. Therefore, the enhanced sorting of phase-markers in CTxB and not BCR clusters could be evidence of a stronger cellular response in CTxB samples. A way to test this would be to compare the Ca^{2+} response in CTxB surface-stimulated cells to the Ca^{2+} response in BCR surface-stimulated cells, where I predict that that CTxB would exhibit a higher Ca^{2+} response as a result of the PC-BCR stimulation and CTxB binding triggering the non-specific BCR signaling. Additional methods for testing this include measuring the enrichment of BCR in CTxB clusters, as well as repeating some of the CTxB experiments on non-stimulatory PC lipid bilayers, composed of 10-20 mol % DOPC rather than 99.5 mol %.

4.5 – Reduced temperature slightly enhances Lo-like domain sorting.

Because CTxB stabilizes Lo-like domains, the goal of Chapter 3 was expanded to identify what physical parameters modulate membrane domain sorting strength. I found that sorting of the Ld phase-marker was slightly enhanced at 4°C, even though the size of CTxB clusters and correlation length-scale between phase markers and CTxB remained unchanged. The measured difference in sorting as a result of the temperature perturbation was weaker than I expected based on predictions from the critical fluctuation model (see section 1.3.7). I suggest the reason the difference was weaker than expected is either due to poor sampling statistics in my measurement, which should affect all of my measurements, or that the effect is simply not as strong as I had anticipated.

One additional parameter that might be affecting the expected difference in signal might be the fixation of cells at 4°C compared to 22°C. The B cells are labeled and clustered at 22°C, the only

temperature difference they experience is a buffer wash and fixation. One possibility is that the difference in temperature fixation is perturbing the organization of the lipids by not fixing the membrane lipids as quickly at 4°C as it does at 22°C thereby providing an altered state of the membrane organization. One way to work around this question would be to repeat this experiment in live cells, which is possible, but would require brighter, more stable fluorescent probes than the one I currently use for fixed-cell experiments.

Lastly, while the slightly enhanced depletion of the Ld phase marker at 4°C doesn't directly inform us of a mechanism cells might use to modulate membrane domain sorting since cells are unable to change the temperature around them, there are compounds like n-chain alcohols, that change the effective temperature of the membranes without changing their physical temperature in model membranes [148, 293]. That is, I could attempt to induce a 10% decrease of TM depletion in CTxB clusters at 22°C (rather than at 4°C) by incubating B cells with n-chain alcohols, since this biochemical treatment is expected to change the membrane's relative temperature without physically doing so based on past studies [148, 293].

4.6 – Concluding Remarks:

Understanding the organization and function of the plasma membrane is of great importance due to the increasing number of reports in which biochemically defined membrane rafts are implicated in some of the highest leading causes of death: HIV [49, 294], cancer [46, 295, 296], and heart disease [45, 297, 298]. Unfortunately, advancement in the fight against these diseases has had limited input from the lipid raft field due to questions related to the proper interpretation of these biochemically defined membrane rafts. My work directly detects the physical

manifestation of this biochemical phenomena, thereby empowering new avenues of investigation into these areas.

It is important to figure out a way to manipulate Lo-like domains on the plasma membrane of B cells with CTxB clusters considering CTxB is a commonly used adjuvant (helper/booster) in therapies to either increase immunogenicity of vaccines, or to dampen autoimmunity of certain antigens [299]. At present, the hypothesized mechanism for how CTxB achieves these functions is due to its partitioning into Lo domains. Here I present a method to study Lo-like domains on the plasma membrane of B cells. It would not only serve the field of biology to expand on these studies to different cell lines, but also for the general health of humans to understand if Lo-like domains are a phenomenon shared by all eukaryotic cells. If this is true, it is vital that we begin to understand these biochemical phenomena, specifically testing which mechanism cells use to modulate the parameters of lipid domains on their own membranes, so that we can attempt to rescue diseased states through manipulation of membrane organization.

Citations

1. Voet, D. and J.G. Voet, *Biochemistry*. 4th ed. 2011: John Wily and Sons.

2. LeBien, T.W. and T.F. Tedder, *B lymphocytes: how they develop and function.* Blood, 2008. **112**(5): p. 1570-1580.

3. Medzhitov, R. and C.A. Janeway, Jr., *Innate immunity: impact on the adaptive immune response.* Curr Opin Immunol, 1997. **9**(1): p. 4-9.

4. Slifka, M.K. and R. Ahmed, *B cell responses and immune memory.* Dev Biol Stand, 1998. **95**: p. 105-15.

5. Slifka, M.K. and R. Ahmed, *Long-lived plasma cells: a mechanism for maintaining persistent antibody production.* Curr Opin Immunol, 1998. **10**(3): p. 252-8.

6. Murphy, K. and C. Weaver, *Janeway's Immunobiology*. 2016: Garland Science.

7. Clark, M.R., et al., *B-cell antigen receptor signaling requirements for targeting antigen to the MHC class II presentation pathway.* Curr Opin Immunol, 2004. **16**(3): p. 382-7.

8. Cheng, P.C., et al., *MHC class II antigen processing in B cells: accelerated intracellular targeting of antigens.* J Immunol, 1999. **162**(12): p. 7171-80.

9. Kurosaki, T., H. Shinohara, and Y. Baba, *B cell signaling and fate decision.* Annual review of immunology, 2009. **28**: p. 21-55.

10. Ron, Y. and J. Sprent, *T cell priming in vivo: a major role for B cells in presenting antigen to T cells in lymph nodes.* J Immunol, 1987. **138**(9): p. 2848-56.

11. Janeway, C.A., J. Ron, and M.E. Katz, *The B-Cell Is the Initiating Antigen-Presenting Cell in Peripheral Lymph-Nodes.* Journal of Immunology, 1987. **138**(4): p. 1051-1055.

12. Lanzavecchia, A., *Antigen-Specific Interaction between T-Cells and B-Cells.* Nature, 1985. **314**(6011): p. 537-539.

13. Janeway, C.A., et al., *Immunobiology: the immune system in health and disease*. Vol. 2. 2001: Garland Pub. New York.

14. Xu, Y.S., et al., *No receptor stands alone: IgG B-cell receptor intrinsic and extrinsic mechanisms contribute to antibody memory.* Cell Research, 2014. **24**(6): p. 651-664.

15. Geier, J.K. and M.S. Schlissel, *Pre-BCR signals and the control of Ig gene rearrangements.* Semin Immunol, 2006. **18**(1): p. 31-9.

16. Meixlsperger, S., et al., *Conventional light chains inhibit the autonomous signaling capacity of the B cell receptor.* Immunity, 2007. **26**(3): p. 323-33.

17. Ubelhart, R., et al., *N-linked glycosylation selectively regulates autonomous precursor BCR function.* Nat Immunol, 2010. **11**(8): p. 759-65.

18. Kurosaki, T., et al., *Unique properties of memory B cells of different isotypes.* Immunol Rev, 2010. **237**(1): p. 104-16.

19. McHeyzer-Williams, L.J. and M.G. McHeyzer-Williams, *Antigen-specific memory B cell development.* Annu Rev Immunol, 2005. **23**: p. 487-513.

20. Pier, G.B., J.B. Lyczak, and L.M. Wetzler, *Immunology, infection, and immunity*. 2004: ASM press.

21. Kurosaki, T., et al., *Role of the Syk autophosphorylation site and SH2 domains in B cell antigen receptor signaling.* J Exp Med, 1995. **182**(6): p. 1815-23.

22. Reth, M., *Antigen receptor tail clue.* Nature, 1989. **338**(6214): p. 383-4.

23. Cambier, J.C., *New nomenclature for the Reth motif (or ARH1/TAM/ARAM/YXXL).* Immunol Today, 1995. **16**(2): p. 110.

24. Schamel, W.W. and M. Reth, *Monomeric and oligomeric complexes of the B cell antigen receptor.* Immunity, 2000. **13**(1): p. 5-14.

25. Kurosaki, T., *Genetic analysis of B cell antigen receptor signaling.* Annu Rev Immunol, 1999. **17**: p. 555-92.

26. Dal Porto, J.M., et al., *B cell antigen receptor signaling 101.* Mol Immunol, 2004. **41**(6-7): p. 599-613.

27. DeFranco, A.L., *The complexity of signaling pathways activated by the BCR.* Curr Opin Immunol, 1997. **9**(3): p. 296-308.

28. Kurosaki, T., *Regulation of B-cell signal transduction by adaptor proteins.* Nat Rev Immunol, 2002. **2**(5): p. 354-63.

29. Reth, M. and J. Wienands, *Initiation and processing of signals from the B cell antigen receptor.* Annu Rev Immunol, 1997. **15**: p. 453-79.

30. Scharenberg, A.M., L.A. Humphries, and D.J. Rawlings, *Calcium signalling and cell-fate choice in B cells.* Nat Rev Immunol, 2007. **7**(10): p. 778-89.

31. Rock, K.L., B. Benacerraf, and A.K. Abbas, *Antigen presentation by hapten-specific B lymphocytes. I. Role of surface immunoglobulin receptors.* J Exp Med, 1984. **160**(4): p. 1102-13.

32. Katagiri, T., et al., *CD45 negatively regulates lyn activity by dephosphorylating both positive and negative regulatory tyrosine residues in immature B cells.* J Immunol, 1999. **163**(3): p. 1321-6.

33. Katagiri, T., et al., *Selective regulation of Lyn tyrosine kinase by CD45 in immature B cells.* J Biol Chem, 1995. **270**(47): p. 27987-90.

34. Saunders, A.E. and P. Johnson, *Modulation of immune cell signalling by the leukocyte common tyrosine phosphatase, CD45.* Cell Signal, 2010. **22**(3): p. 339-48.

35. Harwood, N.E. and F.D. Batista, *Early events in B cell activation.* Annual review of immunology, 2009. **28**: p. 185-210.

36. Pierce, S.K., *Lipid rafts and B-cell activation.* Nat Rev Immunol, 2002. **2**(2): p. 96-105.

37. Sasaki, T., J. Sasaki-Irie, and J.M. Penninger, *New insights into the transmembrane protein tyrosine phosphatase CD45.* Int J Biochem Cell Biol, 2001. **33**(11): p. 1041-6.

38. Rocks, O., et al., *The palmitoylation machinery is a spatially organizing system for peripheral membrane proteins.* Cell, 2010. **141**(3): p. 458-71.

39. Fan, Y.Y., et al., *Dietary docosahexaenoic acid suppresses T cell protein kinase C theta lipid raft recruitment and IL-2 production.* J Immunol, 2004. **173**(10): p. 6151-60.

40. Fan, Y.Y., et al., *Dietary (n-3) polyunsaturated fatty acids remodel mouse T-cell lipid rafts.* J Nutr, 2003. **133**(6): p. 1913-20.

41. Li, Q., et al., *Polyunsaturated eicosapentaenoic acid changes lipid composition in lipid rafts.* Eur J Nutr, 2006. **45**(3): p. 144-51.

42. Li, Q., et al., *Docosahexaenoic acid changes lipid composition and interleukin-2 receptor signaling in membrane rafts.* J Lipid Res, 2005. **46**(9): p. 1904-13.

43. Singer, S.J. and G.L. Nicolson, *The fluid mosaic model of the structure of cell membranes.* Science, 1972. **175**(4023): p. 720-31.

44. Sezgin, E., et al., *The mystery of membrane organization: composition, regulation and roles of lipid rafts.* Nat Rev Mol Cell Biol, 2017. **18**(6): p. 361-374.

45. Maguy, A., T.E. Hebert, and S. Nattel, *Involvement of lipid rafts and caveolae in cardiac ion channel function.* Cardiovasc Res, 2006. **69**(4): p. 798-807.

46. Larsen, J.B., et al., *Membrane curvature enables N-Ras lipid anchor sorting to liquid-ordered membrane phases.* Nat Chem Biol, 2015. **11**(3): p. 192-4.

47. Iwabuchi, K., *Involvement of glycosphingolipid-enriched lipid rafts in inflammatory responses.* Front Biosci (Landmark Ed), 2015. **20**: p. 325-34.

48. Farnoud, A.M., et al., *Raft-like membrane domains in pathogenic microorganisms.* Curr Top Membr, 2015. **75**: p. 233-68.

49. Lorizate, M., et al., *Comparative lipidomics analysis of HIV-1 particles and their producer cell membrane in different cell lines.* Cell Microbiol, 2013. **15**(2): p. 292-304.

50. Stone, M.B., et al., *Protein sorting by lipid phase-like domains supports emergent signaling function in B lymphocyte plasma membranes.* Elife, 2017. **6**.

51. Simons, K. and E. Ikonen, *Functional rafts in cell membranes.* Nature, 1997. **387**(6633): p. 569-72.

52. McIntosh, T.J., *Lipid Rafts*. Methods in Molecular Biology, ed. T.J. McIntosh. Vol. 398. 2007, Totowa, New Jersey: Humana Press. 326.

53. Brown, D.A. and E. London, *Functions of lipid rafts in biological membranes.* Annu Rev Cell Dev Biol, 1998. **14**: p. 111-36.

54. Pike, L.J., *Rafts defined: a report on the Keystone Symposium on Lipid Rafts and Cell Function.* J Lipid Res, 2006. **47**(7): p. 1597-8.

55. Waheed, A.A. and E.O. Freed, *Lipids and membrane microdomains in HIV-1 replication.* Virus Res, 2009. **143**(2): p. 162-76.

56. Ipsen, J.H., et al., *Phase-Equilibria in the Phosphatidylcholine-Cholesterol System.* Biochimica Et Biophysica Acta, 1987. **905**(1): p. 162-172.

57. Veatch, S.L. and S.L. Keller, *Separation of liquid phases in giant vesicles of ternary mixtures of phospholipids and cholesterol.* Biophys J, 2003. **85**(5): p. 3074-83.

58. Kaiser, H.J., et al., *Order of lipid phases in model and plasma membranes.* Proc Natl Acad Sci U S A, 2009. **106**(39): p. 16645-50.

59. Machta, B.B., et al., *Minimal model of plasma membrane heterogeneity requires coupling cortical actin to criticality.* Biophys J, 2011. **100**(7): p. 1668-77.

60. Stier, A. and E. Sackmann, *Spin labels as enzyme substrates. Heterogeneous lipid distribution in liver microsomal membranes.* Biochim Biophys Acta, 1973. **311**(3): p. 400-8.

61. Hui, S.W. and D.F. Parsons, *Direct observation of domains in wet lipid bilayers.* Science, 1975. **190**(4212): p. 383-4.

62. Wunderlich, F., et al., *Thermotropic fluid goes to ordered "discontinuous" phase separation in microsomal lipids of Tetrahymena. An X-ray diffraction study.* Biochemistry, 1978. **17**(10): p. 2005-10.

63. de Laat, S.W., et al., *Lateral diffusion of membrane lipids and proteins is increased specifically in neurites of differentiating neuroblastoma cells.* Biochim Biophys Acta, 1979. **558**(2): p. 247-50.

64. Karnovsky, M.J., et al., *The concept of lipid domains in membranes.* J Cell Biol, 1982. **94**(1): p. 1-6.

65. Xavier, R., et al., *Membrane compartmentation is required for efficient T cell activation.* Immunity, 1998. **8**(6): p. 723-32.

66. Simons, K. and G. van Meer, *Lipid sorting in epithelial cells.* Biochemistry, 1988. **27**(17): p. 6197-202.

67. Brown, D.A. and E. London, *Structure of detergent-resistant membrane domains: does phase separation occur in biological membranes?* Biochem Biophys Res Commun, 1997. **240**(1): p. 1-7.

68. Brown, D.A. and J.K. Rose, *Sorting of GPI-anchored proteins to glycolipid-enriched membrane subdomains during transport to the apical cell surface.* Cell, 1992. **68**(3): p. 533-44.

69. Metzger, H., *It's spring, and thoughts turn to ... allergies.* Cell, 1999. **97**(3): p. 287-290.

70. Baird, B., E.D. Sheets, and D. Holowka, *How does the plasma membrane participate in cellular signaling by receptors for immunoglobulin E?* Biophys Chem, 1999. **82**(2-3): p. 109-19.

71. Field, K.A., D. Holowka, and B. Baird, *Fc epsilon RI-mediated recruitment of p53/56lyn to detergent-resistant membrane domains accompanies cellular signaling.* Proc Natl Acad Sci U S A, 1995. **92**(20): p. 9201-5.

72. Sheets, E.D., D. Holowka, and B. Baird, *Critical role for cholesterol in Lyn-mediated tyrosine phosphorylation of FcepsilonRI and their association with detergent-resistant membranes.* J Cell Biol, 1999. **145**(4): p. 877-87.

73. Martens, J.R., et al., *Differential targeting of Shaker-like potassium channels to lipid rafts.* J Biol Chem, 2000. **275**(11): p. 7443-6.

74. Kabouridis, P.S., et al., *Cholesterol depletion disrupts lipid rafts and modulates the activity of multiple signaling pathways in T lymphocytes.* Eur J Immunol, 2000. **30**(3): p. 954-63.

75. Edidin, M., *The state of lipid rafts: from model membranes to cells.* Annu Rev Biophys Biomol Struct, 2003. **32**: p. 257-83.

76. Pizzo, P., et al., *Lipid rafts and T cell receptor signaling: a critical re-evaluation.* Eur J Immunol, 2002. **32**(11): p. 3082-91.

77. Heerklotz, H., *Triton promotes domain formation in lipid raft mixtures.* Biophys J, 2002. **83**(5): p. 2693-701.

78. Heerklotz, H., et al., *The sensitivity of lipid domains to small perturbations demonstrated by the effect of Triton.* J Mol Biol, 2003. **329**(4): p. 793-9.

79. Lichtenberg, D., F.M. Goni, and H. Heerklotz, *Detergent-resistant membranes should not be identified with membrane rafts.* Trends Biochem Sci, 2005. **30**(8): p. 430-6.

80. Schuck, S., et al., *Resistance of cell membranes to different detergents.* Proc Natl Acad Sci U S A, 2003. **100**(10): p. 5795-800.

81. Kwik, J., et al., *Membrane cholesterol, lateral mobility, and the phosphatidylinositol 4,5-bisphosphate-dependent organization of cell actin.* Proc Natl Acad Sci U S A, 2003. **100**(24): p. 13964-9.

82. van Rheenen, J., et al., *PIP2 signaling in lipid domains: a critical re-evaluation.* EMBO J, 2005. **24**(9): p. 1664-73.

83. Kirkham, M. and R.G. Parton, *Clathrin-independent endocytosis: new insights into caveolae and non-caveolar lipid raft carriers.* Biochim Biophys Acta, 2005. **1745**(3): p. 273-86.

84. Silvius, J.R., D. delGiudice, and M. Lafleur, *Cholesterol at different bilayer concentrations can promote or antagonize lateral segregation of phospholipids of differing acyl chain length.* Biochemistry, 1996. **35**(48): p. 15198-15208.

85. Ahmed, S.N., D.A. Brown, and E. London, *On the origin of sphingolipid/cholesterol-rich detergent-insoluble cell membranes: physiological concentrations of cholesterol and sphingolipid induce formation of a detergent-insoluble, liquid-ordered lipid phase in model membranes.* Biochemistry, 1997. **36**(36): p. 10944-53.

86. Xu, X., *X. Xu and E. London, Biochemistry 39, 844 (2000).* Biochemistry, 2000. **39**: p. 844.

87. Schroeder, R.J., et al., *Cholesterol and sphingolipid enhance the Triton X-100 insolubility of glycosylphosphatidylinositol-anchored proteins by promoting the formation of detergent-insoluble ordered membrane domains.* J Biol Chem, 1998. **273**(2): p. 1150-7.

88. Brown, D.A. and E. London, *Structure and function of sphingolipid- and cholesterol-rich membrane rafts.* J Biol Chem, 2000. **275**(23): p. 17221-4.

89. Scott, R.E., et al., *Plasma membrane vesiculation in 3T3 and SV3T3 cells. I. Morphological and biochemical characterization.* J Cell Sci, 1979. **35**: p. 229-43.

90. Belkin, M. and W.G. Hardy, *Relation between Water Permeability and Integrity of Sulfhydryl Groups in Malignant and Normal Cells.* J Biophys Biochem Cytol, 1961. **9**(4): p. 733-45.

91. Fridriksson, E.K., et al., *Quantitative analysis of phospholipids in functionally important membrane domains from RBL-2H3 mast cells using tandem high-resolution mass spectrometry.* Biochemistry, 1999. **38**(25): p. 8056-63.

92. Holowka, D. and B. Baird, *Structural studies on the membrane-bound immunoglobulin E-receptor complex. 1. Characterization of large plasma membrane vesicles from rat basophilic leukemia cells and insertion of amphipathic fluorescent probes.* Biochemistry, 1983. **22**(14): p. 3466-74.

93. Tank, D.W., E.S. Wu, and W.W. Webb, *Enhanced molecular diffusibility in muscle membrane blebs: release of lateral constraints.* J Cell Biol, 1982. **92**(1): p. 207-12.

94. Ge, M., et al., *Ordered and disordered phases coexist in plasma membrane vesicles of RBL-2H3 mast cells. An ESR study.* Biophys J, 2003. **85**(2): p. 1278-88.

95. Dai, J. and M.P. Sheetz, *Membrane tether formation from blebbing cells.* Biophys J, 1999. **77**(6): p. 3363-70.

96. Sezgin, E., et al., *Elucidating membrane structure and protein behavior using giant plasma membrane vesicles.* Nat Protoc, 2012. **7**(6): p. 1042-51.

97. Baumgart, T., et al., *Large-scale fluid/fluid phase separation of proteins and lipids in giant plasma membrane vesicles.* Proc Natl Acad Sci U S A, 2007. **104**(9): p. 3165-70.

98. Levental, K.R. and I. Levental, *Giant plasma membrane vesicles: models for understanding membrane organization*, in *Current topics in membranes*. 2015, Elsevier. p. 25-57.

99. Levental, K.R., et al., *Polyunsaturated Lipids Regulate Membrane Domain Stability by Tuning Membrane Order.* Biophys J, 2016. **110**(8): p. 1800-1810.

100. Levental, I., et al., *Cholesterol-dependent phase separation in cell-derived giant plasma-membrane vesicles.* Biochem J, 2009. **424**(2): p. 163-7.

101. Veatch, S.L., et al., *Critical fluctuations in plasma membrane vesicles.* ACS Chem Biol, 2008. **3**(5): p. 287-93.

102. Fisher, M.E., *Correlation functions and the critical region of simple fluids.* Journal of Mathematical Physics, 1964. **5**(7): p. 944-962.

103. Sengers, J.V. and J.M.H.L. Sengers, *Thermodynamic Behavior of Fluids near the Critical-Point.* Annual Review of Physical Chemistry, 1986. **37**(1): p. 189-222.

104. Sethna, J.P., *Statistical mechanics : entropy, order parameters, and complexity*. Oxford master series in statistical, computational, and theoretical physics. 2006, Oxford ; New York: Oxford University Press. xix, 349 p.

105. Honerkamp-Smith, A.R., S.L. Veatch, and S.L. Keller, *An introduction to critical points for biophysicists; observations of compositional heterogeneity in lipid membranes.* Biochim Biophys Acta, 2009. **1788**(1): p. 53-63.

106. Ingley, E., *Functions of the Lyn tyrosine kinase in health and disease.* Cell Commun Signal, 2012. **10**(1): p. 21.

107. Janes, P.W., S.C. Ley, and A.I. Magee, *Aggregation of lipid rafts accompanies signaling via the T cell antigen receptor.* J Cell Biol, 1999. **147**(2): p. 447-61.

108. Kawabuchi, M., et al., *Transmembrane phosphoprotein Cbp regulates the activities of Src-family tyrosine kinases.* Nature, 2000. **404**(6781): p. 999-1003.

109. Brdicka, T., et al., *Phosphoprotein associated with glycosphingolipid-enriched microdomains (PAG), a novel ubiquitously expressed transmembrane adaptor protein, binds the protein tyrosine kinase csk and is involved in regulation of T cell activation.* J Exp Med, 2000. **191**(9): p. 1591-604.

110. Horejsi, V., W. Zhang, and B. Schraven, *Transmembrane adaptor proteins: organizers of immunoreceptor signalling.* Nat Rev Immunol, 2004. **4**(8): p. 603-16.

111. Thome, C.H., et al., *Linker for activation of T-cell family member2 (LAT2) a lipid raft adaptor protein for AKT signaling, is an early mediator of alkylphospholipid anti-leukemic activity.* Mol Cell Proteomics, 2012. **11**(12): p. 1898-912.

112. Hur, E.M., et al., *LIME, a novel transmembrane adaptor protein, associates with p56lck and mediates T cell activation.* J Exp Med, 2003. **198**(10): p. 1463-73.

113. Levental, I., et al., *Palmitoylation regulates raft affinity for the majority of integral raft proteins.* Proc Natl Acad Sci U S A, 2010. **107**(51): p. 22050-4.

114. Cherukuri, A., P.C. Cheng, and S.K. Pierce, *The role of the CD19/CD21 complex in B cell processing and presentation of complement-tagged antigens.* J Immunol, 2001. **167**(1): p. 163-72.

115. Cherukuri, A., et al., *The tetraspanin CD81 is necessary for partitioning of coligated CD19/CD21-B cell antigen receptor complexes into signaling-active lipid rafts.* Journal of Immunology, 2004. **172**(1): p. 370-380.

116. Muta, T., et al., *A 13-amino-acid motif in the cytoplasmic domain of Fc gamma RIIB modulates B-cell receptor signalling.* Nature, 1994. **368**(6466): p. 70-3.

117. Amigorena, S., et al., *Cytoplasmic domain heterogeneity and functions of IgG Fc receptors in B lymphocytes.* Science, 1992. **256**(5065): p. 1808-12.

118. Ono, M., et al., *Deletion of SHIP or SHP-1 reveals two distinct pathways for inhibitory signaling.* Cell, 1997. **90**(2): p. 293-301.

119. Ono, M., et al., *Role of the inositol phosphatase SHIP in negative regulation of the immune system by the receptor Fc(gamma)RIIB.* Nature, 1996. **383**(6597): p. 263-6.

120. Sohn, H.W., S.K. Pierce, and S.-J. Tzeng, *Live cell imaging reveals that the inhibitory FcγRIIB destabilizes B cell receptor membrane-lipid interactions and blocks immune synapse formation.* The Journal of Immunology, 2008. **180**(2): p. 793-799.

121. Levental, K.R. and I. Levental, *Isolation of giant plasma membrane vesicles for evaluation of plasma membrane structure and protein partitioning.* Methods Mol Biol, 2015. **1232**: p. 65-77.

122. Bagatolli, L.A., et al., *Laurdan properties in glycosphingolipid-phospholipid mixtures: a comparative fluorescence and calorimetric study.* Biochim Biophys Acta, 1997. **1325**(1): p. 80-90.

123. Goswami, D., et al., *Nanoclusters of GPI-anchored proteins are formed by cortical actin-driven activity.* Cell, 2008. **135**(6): p. 1085-97.

124. Rao, M. and S. Mayor, *Use of Forster's resonance energy transfer microscopy to study lipid rafts.* Biochim Biophys Acta, 2005. **1746**(3): p. 221-33.

125. Sharma, P., et al., *Nanoscale organization of multiple GPI-anchored proteins in living cell membranes.* Cell, 2004. **116**(4): p. 577-89.

126. Zacharias, D.A., et al., *Partitioning of lipid-modified monomeric GFPs into membrane microdomains of live cells.* Science, 2002. **296**(5569): p. 913-6.

127. Varma, R. and S. Mayor, *GPI-anchored proteins are organized in submicron domains at the cell surface.* Nature, 1998. **394**(6695): p. 798-801.

128. Kenworthy, A.K. and M. Edidin, *Distribution of a glycosylphosphatidylinositol-anchored protein at the apical surface of MDCK cells examined at a resolution of <100 A using imaging fluorescence resonance energy transfer.* J Cell Biol, 1998. **142**(1): p. 69-84.

129. Pyenta, P.S., D. Holowka, and B. Baird, *Cross-correlation analysis of inner-leaflet-anchored green fluorescent protein co-redistributed with IgE receptors and outer leaflet lipid raft components.* Biophys J, 2001. **80**(5): p. 2120-32.

130. Sengupta, P., D. Holowka, and B. Baird, *Fluorescence resonance energy transfer between lipid probes detects nanoscopic heterogeneity in the plasma membrane of live cells.* Biophys J, 2007. **92**(10): p. 3564-74.

131. Sohn, H.W., et al., *Fluorescence resonance energy transfer in living cells reveals dynamic membrane changes in the initiation of B cell signaling.* Proc Natl Acad Sci U S A, 2006. **103**(21): p. 8143-8.

132. Sohn, H.W., P. Tolar, and S.K. Pierce, *Membrane heterogeneities in the formation of B cell receptor-Lyn kinase microclusters and the immune synapse.* J Cell Biol, 2008. **182**(2): p. 367-79.

133. Saha, S., R. Raghupathy, and S. Mayor, *Homo-FRET imaging highlights the nanoscale organization of cell surface molecules.* Methods Mol Biol, 2015. **1251**: p. 151-73.

134. Pathak, P. and E. London, *The Effect of Membrane Lipid Composition on the Formation of Lipid Ultrananodomains.* Biophys J, 2015. **109**(8): p. 1630-8.

135. Engel, S., et al., *FLIM-FRET and FRAP reveal association of influenza virus haemagglutinin with membrane rafts.* Biochem J, 2010. **425**(3): p. 567-73.

136. Heberle, F.A., et al., *Comparison of three ternary lipid bilayer mixtures: FRET and ESR reveal nanodomains.* Biophys J, 2010. **99**(10): p. 3309-18.

137. Eggeling, C., *Super-resolution optical microscopy of lipid plasma membrane dynamics.* Essays Biochem, 2015. **57**: p. 69-80.

138. Sezgin, E. and P. Schwille, *Fluorescence techniques to study lipid dynamics.* Cold Spring Harb Perspect Biol, 2011. **3**(11): p. a009803.

139. Sengupta, P., et al., *Probing protein heterogeneity in the plasma membrane using PALM and pair correlation analysis.* Nat Methods, 2011. **8**(11): p. 969-75.

140. Simons, K. and W.L. Vaz, *Model systems, lipid rafts, and cell membranes.* Annu Rev Biophys Biomol Struct, 2004. **33**: p. 269-95.

141. de Almeida, R.F., A. Fedorov, and M. Prieto, *Sphingomyelin/phosphatidylcholine/cholesterol phase diagram: boundaries and composition of lipid rafts.* Biophys J, 2003. **85**(4): p. 2406-16.

142. Dykstra, M., et al., *Location is everything: lipid rafts and immune cell signaling.* Annu Rev Immunol, 2003. **21**: p. 457-81.

143. Cherukuri, A., M. Dykstra, and S.K. Pierce, *Floating the raft hypothesis: lipid rafts play a role in immune cell activation.* Immunity, 2001. **14**(6): p. 657-60.

144. Johnson, S.A., et al., *Phosphorylated immunoreceptor signaling motifs (ITAMs) exhibit unique abilities to bind and activate Lyn and Syk tyrosine kinases.* J Immunol, 1995. **155**(10): p. 4596-603.

145. Zhao, J., J. Wu, and S.L. Veatch, *Adhesion stabilizes robust lipid heterogeneity in supercritical membranes at physiological temperature.* Biophys J, 2013. **104**(4): p. 825-34.

146. Calder, P.C., *Polyunsaturated fatty acids and inflammation.* Prostaglandins, Leukotrienes and Essential Fatty Acids, 2006. **75**(3): p. 197-202.

147. Jaffres, P.A., et al., *Alkyl ether lipids, ion channels and lipid raft reorganization in cancer therapy.* Pharmacol Ther, 2016. **165**: p. 114-31.

148. Gray, E., et al., *Liquid general anesthetics lower critical temperatures in plasma membrane vesicles.* Biophys J, 2013. **105**(12): p. 2751-9.

149. Petrie, R.J., et al., *Transient translocation of the B cell receptor and Src homology 2 domain-containing inositol phosphatase to lipid rafts: evidence toward a role in calcium regulation.* J Immunol, 2000. **165**(3): p. 1220-7.

150. Awasthi-Kalia, M., P.P. Schnetkamp, and J.P. Deans, *Differential effects of filipin and methyl-beta-cyclodextrin on B cell receptor signaling.* Biochem Biophys Res Commun, 2001. **287**(1): p. 77-82.

151. Katkere, B., et al., *Physiological-range temperature changes modulate cognate antigen processing and presentation mediated by lipid raft-restricted ubiquitinated B cell receptor molecules.* J Immunol, 2010. **185**(9): p. 5032-9.

152. Saitou, T., et al., *Roles of raft-anchored adaptor Cbp/PAG1 in spatial regulation of c-Src kinase.* PLoS One, 2014. **9**(3): p. e93470.

153. O'Shea, J.J., A. Laurence, and I.B. McInnes, *Back to the future: oral targeted therapy for RA and other autoimmune diseases.* Nat Rev Rheumatol, 2013. **9**(3): p. 173-82.

154. Bernardino de la Serna, J., et al., *There Is No Simple Model of the Plasma Membrane Organization.* Front Cell Dev Biol, 2016. **4**: p. 106.

155. Yang, J. and M. Reth, *The dissociation activation model of B cell antigen receptor triggering.* FEBS Lett, 2010. **584**(24): p. 4872-7.

156. Moore, K.W., et al., *Expression of Igd May Use Both DNA Rearrangement and Rna Splicing Mechanisms.* Proceedings of the National Academy of Sciences of the United States of America-Biological Sciences, 1981. **78**(3): p. 1800-1804.

157. Kerr, W.G., L.M. Hendershot, and P.D. Burrows, *Regulation of IgM and IgD expression in human B-lineage cells.* J Immunol, 1991. **146**(10): p. 3314-21.

158. Wienands, J. and M. Reth, *The B-Cell Antigen Receptor of Class-Igd Can Be Expressed on the Cell-Surface in 2 Different Forms.* European Journal of Immunology, 1991. **21**(10): p. 2373-2378.

159. Campbell, K.S., E.J. Hager, and J.C. Cambier, *Alpha-chains of IgM and IgD antigen receptor complexes are differentially N-glycosylated MB-1-related molecules.* J Immunol, 1991. **147**(5): p. 1575-80.

160. Venkitaraman, A.R., et al., *The B-cell antigen receptor of the five immunoglobulin classes.* Nature, 1991. **352**(6338): p. 777-81.

161. Geisberger, R., M. Lamers, and G. Achatz, *The riddle of the dual expression of IgM and IgD.* Immunology, 2006. **118**(4): p. 429-37.

162. Peckham, D., et al., *Difference in apoptosis induction between surface IgD and IgM.* International Immunology, 2001. **13**(3): p. 285-295.

163. Kim, K.M. and M. Reth, *The B cell antigen receptor of class IgD induces a stronger and more prolonged protein tyrosine phosphorylation than that of class IgM.* J Exp Med, 1995. **181**(3): p. 1005-14.

164. Tolar, P., H.W. Sohn, and S.K. Pierce, *The initiation of antigen-induced B cell antigen receptor signaling viewed in living cells by fluorescence resonance energy transfer.* Nat Immunol, 2005. **6**(11): p. 1168-76.

165. Reth, M., J. Wienands, and W.W. Schamel, *An unsolved problem of the clonal selection theory and the model of an oligomeric B-cell antigen receptor.* Immunol Rev, 2000. **176**: p. 10-8.

166. Yang, J. and M. Reth, *Oligomeric organization of the B-cell antigen receptor on resting cells.* Nature, 2010. **467**(7314): p. 465-9.

167. Mattila, P.K., et al., *The actin and tetraspanin networks organize receptor nanoclusters to regulate B cell receptor-mediated signaling.* Immunity, 2013. **38**(3): p. 461-74.

168. Maity, P.C., et al., *B cell antigen receptors of the IgM and IgD classes are clustered in different protein islands that are altered during B cell activation.* Sci Signal, 2015. **8**(394): p. ra93.

169. Muller, J., et al., *CD22 ligand-binding and signaling domains reciprocally regulate B-cell Ca2+ signaling.* Proceedings of the National Academy of Sciences of the United States of America, 2013. **110**(30): p. 12402-12407.

170. Soderberg, O., et al., *Characterizing proteins and their interactions in cells and tissues using the in situ proximity ligation assay.* Methods, 2008. **45**(3): p. 227-232.

171. Klasener, K., et al., *B cell activation involves nanoscale receptor reorganizations and inside-out signaling by Syk.* Elife, 2014. **3**: p. e02069.

172. Yang, J. and M. Reth, *Receptor dissociation and B-cell activation*, in *B Cell Receptor Signaling*. 2015, Springer. p. 27-43.

173. Dustin, M.L. and D. Depoil, *New insights into the T cell synapse from single molecule techniques.* Nat Rev Immunol, 2011. **11**(10): p. 672-84.

174. Choudhuri, K., et al., *T-cell receptor triggering is critically dependent on the dimensions of its peptide-MHC ligand.* Nature, 2005. **436**(7050): p. 578-582.

175. Davis, S.J. and P.A. van der Merwe, *The kinetic-segregation model: TCR triggering and beyond.* Nat Immunol, 2006. **7**(8): p. 803-9.

176. Huppa, J.B. and M.M. Davis, *T-cell-antigen recognition and the immunological synapse.* Nat Rev Immunol, 2003. **3**(12): p. 973-83.

177. Yuseff, M.I., et al., *How B cells capture, process and present antigens: a crucial role for cell polarity.* Nat Rev Immunol, 2013. **13**(7): p. 475-86.

178. Davis, S.J. and P.A. van der Merwe, *The structure and ligand interactions of CD2: implications for T-cell function.* Immunol Today, 1996. **17**(4): p. 177-87.

179. Carbone, C.B., et al., *In vitro reconstitution of T cell receptor-mediated segregation of the CD45 phosphatase.* Proc Natl Acad Sci U S A, 2017. **114**(44): p. E9338-E9345.

180. James, J.R. and R.D. Vale, *Biophysical mechanism of T-cell receptor triggering in a reconstituted system.* Nature, 2012. **487**(7405): p. 64-9.

181. Irles, C., et al., *CD45 ectodomain controls interaction with GEMs and Lck activity for optimal TCR signaling.* Nat Immunol, 2003. **4**(2): p. 189-97.

182. Kuokkanen, E., V. Sustar, and P.K. Mattila, *Molecular control of B cell activation and immunological synapse formation.* Traffic, 2015. **16**(4): p. 311-26.

183. Ketchum, C., et al., *Ligand mobility regulates B cell receptor clustering and signaling activation.* Biophys J, 2014. **106**(1): p. 26-36.

184. Kim, Y.M., et al., *Monovalent ligation of the B cell receptor induces receptor activation but fails to promote antigen presentation.* Proc Natl Acad Sci U S A, 2006. **103**(9): p. 3327-32.

185. Minguet, S., E.-P. Dopfer, and W.W. Schamel, *Low-valency, but not monovalent, antigens trigger the B-cell antigen receptor (BCR).* International immunology, 2010. **22**(3): p. 205-212.

186. Thyagarajan, R., N. Arunkumar, and W. Song, *Polyvalent antigens stabilize B cell antigen receptor surface signaling microdomains.* J Immunol, 2003. **170**(12): p. 6099-106.

187. Woodruff, M.F., B. Reid, and K. James, *Effect of antilymphocytic antibody and antibody fragments on human lymphocytes in vitro.* Nature, 1967. **215**(5101): p. 591-4.

188. Fleire, S.J., et al., *B cell ligand discrimination through a spreading and contraction response.* Science, 2006. **312**(5774): p. 738-41.

189. Liu, W.L., et al., *Antigen affinity discrimination is an intrinsic function of the B cell receptor.* Journal of Experimental Medicine, 2010. **207**(5): p. 1095-1111.

190. Pape, K.A., et al., *The humoral immune response is initiated in lymph nodes by B cells that acquire soluble antigen directly in the follicles.* Immunity, 2007. **26**(4): p. 491-502.

191. Tew, J.G., et al., *Follicular Dendritic Cells as Accessory Cells.* Immunological Reviews, 1990. **117**(1): p. 185-211.

192. Wykes, M., et al., *Dendritic cells interact directly with naive B lymphocytes to transfer antigen and initiate class switching in a primary T-dependent response.* J Immunol, 1998. **161**(3): p. 1313-9.

193. Haberman, A.M. and M.J. Shlomchik, *Reassessing the function of immune-complex retention by follicular dendritic cells.* Nat Rev Immunol, 2003. **3**(9): p. 757-64.

194. Kosco-Vilbois, M.H., *Are follicular dendritic cells really good for nothing?* Nature Reviews Immunology, 2003. **3**(9): p. 764.

195. Bergtold, A., et al., *Cell surface recycling of internalized antigen permits dendritic cell priming of B cells.* Immunity, 2005. **23**(5): p. 503-14.

196. Nossal, G.J., et al., *Antigens in immunity. XV. Ultrastructural features of antigen capture in primary and secondary lymphoid follicles.* J Exp Med, 1968. **127**(2): p. 277-90.

197. Lindquist, R.L., et al., *Visualizing dendritic cell networks in vivo.* Nat Immunol, 2004. **5**(12): p. 1243-50.

198. Clark, S.L., Jr., *The reticulum of lymph nodes in mice studied with the electron microscope.* Am J Anat, 1962. **110**: p. 217-57.

199. van der Merwe, P.A., *The TCR triggering puzzle.* Immunity, 2001. **14**(6): p. 665-8.

200. Rudolph, M.G., R.L. Stanfield, and I.A. Wilson, *How TCRs bind MHCs, peptides, and coreceptors.* Annu Rev Immunol, 2006. **24**: p. 419-66.

201. Liu, W., et al., *It's all about change: the antigen-driven initiation of B-cell receptor signaling.* Cold Spring Harb Perspect Biol, 2010. **2**(7): p. a002295.

202. Saphire, E.O., et al., *Contrasting IgG structures reveal extreme asymmetry and flexibility.* J Mol Biol, 2002. **319**(1): p. 9-18.

203. Wurzburg, B.A., S.C. Garman, and T.S. Jardetzky, *Structure of the human IgE-Fc C epsilon 3-C epsilon 4 reveals conformational flexibility in the antibody effector domains.* Immunity, 2000. **13**(3): p. 375-85.

204. Sondermann, P., et al., *The 3.2-A crystal structure of the human IgG1 Fc fragment-Fc gammaRIII complex.* Nature, 2000. **406**(6793): p. 267-73.

205. Radaev, S., et al., *Structural and functional studies of Igalphabeta and its assembly with the B cell antigen receptor.* Structure, 2010. **18**(8): p. 934-43.

206. Tolar, P. and S.K. Pierce, *A conformation-induced oligomerization model for B cell receptor microclustering and signaling*, in *Immunological Synapse*. 2010, Springer. p. 155-169.

207. Tolar, P., et al., *The constant region of the membrane immunoglobulin mediates B cell-receptor clustering and signaling in response to membrane antigens.* Immunity, 2009. **30**(1): p. 44-55.

208. Wan, T., et al., *The crystal structure of IgE Fc reveals an asymmetrically bent conformation.* Nat Immunol, 2002. **3**(7): p. 681-6.

209. Huber, R., et al., *Crystallographic structure studies of an IgG molecule and an Fc fragment.* Nature, 1976. **264**(5585): p. 415-20.

210. Herr, A.B., E.R. Ballister, and P.J. Bjorkman, *Insights into IgA-mediated immune responses from the crystal structures of human FcalphaRI and its complex with IgA1-Fc.* Nature, 2003. **423**(6940): p. 614-20.

211. Yang, F., et al., *Origin of the Stokes shift: A geometrical model of exciton spectra in 2D semiconductors.* Phys Rev Lett, 1993. **70**(3): p. 323-326.

212. Axelrod, D., *Cell-substrate contacts illuminated by total internal reflection fluorescence.* J Cell Biol, 1981. **89**(1): p. 141-5.

213. Axelrod, D., N.L. Thompson, and T.P. Burghardt, *Total internal inflection fluorescent microscopy.* J Microsc, 1983. **129**(Pt 1): p. 19-28.

214. Huang, B., H. Babcock, and X. Zhuang, *Breaking the diffraction barrier: super-resolution imaging of cells.* Cell, 2010. **143**(7): p. 1047-58.

215. Davidson, M.W. *Resolution*. 2019 [cited 2019 03/04/2019]; Available from: https://www.microscopyu.com/microscopy-basics/resolution.

216. Saxena, M., G. Eluru, and S.S. Gorthi, *Structured illumination microscopy.* Advances in Optics and Photonics, 2015. **7**(2): p. 241-275.

217. Heintzmann, R. and M.G.L. Gustafsson, *Subdiffraction resolution in continuous samples.* Nature Photonics, 2009. **3**(7): p. 362-364.

218. Rego, E.H., et al., *Nonlinear structured-illumination microscopy with a photoswitchable protein reveals cellular structures at 50-nm resolution.* Proc Natl Acad Sci U S A, 2012. **109**(3): p. E135-43.

219. Gustafsson, M.G., *Surpassing the lateral resolution limit by a factor of two using structured illumination microscopy.* J Microsc, 2000. **198**(Pt 2): p. 82-7.

220. Heintzmann, R. and C. Cremer, *Laterally modulated excitation microscopy: Improvement of resolution by using a diffraction grating.* Optical Biopsies and Microscopic Techniques Iii, Proceedings Of, 1999. **3568**: p. 185-196.

221. Hell, S.W. and J. Wichmann, *Breaking the diffraction resolution limit by stimulated emission: stimulated-emission-depletion fluorescence microscopy.* Opt Lett, 1994. **19**(11): p. 780-2.

222. Klar, T.A. and S.W. Hell, *Subdiffraction resolution in far-field fluorescence microscopy.* Opt Lett, 1999. **24**(14): p. 954-6.

223. Klar, T.A., et al., *Fluorescence microscopy with diffraction resolution barrier broken by stimulated emission.* Proc Natl Acad Sci U S A, 2000. **97**(15): p. 8206-10.

224. Vicidomini, G., P. Bianchini, and A. Diaspro, *STED super-resolved microscopy.* Nat Methods, 2018. **15**(3): p. 173-182.

225. Muller, T., C. Schumann, and A. Kraegeloh, *STED microscopy and its applications: new insights into cellular processes on the nanoscale.* Chemphyschem, 2012. **13**(8): p. 1986-2000.

226. Gottfert, F., et al., *Coaligned dual-channel STED nanoscopy and molecular diffusion analysis at 20 nm resolution.* Biophys J, 2013. **105**(1): p. L01-3.

227. Thompson, R.E., D.R. Larson, and W.W. Webb, *Precise nanometer localization analysis for individual fluorescent probes.* Biophys J, 2002. **82**(5): p. 2775-83.

228. Yildiz, A., et al., *Myosin V walks hand-over-hand: single fluorophore imaging with 1.5-nm localization.* Science, 2003. **300**(5628): p. 2061-5.

229. Mortensen, K.I., et al., *Optimized localization analysis for single-molecule tracking and super-resolution microscopy.* Nat Methods, 2010. **7**(5): p. 377-81.

230. Schermelleh, L., R. Heintzmann, and H. Leonhardt, *A guide to super-resolution fluorescence microscopy.* J Cell Biol, 2010. **190**(2): p. 165-75.

231. Pertsinidis, A., Y. Zhang, and S. Chu, *Subnanometre single-molecule localization, registration and distance measurements.* Nature, 2010. **466**(7306): p. 647-51.

232. Sharonov, A. and R.M. Hochstrasser, *Wide-field subdiffraction imaging by accumulated binding of diffusing probes.* Proc Natl Acad Sci U S A, 2006. **103**(50): p. 18911-6.

233. Rice, J.H., *Beyond the diffraction limit: far-field fluorescence imaging with ultrahigh resolution.* Mol Biosyst, 2007. **3**(11): p. 781-93.

234. Delcanale, P., et al., *Nanoscale Mapping Functional Sites on Nanoparticles by Points Accumulation for Imaging in Nanoscale Topography (PAINT).* ACS Nano, 2018. **12**(8): p. 7629-7637.

235. Jahn, K., et al., *Functional patterning of DNA origami by parallel enzymatic modification.* Bioconjug Chem, 2011. **22**(4): p. 819-23.

236. Rust, M.J., M. Bates, and X. Zhuang, *Sub-diffraction-limit imaging by stochastic optical reconstruction microscopy (STORM).* Nat Methods, 2006. **3**(10): p. 793-5.

237. Heilemann, M., et al., *Carbocyanine dyes as efficient reversible single-molecule optical switch.* J Am Chem Soc, 2005. **127**(11): p. 3801-6.

238. Betzig, E., et al., *Imaging intracellular fluorescent proteins at nanometer resolution.* Science, 2006. **313**(5793): p. 1642-5.

239. Dempsey, G.T., et al., *Photoswitching mechanism of cyanine dyes.* J Am Chem Soc, 2009. **131**(51): p. 18192-3.

240. Heilemann, M., et al., *Super-resolution imaging with small organic fluorophores.* Angew Chem Int Ed Engl, 2009. **48**(37): p. 6903-8.

241. Zhang, M., et al., *Rational design of true monomeric and bright photoactivatable fluorescent proteins.* Nat Methods, 2012. **9**(7): p. 727-9.

242. Lee, J., et al., *The nanoscale spatial organization of B-cell receptors on immunoglobulin M- and G-expressing human B-cells.* Mol Biol Cell, 2017. **28**(4): p. 511-523.

243. Pore, D., et al., *Ezrin tunes the magnitude of humoral immunity.* J Immunol, 2013. **191**(8): p. 4048-58.

244. Zuidscherwoude, M., et al., *The tetraspanin web revisited by super-resolution microscopy.* Sci Rep, 2015. **5**: p. 12201.

245. Stone, M.B. and S.L. Veatch, *Steady-state cross-correlations for live two-colour super-resolution localization data sets.* Nat Commun, 2015. **6**: p. 7347.

246. Righolt, C.H., et al., *Differences in Nuclear DNA Organization Between Lymphocytes, Hodgkin and Reed-Sternberg Cells Revealed by Structured Illumination Microscopy.* Journal of Cellular Biochemistry, 2014. **115**(8): p. 1441-1448.

247. Hell, S.W., et al., *The 2015 super-resolution microscopy roadmap.* Journal of Physics D-Applied Physics, 2015. **48**(44).

248. Guo, B., T.T. Su, and D.J. Rawlings, *Protein kinase C family functions in B-cell activation.* Curr Opin Immunol, 2004. **16**(3): p. 367-73.

249. Ulivieri, C. and C.T. Baldari, *The BCR signalosome: Where cell fate is decided.* Journal of Biological Regulators and Homeostatic Agents, 2005. **19**(1-2): p. 1-16.

250. Kner, P., et al., *Super-resolution video microscopy of live cells by structured illumination.* Nat Methods, 2009. **6**(5): p. 339-42.

251. Shelby, S.A., et al., *Distinct stages of stimulated FcepsilonRI receptor clustering and immobilization are identified through superresolution imaging.* Biophys J, 2013. **105**(10): p. 2343-54.

252. Veatch, S.L., et al., *Correlation functions quantify super-resolution images and estimate apparent clustering due to over-counting.* PLoS One, 2012. **7**(2): p. e31457.

253. Kwak, B., et al., *Statins as a newly recognized type of immunomodulator.* Nat Med, 2000. **6**(12): p. 1399-402.

254. DiLillo, D.J., M. Horikawa, and T.F. Tedder, *B-lymphocyte effector functions in health and disease.* Immunologic research, 2011. **49**(1-3): p. 281-292.

255. Youinou, P., *B cell conducts the lymphocyte orchestra.* Journal of autoimmunity, 2007. **28**(2-3): p. 143-151.

256. Howard, M. and W.E. Paul, *Regulation of B-cell growth and differentiation by soluble factors.* Annual review of immunology, 1983. **1**(1): p. 307-327.

257. Monroe, J.G. and K. Dorshkind, *Fate decisions regulating bone marrow and peripheral B lymphocyte development.* Advances in immunology, 2007. **95**: p. 1-50.

258. Niiro, H. and E.A. Clark, *Decision making in the immune system: regulation of B-cell fate by antigen-receptor signals.* Nature Reviews Immunology, 2002. **2**(12): p. 945.

259. Volkmann, C., et al., *Molecular requirements of the B-cell antigen receptor for sensing monovalent antigens.* EMBO J, 2016. **35**(21): p. 2371-2381.

260. Yamanashi, Y., et al., *Association of B cell antigen receptor with protein tyrosine kinase Lyn.* Science, 1991. **251**(4990): p. 192-4.

261. Cheng, P.C., et al., *A role for lipid rafts in B cell antigen receptor signaling and antigen targeting.* J Exp Med, 1999. **190**(11): p. 1549-60.

262. Zhu, J.W., et al., *Structurally distinct Phosphatases CD45 and CD148 both regulate B cell and macrophage immunoreceptor signaling.* Immunity, 2008. **28**(2): p. 183-196.

263. Honerkamp-Smith, A.R., et al., *Line tensions, correlation lengths, and critical exponents in lipid membranes near critical points.* Biophys J, 2008. **95**(1): p. 236-46.

264. Lorent, J.H., et al., *Structural determinants and functional consequences of protein affinity for membrane rafts.* Nat Commun, 2017. **8**(1): p. 1219.

265. Diaz-Rohrer, B.B., et al., *Membrane raft association is a determinant of plasma membrane localization.* Proc Natl Acad Sci U S A, 2014. **111**(23): p. 8500-5.

266. Haughton, G., et al., *The CH series of murine B cell lymphomas: neoplastic analogues of Ly-1+ normal B cells.* Immunol Rev, 1986. **93**(1): p. 35-51.

267. Edwald, E., et al., *Oxygen depletion speeds and simplifies diffusion in HeLa cells.* Biophys J, 2014. **107**(8): p. 1873-1884.

268. Carrasco, Y.R., et al., *LFA-1/ICAM-1 interaction lowers the threshold of B cell activation by facilitating B cell adhesion and synapse formation.* Immunity, 2004. **20**(5): p. 589-99.

269. Carrasco, Y.R. and F.D. Batista, *B‐cell activation by membrane‐bound antigens is facilitated by the interaction of VLA‐4 with VCAM‐1.* The EMBO journal, 2006. **25**(4): p. 889-899.

270. Stone, M.B., S.A. Shelby, and S.L. Veatch, *Super-Resolution Microscopy: Shedding Light on the Cellular Plasma Membrane.* Chem Rev, 2017. **117**(11): p. 7457-7477.

271. Tolar, P., et al., *The molecular assembly and organization of signaling active B-cell receptor oligomers.* Immunol Rev, 2009. **232**(1): p. 34-41.

272. Batista, F.D., D. Iber, and M.S. Neuberger, *B cells acquire antigen from target cells after synapse formation.* Nature, 2001. **411**(6836): p. 489-94.

273. Goodnow, C.C., *Transgenic mice and analysis of B-cell tolerance.* Annu Rev Immunol, 1992. **10**(1): p. 489-518.

274. Koopman, G., et al., *Adhesion through the Lfa-1 (Cd11a/Cd18)-Icam-1 (Cd54) and the Vla-4 (Cd49d)-Vcam-1 (Cd106) Pathways Prevents Apoptosis of Germinal Center B-Cells.* Journal of Immunology, 1994. **152**(8): p. 3760-3767.

275. Hayashida, K., et al., *Rheumatoid arthritis synovial stromal cells inhibit apoptosis and up-regulate Bcl-xL expression by B cells in a CD49/CD29-CD106-dependent mechanism.* J Immunol, 2000. **164**(2): p. 1110-6.

276. Harwood, N.E. and F.D. Batista, *New insights into the early molecular events underlying B cell activation.* Immunity, 2008. **28**(5): p. 609-619.

277. Xu, Y., et al., *Lyn tyrosine kinase: accentuating the positive and the negative.* Immunity, 2005. **22**(1): p. 9-18.

278. Chan, V.W., et al., *Characterization of the B lymphocyte populations in Lyn-deficient mice and the role of Lyn in signal initiation and down-regulation.* Immunity, 1997. **7**(1): p. 69-81.

279. Davis, R.E., et al., *Chronic active B-cell-receptor signalling in diffuse large B-cell lymphoma.* Nature, 2010. **463**(7277): p. 88-92.

280. Hartley, J.M., et al., *Super-Resolution Imaging and Quantitative Analysis of Membrane Protein/Lipid Raft Clustering Mediated by Cell-Surface Self-Assembly of Hybrid Nanoconjugates.* Chembiochem, 2015. **16**(12): p. 1725-9.

281. Levental, I. and S. Veatch, *The Continuing Mystery of Lipid Rafts.* J Mol Biol, 2016. **428**(24 Pt A): p. 4749-4764.

282. Razvag, Y., et al., *Nanoscale kinetic segregation of TCR and CD45 in engaged microvilli facilitates early T cell activation.* Nat Commun, 2018. **9**(1): p. 732.

283. Depoil, D., et al., *CD19 is essential for B cell activation by promoting B cell receptor-antigen microcluster formation in response to membrane-bound ligand.* Nat Immunol, 2008. **9**(1): p. 63-72.

284. Mustelin, T., K.M. Coggeshall, and A. Altman, *Rapid activation of the T-cell tyrosine protein kinase pp56lck by the CD45 phosphotyrosine phosphatase.* Proc Natl Acad Sci U S A, 1989. **86**(16): p. 6302-6.

285. Byth, K., et al., *CD45-null transgenic mice reveal a positive regulatory role for CD45 in early thymocyte development, in the selection of CD4+ CD8+ thymocytes, and B cell maturation.* Journal of Experimental Medicine, 1996. **183**(4): p. 1707-1718.

286. Kishihara, K., et al., *Normal B lymphocyte development but impaired T cell maturation in CD45-exon6 protein tyrosine phosphatase-deficient mice.* Cell, 1993. **74**(1): p. 143-156.

287. Hammond, A.T., et al., *Crosslinking a lipid raft component triggers liquid ordered-liquid disordered phase separation in model plasma membranes.* Proc Natl Acad Sci U S A, 2005. **102**(18): p. 6320-5.

288. Blank, N., et al., *Cholera toxin binds to lipid rafts but has a limited specificity for ganglioside GM1.* Immunol Cell Biol, 2007. **85**(5): p. 378-82.

289. Toulmay, A. and W.A. Prinz, *Direct imaging reveals stable, micrometer-scale lipid domains that segregate proteins in live cells.* Journal of Cell Biology, 2013. **202**(1): p. 35-44.

290. Shelby, S.A., et al., *Functional nanoscale coupling of Lyn kinase with IgE-FcepsilonRI is restricted by the actin cytoskeleton in early antigen-stimulated signaling.* Mol Biol Cell, 2016. **27**(22): p. 3645-3658.

291. Mercolino, T.J., L.W. Arnold, and G. Haughton, *Phosphatidyl choline is recognized by a series of Ly-1+ murine B cell lymphomas specific for erythrocyte membranes.* J Exp Med, 1986. **163**(1): p. 155-65.

292. Schnitzler, A.C., J.M. Burke, and L.M. Wetzler, *Induction of cell signaling events by the cholera toxin B subunit in antigen-presenting cells.* Infect Immun, 2007. **75**(6): p. 3150-9.

293. Machta, B.B., et al., *Conditions that Stabilize Membrane Domains Also Antagonize n-Alcohol Anesthesia.* Biophysical Journal, 2016. **111**(3): p. 537-545.

294. Dick, R.A., et al., *HIV-1 Gag protein can sense the cholesterol and acyl chain environment in model membranes.* Proc Natl Acad Sci U S A, 2012. **109**(46): p. 18761-6.

295. Staubach, S., H. Razawi, and F.G. Hanisch, *Proteomics of MUC1-containing lipid rafts from plasma membranes and exosomes of human breast carcinoma cells MCF-7.* Proteomics, 2009. **9**(10): p. 2820-35.

296. Raghu, H., et al., *Localization of uPAR and MMP-9 in lipid rafts is critical for migration, invasion and angiogenesis in human breast cancer cells.* BMC Cancer, 2010. **10**: p. 647.

297. Shashkin, P., B. Dragulev, and K. Ley, *Macrophage differentiation to foam cells.* Curr Pharm Des, 2005. **11**(23): p. 3061-72.

298. Rios, F.J., et al., *Uptake of oxLDL and IL-10 production by macrophages requires PAFR and CD36 recruitment into the same lipid rafts.* PLoS One, 2013. **8**(10): p. e76893.

299. Stratmann, T., *Cholera Toxin Subunit B as Adjuvant-An Accelerator in Protective Immunity and a Break in Autoimmunity.* Vaccines, 2015. **3**(3): p. 579-596.